Geometric Estimation

Of

Strains

In

Car Body Panels

by

Graham Stewart Heap

A Doctoral thesis submitted in partial fulfilment of
the requirements for the award of the degree of
Doctor of Philosophy of
Loughborough University of Technology.
October 1988.

Supervisor : A.A. Ball, B.Sc., Ph.D.
Institute of Engineering Design,
Loughborough University of Technology.

Acknowledgement

I acknowledge the help and committed involvement of my supervisor, Dr. Alan Ball, and the structured step by step development of my work. His ideas and motivation have been crucial for the task I have undertaken and the criticism and comments made on the thesis have greatly enhanced its presentation.

I must thank the Department of Engineering Mathematics, under Professor A. C. Bajpai, OBE, for support and making available the facilities required to complete the thesis.

I give credit to the Science and Engineering Research Council and Austin Rover for funding the Case Studentship. Further I thank Bob Coltman of Austin Rover for organizing the collection of strain data.

I also thank Dr. Robert Cripps for help on software development and criticism for the flowcharts presented. The programs were all written on the University Honeywell DPS8 mainframe using FORTRAN 77 and to departmental standards identified in Internal reports : NO. 85/37, 'Programming Standards' and No. 86/39, 'Documentation Standards', written by Dr. Robert Cripps.

I express my appreciation to my girl friend Debbie Brown for her personal support and tolerance of my strained thinking during the completion of the write-up. I also value the work done by the University Counselling Service and I am especially indebted to Alan Lilley for his patient ear and mature advise.

SYNOPSIS

The thesis focuses on the manufacture of car body panels at Austin Rover and in particular the phenomenon of springback. After pressing of a shallow drawn panel its shape is often flatter than required. This loss of shape control corresponds to areas of small strains. The aim of the thesis is to describe the generation of a database of small strain information at discrete points on a drawn panel, which could be used in the numerical modelling of the drawing process.

Chapter 2 discusses the background for small strain analysis and gives an outline system specification for a suite of programs to determine the principal strains and directions at discrete points on a drawn panel.
Chapter 3 presents the basic theory of geodesics, based on the differential geometry of curves and surfaces. Curvature and torsion properties are established for the rational cubic segment.

Chapter 4 presents the radial plane subdivision method, for evaluating the shortest planar distance between two points on a surface patch. The results of this algorithm applied to two production panels are presented in Chapter 5. The final chapter discusses these results and identifies areas for further work.

TABLE OF CONTENTS

CHAPTER 1

INTRODUCTION

In this thesis we focus on the manufacture of car body panels at Austin Rover and in particular the phenomenon of springback. After pressing of a shallow drawn panel its shape is often flatter than required e.g., a car bonnet or roof panel. This loss of shape control corresponds to areas of small strains. The aim of the thesis is to describe the generation of a database of small strain information at discrete points on a drawn panel, which could be used in the numerical modelling of the drawing process.

The numerical modelling of sheet metal forming [Duncan et al; 1985] is important in the context of fully integrated CADCAM and the potential benefits for the sheet metal forming industry are documented [Lee; 1983, Kokkonen; 1985].

In section(1.1) the drawing process is described and factors which influence the quality of the drawn panel are also identified. In section(1.2) an overview of the activities for the design and manufacture of press tools at Austin Rover is presented. The contents of the thesis are outlined in section(1.3).

1.1 The drawing process.

The drawing process can be illustrated by the operation of a double action press with the following sequence of actions which correspond to Figures(1.1) to (1.3) :

a) a sheet of metal or blank is placed in its initial position.
b) the outer ram moves downwards and secures the blank for pressing.
c) the punch descends with the inner ram, and stretches and draws the blank into its shape.

The blank holder secures the sheet of metal for pressing. The presence of draw beads, and complementary grooves which are cut into the mating blank holder, affect the flow of metal into the forming part. Similarly, other process parameters such as friction between contact surfaces, lubrication, stroke force and blank holder pressure affect the shape of the drawn panel.

There are a number of factors which influence the quality of a pressed panel and can be broadly categorized by :

a) the shape and thickness of the design part.
b) the material properties of the blank.
c) the process parameters.

A detailed review of these factors is reported in the work by Caddell and Hosford [1983], and Richard [1981a, 1981b].

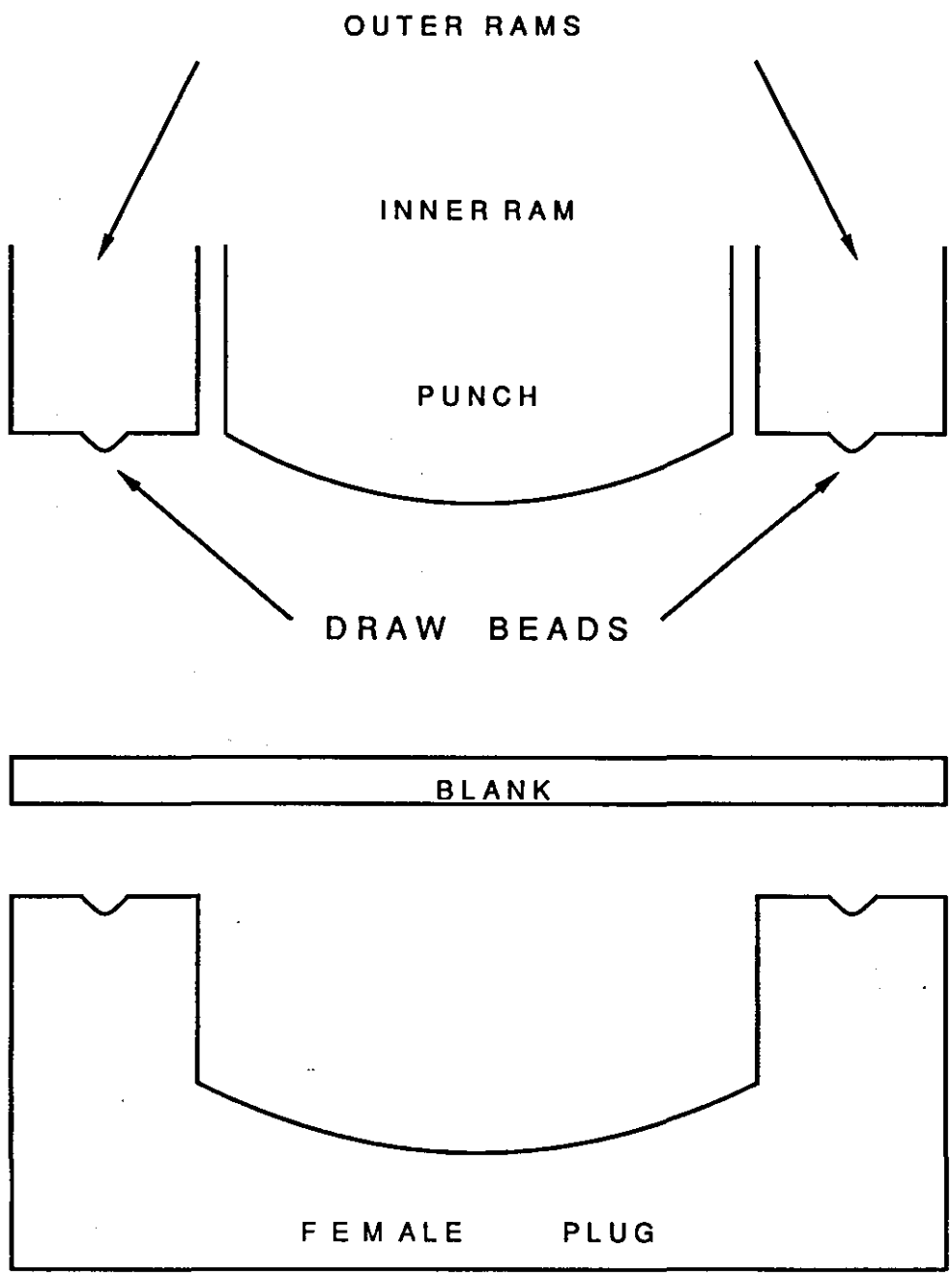

Figure (1.1) : Blank in its initial position .

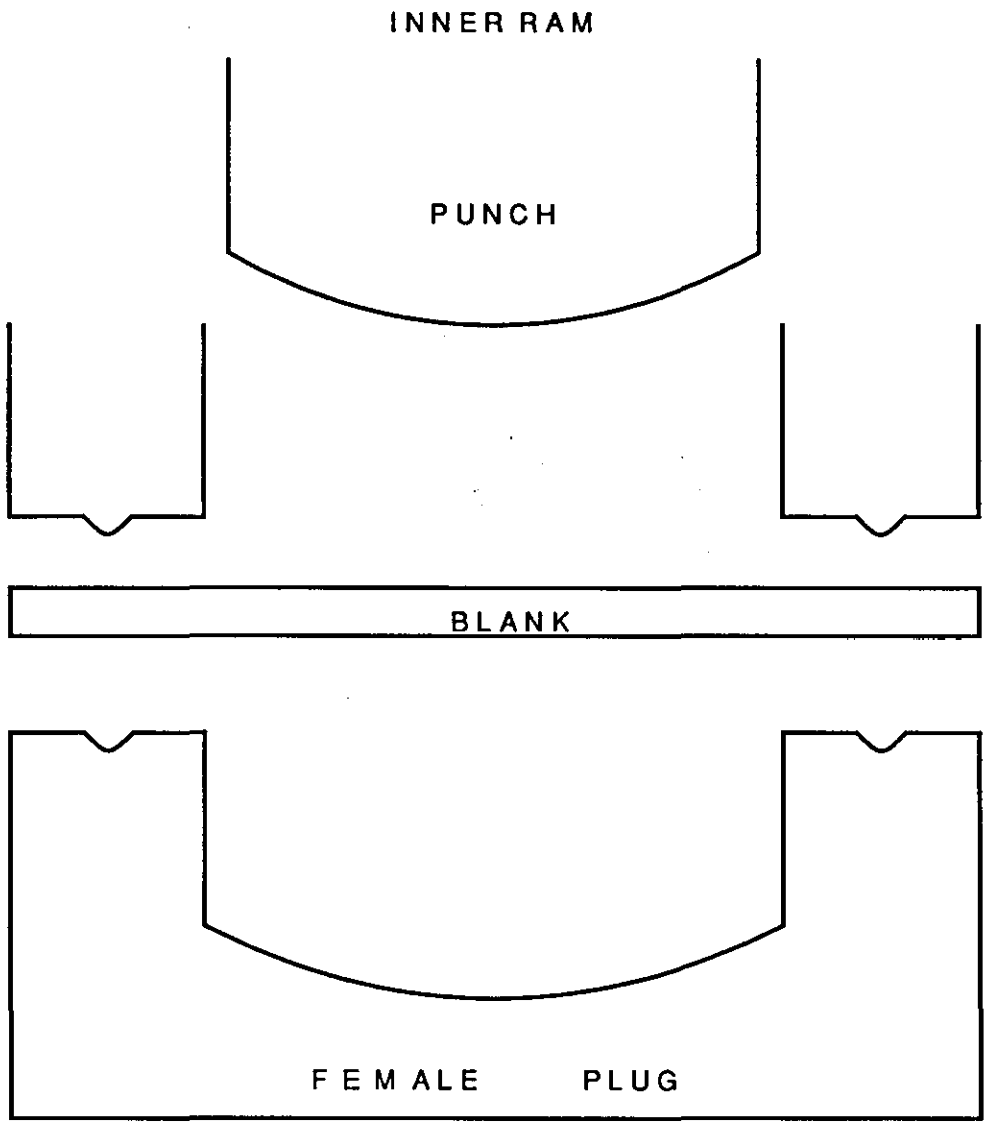

Figure (1.2) : Blank is secured by outer ram .

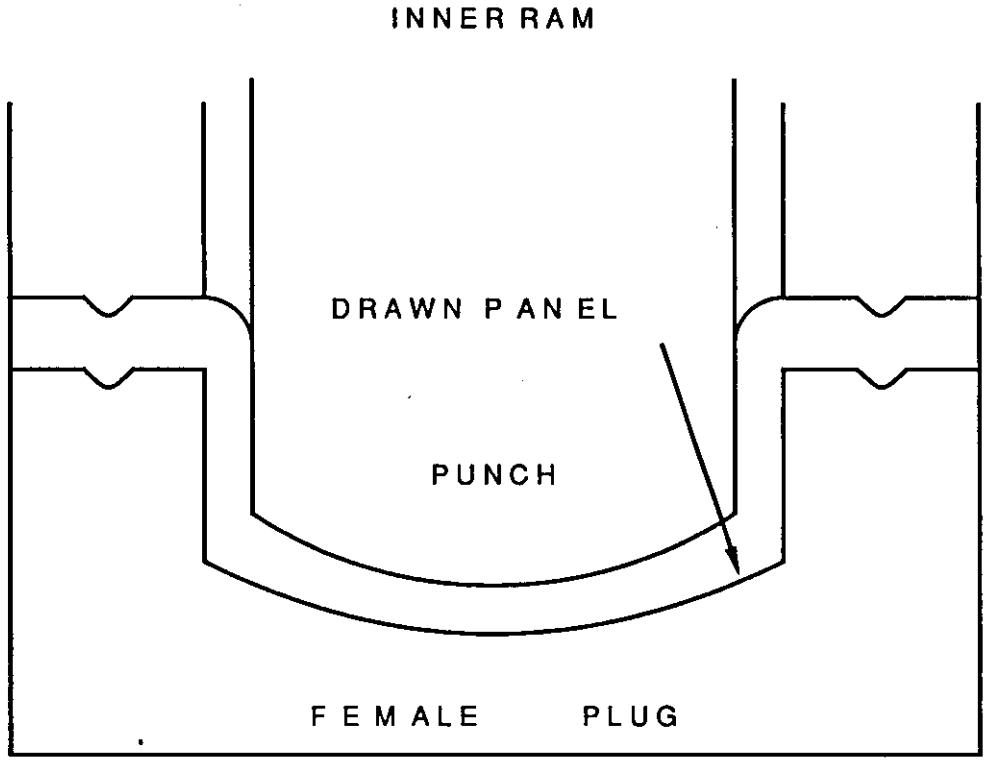

Figure (1.3) : The panel is formed from the blank being stetched over the punch, which descends on the inner ram.

1.2 Tool design and manufacture at Austin Rover.

The departmental structure for the design and manufacture of press tools for the production of car body panels at Austin Rover [Coltman; 1988] is illustrated in Figures(1.4) to (1.6). The activities within each department are summarized in **Tables 1.1** to **1.3**.

The problem of springback is usually dealt with at Tryout. The punch is overshaped or overcrowned, so that the panel springs back to the required shape. This is done on a trial and error basis with the experience of press shop personnel, and highlights a missing link in the CADCAM chain : given the shape, material properties and thickness of a drawn panel the overcrown required on the punch cannot be predicted, before the panel is pressed.

Ball and Cripps [1987] describe a geometric approach for the development of an overcrown prediction program. We consider one aspect of the overcrown project, which is the generation of small strain information at discrete points on a drawn panel. In the next section we outline the content and structure of the thesis.

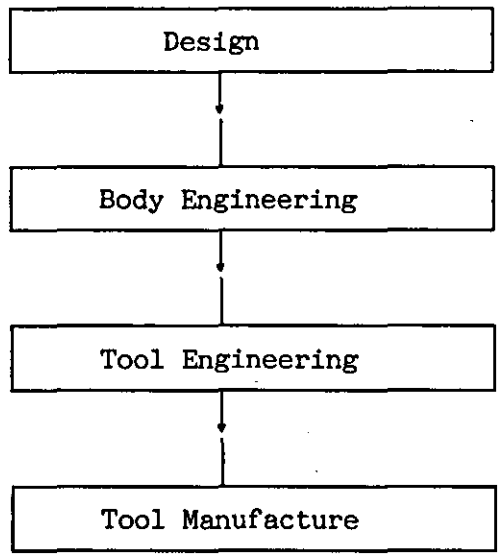

Figure(1.4) : The departments involved in the design and manufacture of press tools.

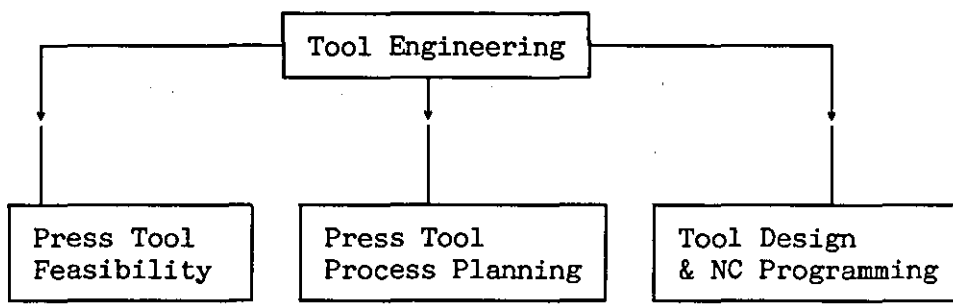

Figure(1.5) : The departmental structure of Tool Engineering at Austin Rover.

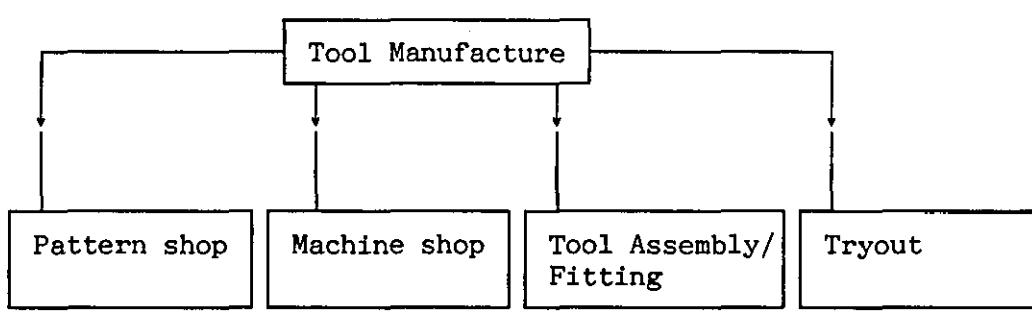

Figure(1.6) : The departmental structure of Tool Manufacture at Austin Rover.

Table 1.1 : The production of car body panels

Department	Activity
Design	A geometric database of the new car is generated, from a full scale clay model, which serves as a Master model for reference in the design and manufacture of press tools.
Body Engineering	The car body panels are defined by dividing up the outside shell of the car with curves.
Tool Engineering	See **Table 1.2**
Tool Manufacture	See **Table 1.3**

Table 1.2 : Tool Engineering

Department	Activity
Press Tool Feasibility	The panels required for the car are approved, in liaison with Body Engineering.
Press Tool Process Planning	A manufacturing scheme is devised which details the number and type of tool(s) for each panel required.
Tool Design & NC Programming	The press tools are designed from the component drawing of the part and with the aid of a CADCAM system and NC programmed.

Table 1.3 : Tool Manufacture

Department	Activity
Pattern shop	Manufacture reference media and casting patterns for press tool geometry, assembly fixtures and inspection media.
Machine shop	Machine castings and polish piece surfaces.
Tool Assembly /Fitting	Assemble tools.
Tryout	Produce a panel acceptable at inspection. Problems encountered : wrinkling, splitting and springback.

1.3 Outline of thesis contents.

In Chapter 2 we discuss the background for small strain analysis. We describe the calculation of principal strains and directions at discrete points on a drawn panel. We outline a system specification for a suite of programs to determine the principal strains and directions at discrete points on a drawn panel.

To estimate small strains we consider the deformation of straight lines on a blank to curves on the drawn panel. We can obtain a lower bound for small strains by considering curves of shortest distance i.e., geodesic curves.

In Chapter 3 we present the basic theory of geodesics, which is based on the differential geometry of curves and surfaces. In particular the parametric cubic (PC) segment, widely used in CAD [Faux and Pratt; 1983], is considered, and curvature and torsion properties are established as a by-product of this work with generalizations for the rational cubic segment presented in Appendices A and B.

In Chapter 4 we present a naïve algorithm, the radial plane subdivision method, for evaluating the shortest planar distance between two points on a surface patch; this gives a greater value than the geodesic curve length, which by definition would be the minimum distance. The background mathematics of the shortest path problem is presented and underlying assumptions are highlighted. The algorithm is based on the lattice technique for a surface/plane intersection. The choice of mesh parameters is investigated using roof and bonnet information.

In Chapter 5 we present the results of applying the radial range subdivision methods to two production panels : the R8-bonnet and R8-roof. The problem of presenting large amounts of strain data is identified and graphical solutions are discussed.

In Chapter 6 we discuss the physical interpretation of these results. Some limitations of the radial range subdivision method are examined and possible improvements are suggested. We discuss the motivation for further work and conclude with the development of shortest path algorithms by finding the geodesic curves between two points on a surface.

In Appendix D we apply the torsion property of the rational cubic segment, presented in Appendix B, to composite rational cubic curves and to the rational bicubic surface; the results are placed in the context of a new area of research, visual continuity [Boehm;1988].

CHAPTER 2

STRAIN ANALYSIS OF DRAWN PANELS

2.1 Introduction.

In this chapter we consider the estimation of small strains in drawn panels. A brief overview of the literature for numerical modelling of stretch forming and deep-drawing with sheet metal is presented in this section. The background for small strain analysis is discussed in section(2.2). The determination of principal strains and directions at discrete points on a drawn panel is described in section(2.3). A system specification for a suite of programs to determine the principal strains and directions at discrete points on a drawn panel is outlined in section(2.4).

The pioneering efforts by Chung and Swift [1951], in the forming and deep-drawing of cups with a hemispherical punch were initiated when computing power was fairly limited. Wood [1981] reports the successful application of a versatile numerical technique, the finite element (FE) method and more details are discussed in a number of texts [Zienkiewicz; 1985, Mitchell and Wait; 1985] : he indicates the future numerical modelling of arbitrary shapes, material properties and process parameters, in the stretch forming and deep-drawing of sheet metals using FE methods.

Success in predicting forming and failure in parts, of arbitrary shapes, at the design stage is described by Chu et al. [1982] and Lee [1982]. The potential of a tested FE code for general tooling is identified by Baynham and Zienkiewicz [1982].

There are two FE approaches for modelling the deformation of material : the rigid - plastic and elastic - viscoplastic. The former essentially models the behaviour of the metal as a non-newtonian viscous fluid, and ignores the elasticity of the material : the latter models the metal as a deformable solid. The formulation and implementation of the two approaches is compared by Honner et al. [1985].

Several authors [Baynham and Zienkiewicz; 1982, Chu et al.; 1982, Honner et al.; 1985 , Lee; 1982] have modelled process parameters, such as friction between the punch and panel, the effect of changing process parameters on the drawing process is also considered in detail by Chandra [1986] and Kobayashi et al. [1986].

The comparison of numerical results with the forming of simple shapes using hemispherical, elliptical and flat punches has been documented [Chu et al.; 1982, Kobayashi et al.; 1986, Lee ;1982 , Wang; 1982]. However, the evaluation of general FE codes is restricted by the limited experimental data available [Baynham and Zienkiewicz; 1982].

Alternative numerical approaches for the modelling of stretch forming and deep-drawing of sheet metal are suggested by Duncan et al. [1985] and Ball and Cripps [1987].

2.2 Background for small strain analysis.

Ball and Cripps [1987] are involved in the development of an overcrown prediction program in collaboration with Austin Rover. Their aim is to characterize the geometric nature of springback. This is done by generating a knowledge base of punch and panel shapes, for a range of materials and thicknesses. The difference between the punch and panel shapes defines the geometric nature of springback. A punch or panel is defined by an assembly of surface patches. Each surface patch is defined by polynomial approximation of points taken off, using the LK 3D digitizer at Austin Rover, the punch or panel and the numerical definition is represented parametrically by :

$$\mathbf{r} = \mathbf{r}(u,v) = (x(u,v), y(u,v), z(u,v)); \; 0 \leq u,v \leq 1$$

where $x(u,v)$, $y(u,v)$ and $z(u,v)$ are polynomials in u and v.

In addition a database of small strain information is generated. The panels of interest are regions of low strain, where springback is most noticeable eg. roofs or bonnets. From the strain information generated we can determine the principal strains and directions at discrete points, and this is described in section(2.3).

2.3 Principal strains and directions.

In this section we discuss the determination of principal strains and directions at discrete points on a drawn panel. In section(2.3.1) we define a strain state with reference to a co-ordinate system. In section(2.3.2) we apply this definition to discrete points on a drawn panel, for which we require two estimated strains and their directions. The source and processing of strain data is described in sections(2.3.3) and (2.3.4).

2.3.1) Definition of strain state .

We consider two perpendicular lines on a flat plate. Let the point x_1 lie on one of these lines and let the point y_1 lie on the other line. Let the point **o** be the intersection of the two lines. Our co-ordinate system is defined by unit vectors **ox** and **oy**; which are parallel to the vectors ox_1 and oy_1, respectively. The flat plate is deformed in the plane, and the points **o**, x_1 and y_1 take up new positions : o^*, x_1^* and y_1^*, respectively. This configuration is illustrated by Figure(2.1). We perform a rigid body translation and rotation; such that $o = o^*$ and the angle between **ox** and ox_1^* and the angle between **oy** and oy_1^* are equal.

The state of strain at o^* is defined by the three scalars; ϵ_{xx}, ϵ_{xy} and ϵ_{yy} [Hall; 1968] where :

$$\epsilon_{xx} = |o^*x_1^* - ox_1|/|ox_1|$$
$$\epsilon_{xy} = \tfrac{1}{2}(\pi/2 - \alpha_{xy}); \quad \alpha_{xy} = \cos^{-1}(o^*x_1^*.o^*y_1^*/|o^*x_1^*||o^*y_1^*|)$$
$$\epsilon_{yy} = |o^*y_1^* - oy_1|/|oy_1|$$

To calculate the principal strains and directions we consider an anti-clockwise rotation, σ_r, about the **oz** axis, where **oz** = **ox** X **oy**, of the coordinate system **ox**, **oy** to ox_r, oy_r, this coordinate system is illustrated in Figure(2.2). The strain state is now defined by three scalars; ϵ_{xxr}, ϵ_{xyr} ,ϵ_{yyr} where :

$$\begin{aligned}
\epsilon_{xxr} &= \cos^2(\sigma_r)\epsilon_{xx} + \sin(2\sigma_r)\epsilon_{xy} + \sin^2(\sigma_r)\epsilon_{yy} \\
\epsilon_{xyr} &= \tfrac{1}{2}\sin(2\sigma_r)(\epsilon_{yy} - \epsilon_{xx}) + \cos(2\sigma_r)\epsilon_{xy} \\
\epsilon_{yyr} &= \sin^2(\sigma_r)\epsilon_{xx} - \sin(2\sigma_r)\epsilon_{xy} + \cos^2(\sigma_r)\epsilon_{yy}
\end{aligned} \qquad (2.1)$$

and

$$ox_r = ox\cos(\sigma_r) + oy\sin(\sigma_r)$$
$$oy_r = -ox\sin(\sigma_r) + oy\cos(\sigma_r).$$

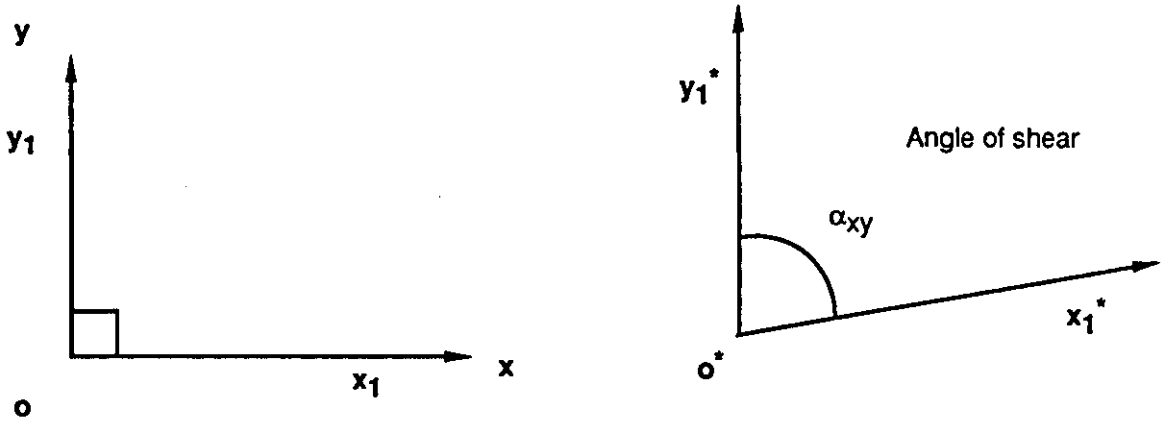

Figure(2.1) : Definition of a strain state .

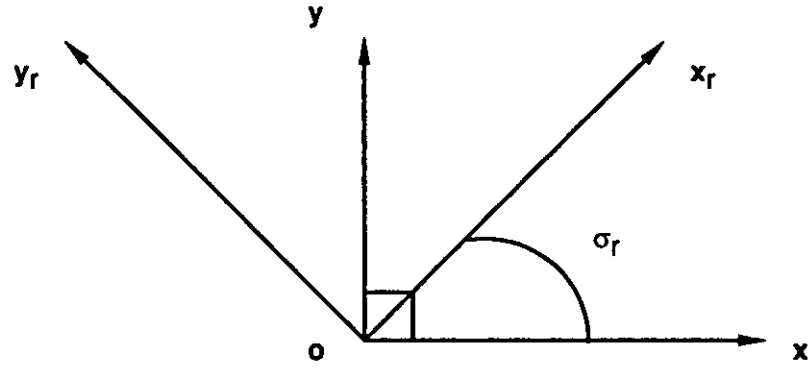

Figure(2.2) : Rotation of coordinate axes **ox** and **oy**.

Now the principal strains, $\epsilon_{x'}$ and $\epsilon_{y'}$, occur where $\epsilon_{xyp} = 0$.

Let $\epsilon_x' = \epsilon_{xxp}$ and $\epsilon_y' = \epsilon_{yyp}$, then :

$$\begin{aligned}\epsilon_{x'} &= \cos^2(\sigma_p)\epsilon_{xx} + \sin(2\sigma_p)\epsilon_{xy} + \sin^2(\sigma_p)\epsilon_{yy} \\ \epsilon_{y'} &= \sin^2(\sigma_p)\epsilon_{xx} - \sin(2\sigma_p)\epsilon_{xy} + \cos^2(\sigma_p)\epsilon_{yy}\end{aligned} \qquad (2.2)$$

where,

$$\tan(2\sigma_p) = \frac{2\epsilon_{xy}}{\epsilon_{xx} - \epsilon_{yy}}$$

and the principal directions, ox' and oy', are defined by :

$$\begin{aligned}ox' &= ox\cos(\sigma_p) + oy\sin(\sigma_p) \\ oy' &= -ox\sin(\sigma_p) + oy\cos(\sigma_p).\end{aligned} \qquad (2.3)$$

2.3.2) Principal strains and directions at discrete points

To calculate the principal strains and directions at a discrete point, **p***, we first define a coordinate system **ox**,**oy** in the tangent plane at **p***. We assume that the unit tangent directions t_1 and t_2 associated with strains S_1 and S_2 are inclined by an angle ϵ_{xy} [Hall; 1968] to the coordinate axes **ox** and **oy**, respectively; as illustrated in Figure(2.3). Thus the coordinate axes with unit vectors **ox** ,**oy** are defined by :

$$\begin{aligned}ox &= (t_1\cos(\epsilon xy) - t_2\sin(\epsilon xy))/\cos(2\epsilon xy) \\ oy &= (-t_1\sin(\epsilon xy) + t_2\cos(\epsilon xy))/\cos(2\epsilon xy)\end{aligned}$$

For small angles $|\epsilon_{xy}| \ll 1$ then :

$$\begin{aligned}ox &= t_1 - t_2\epsilon_{xy} \\ oy &= -t_1\epsilon_{xy} + t_2\end{aligned}$$

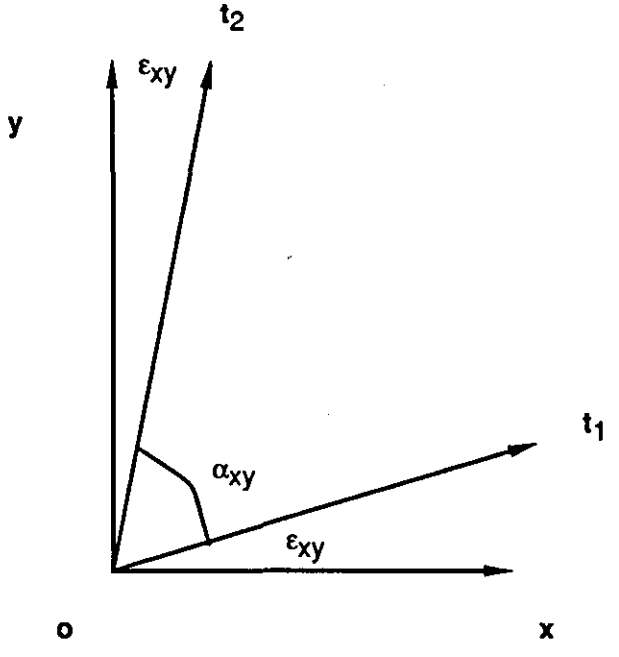

Figure(2.3) : The coordinate system in the tangent plane at p^*

We can now define a strain state, as discussed in section(2.3.1), in the tangent plane at **p***, by three scalars ϵ_{xx},ϵ_{xy} and ϵ_{yy} where :

$$\epsilon_{xx} = S_1$$
$$\epsilon_{xy} = \tfrac{1}{2}(\pi/2 - \alpha_{xy}) \ , \ \alpha_{xy} = \cos^{-1}(t_1.t_2)$$
$$\epsilon_{yy} = S_2$$

From equations (2.1) and (2.2) the principal strains ϵ_x',ϵ_y' at **p*** are defined by :

$$\epsilon_x' = \cos^2(\sigma_p)\epsilon_{xx} + \sin(2\sigma_p)\epsilon_{xy} + \sin^2(\sigma_p)\epsilon_{yy}$$

$$\epsilon_y' = \sin^2(\sigma_p)\epsilon_{xx} - \sin(2\sigma_p)\epsilon_{xy} + \cos^2(\sigma_p)\epsilon_{yy}$$

where,

$$\tan(2\sigma_p) = \frac{2\epsilon_{xy}}{\epsilon_{xx} - \epsilon_{yy}}$$

and the principal directions, **ox'** and **oy'**, in the tangent plane at **p***, are defined by :

$$\mathbf{ox'} = \mathbf{ox}\cos(\sigma_p) + \mathbf{oy}\sin(\sigma_p)$$

$$\mathbf{oy'} = -\mathbf{ox}\sin(\sigma_p) + \mathbf{oy}\cos(\sigma_p).$$

2.3.3) Description of strain data.

The strain data required is derived from 3x3 arrays of points, strain sets, which are etched onto a sheet of metal or blank, to an accuracy of ±0.01mm. We consider a strain set, p_i, i=1,2,...,9, and its numbering is illustrated in Figure(2.4). We refer, for the purpose of discussion in this section, to the parallel lines defined by points p_1,p_3; p_4,p_6; p_7,p_9 as horizontal lines and, similarly, to the parallel lines defined by points p_1,p_7; p_2,p_8; p_3,p_9 as vertical lines.

After pressing, the new positions on the drawn panel for each set of strain points, p_i^*, i=1,2,...,9, are recorded by the LK digitizer at Austin Rover, to an accuracy of ± 0.025mm. The drawn panel is represented by an assembly of polynomial surface patches and each strain set is located, in general, within a surface patch.

To determine the principal strains and directions at a discrete or digitized point, p_i^*, within a strain set we require two estimated strains S_1, S_2 and their associated unit tangent directions, t_1 and t_2, as introduced in section(2.3.2). To define a strain state in the tangent plane at p_i^*, we assume that the strains are generated from the in-plane deformation of perpendicular lines.

Let L_{ij} be a horizontal line joining two neighbouring points p_i and p_j, within a strain set, and let l_{ij} be there distance apart upon the blank. After pressing, the line L_{ij} is deformed to a curve L_{ij}^* on the drawn panel with end tangents t_{ij} and t_{ji}; which lie in the tangent planes at p_i^* and p_j^* , respectively. This curve has an arc length of l_{ij}^* . The average strain S_{ij} at a point p_i^* or p_j^* can be expressed immediately as :

$$S_{ij} = (l_{ij}^* - l_{ij})/ l_{ij}$$

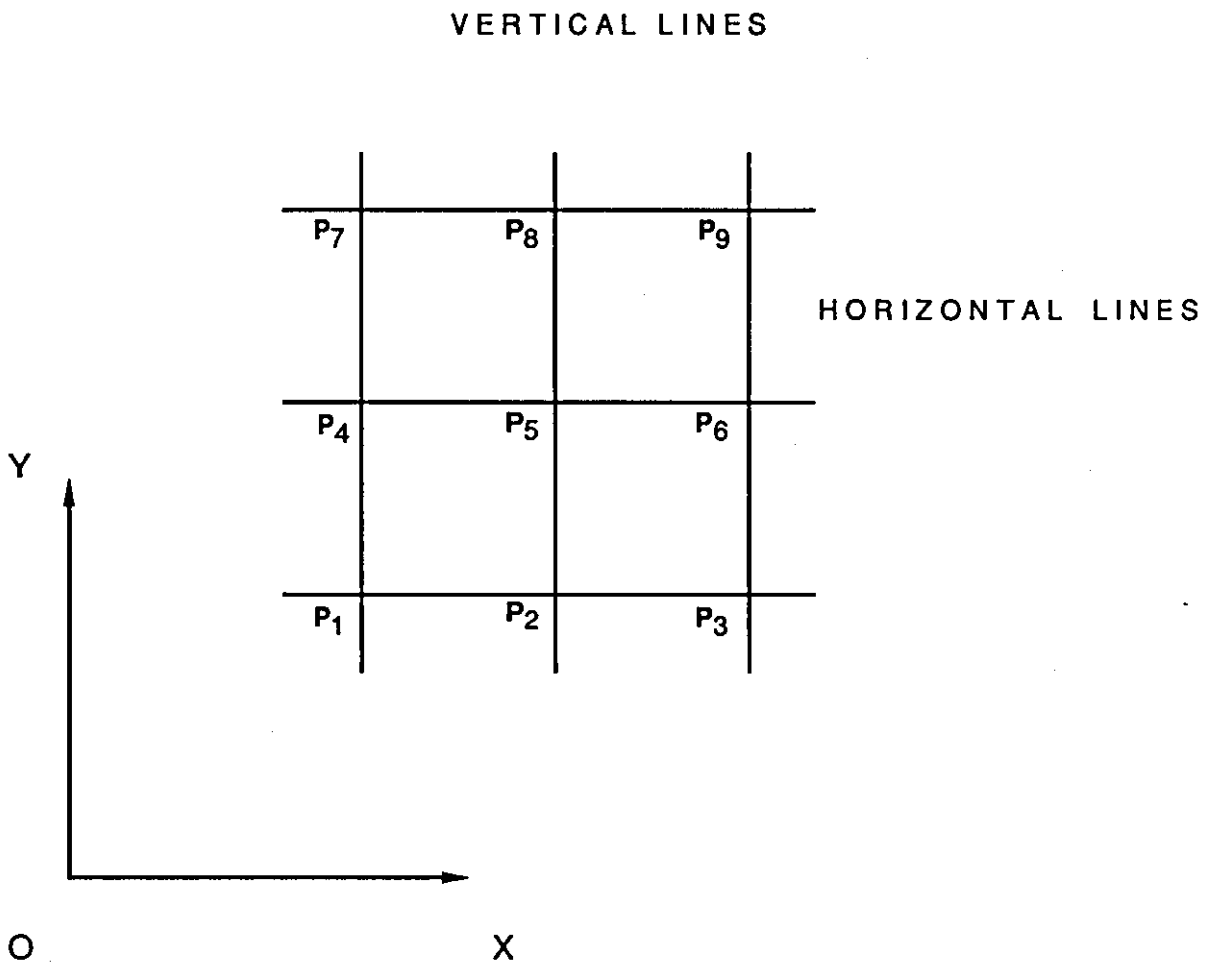

Figure(2.4) : A strain set of points etched upon a blank; the configuration is shown in relation to the horizontal and vertical lines.

If L_{ij} is a horizontal line on the blank then we refer to strain S_{ij} as a horizontal strain. Similarly, if L_{ik} is a vertical then we refer to the average strain S_{ik} as a vertical strain. In general it is not possible to find l_{ij}^* exactly and therefore this arc length must be approximated to estimate the strain.

We can now define a strain state at a point p_i^* , with a horizontal strain S_{ij} and vertical strain S_{ik}. The required strains S_1 and S_2 and their associated tangents t_1 and t_2 can now be defined by :

$$S_1 = S_{ij} \ , \ t_1 = t_{ij}; \ S_2 = S_{ik} \ , \ t_2 = t_{ik}$$

If we consider a strain set the overall number of strains and associated tangent directions to determine the principal strains and directions at points p_i^*, i=1,2,...,9, are : 6 horizontal and 6 vertical strains with 24 associated directions. This means at the centre point p_5^*, and mid-side points p_2^*, p_4^*, p_6^* and p_8^* we have more information than required. In the next section we consider the effect of errors present in the strain data on the calculation of strain states. In the next section we determine the best approach to process extra strain data.

2.3.4) Discussion of errors.

Let the strain state, relative to axes ox and oy, be defined by the numbers ϵ_{xx}, ϵ_{xy} and ϵ_{yy}. We suppose that the estimated strains, ϵ^*_{xx} and ϵ^*_{yy}, have discrepancies e_{xx} and e_{yy} where :

$$\begin{aligned} \epsilon^*_{xx} &= \epsilon_{xx} + e_{xx} \\ \epsilon^*_{yy} &= \epsilon_{yy} + e_{yy} \end{aligned} \qquad (2.4)$$

We consider the effect of errors e_{xx} and e_{yy} on the calculation of strain states. We replace ϵ_{xx} by ϵ^*_{xx} and ϵ_{yy} by ϵ^*_{yy} in equation(2.1) for estimated strains ϵ^*_{xxr}, ϵ^*_{xyr} and ϵ^*_{yyr} where :

$$\epsilon^*_{xxr} = \cos^2(\sigma_r)\epsilon^*_{xx} + \sin(2\sigma_r)\epsilon_{xy} + \sin^2(\sigma_r)\epsilon^*_{yy}$$
$$\epsilon^*_{xyr} = \tfrac{1}{2}\sin(2\sigma_r)(\epsilon^*_{yy} - \epsilon^*_{xx}) + \cos(2\sigma_r)\epsilon_{xy}$$
$$\epsilon^*_{yyr} = \sin^2(\sigma_r)\epsilon^*_{xx} - \sin(2\sigma_r)\epsilon_{xy} + \cos^2(\sigma_r)\epsilon^*_{yy}$$

Substituting relations(2.4) and comparing with (2.1) gives :

$$\epsilon^*_{xxr} = \epsilon_{xxr} + \cos^2(\sigma_r)e_{xx} + \sin^2(\sigma_r)e_{yy}$$
$$\epsilon^*_{xyr} = \epsilon_{xyr} + \tfrac{1}{2}\sin(2\sigma_r)(e_{yy} - e_{xx})$$
$$\epsilon^*_{yyr} = \epsilon_{yyr} + \sin^2(\sigma_r)e_{xx} + \cos^2(\sigma_r)e_{yy}$$

So the discrepancies e_{xxr}, e_{xyr} and e_{yyr} are :

$$e_{xxr} = \cos^2(\sigma_r)e_{xx} + \sin^2(\sigma_r)e_{yy}$$
$$e_{xyr} = \tfrac{1}{2}\sin(2\sigma_r)(e_{yy} - e_{xx})$$
$$e_{yyr} = \sin^2(\sigma_r)e_{xx} + \cos^2(\sigma_r)e_{yy}$$

It follows that :

$$|e_{xxr}| \le \cos^2(\sigma_r)|e_{xx}| + \sin^2(\sigma_r)|e_{yy}|$$
$$|e_{xyr}| \le \tfrac{1}{2}|\sin(2\sigma_r)|(|e_{yy}| + |e_{xx}|) \qquad (2.5)$$
$$|e_{yyr}| \le \sin^2(\sigma_r)|e_{xx}| + \cos^2(\sigma_r)|e_{yy}|$$

Let $e = \max(|e_{xx}|, |e_{yy}|)$ and substitute for $|e_{xx}|, |e_{yy}|$ in equations(2.5) then :

$$|e_{xxr}|, |e_{xyr}|, |e_{yyr}| \le e$$

Hence the errors present in the estimated strain state defined by the numbers ϵ^*_{xxr}, ϵ^*_{xyr} and ϵ^*_{yyr} determined by the estimated strains ϵ^*_{xx} and ϵ^*_{yy} are bounded by the maximum error e. There is no apparent disadvantage in averaging the extra strain data before the principal strains are determined. We now consider the effect of errors e_{xx} and e_{yy} on the estimated principal directions **ox*'** and **oy*'** defined by :

$$\mathbf{ox^{*\prime}} = \mathbf{ox}\cos(\sigma^*_p) + \mathbf{oy}\sin(\sigma^*_p)$$
$$\mathbf{oy^{*\prime}} = -\mathbf{ox}\sin(\sigma^*_p) + \mathbf{oy}\cos(\sigma^*_p),$$

where the estimated principal angle, σ^*_p, is defined by :

$$\tan(2\sigma^*_p) = \frac{2\epsilon_{xy}}{\epsilon^*_{xx} - \epsilon^*_{yy}} \qquad (2.6)$$

Substituting relations(2.4) and rearranging gives :

$$\tan(2\sigma^*_p) = \frac{2\epsilon_{xy}}{\epsilon_{xx} - \epsilon_{yy}} \quad [1 + (e_{xx} - e_{yy})/(\epsilon_{xx} - \epsilon_{yy})]^{-1}$$

From equation(2.6) then :

$$\tan(2\sigma^*_p) = \tan(2\sigma_p)\ [1 + (e_{xx} - e_{yy})/(\epsilon_{xx} - \epsilon_{yy})]^{-1} \qquad (2.7)$$

For $\epsilon_{xx} \approx \epsilon_{yy}$ we can deduce that equation(2.7) is not well defined and the estimated principal directions **ox*'** and **oy*'** do not correspond to the principal directions **ox'** and **oy'**. We conclude that when the estimated strains are almost uniform the principal directions are not stable, when this is not the case the principal directions are well defined.

2.4) Outline of system specification.

This section outlines two system specifications : **system 2.1** and system 2.2.

System 2.1 : Main system

The system specification is illustrated in Figure(2.5). Its purpose is detailed below :

To evaluate and record the principal strains and their directions for digitized or strain points, taken from a drawn panel. Before forming the points are etched on a blank in sets of 3x3 arrays, and after forming each set is located, approximately, on a surface patch. The following information is available :

a) the numerical definition of the drawn panel(The model database).
b) the position of the etched points before forming.
c) the position of the etched points after forming.

System 2.2 : Principal strains

The system specification is illustrated in Figure(2.6). Its purpose is detailed below :

To calculate and record the principal strains and their directions at each strain point within a set of strain points. The following information is available :

a) the set of strain points.
b) the corresponding surface patch.
c) the position of strain points on the blank.

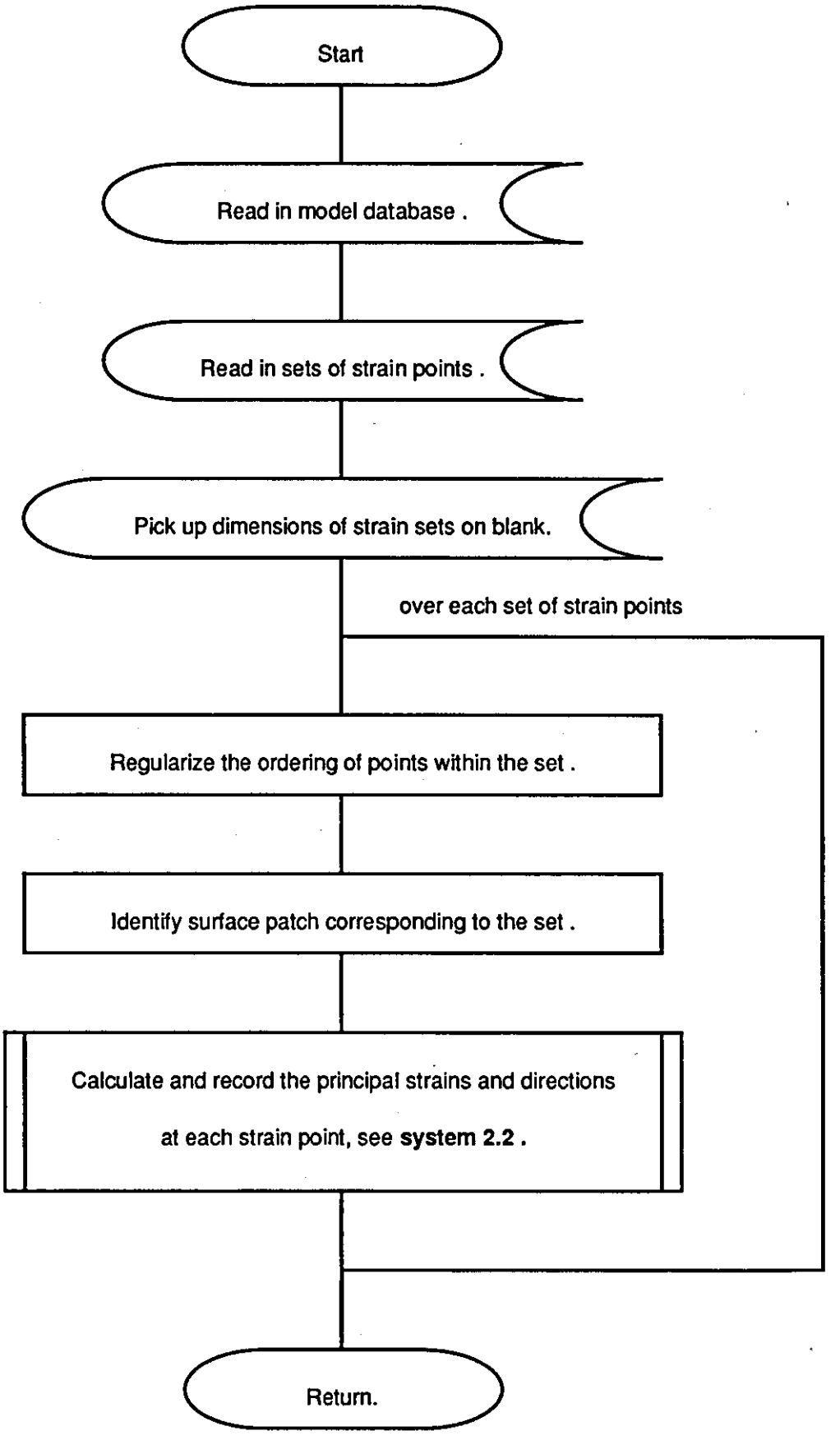

Figure(2.5) : **System 2.1** flowchart for calculation of the principal strains and directions at digitized points .

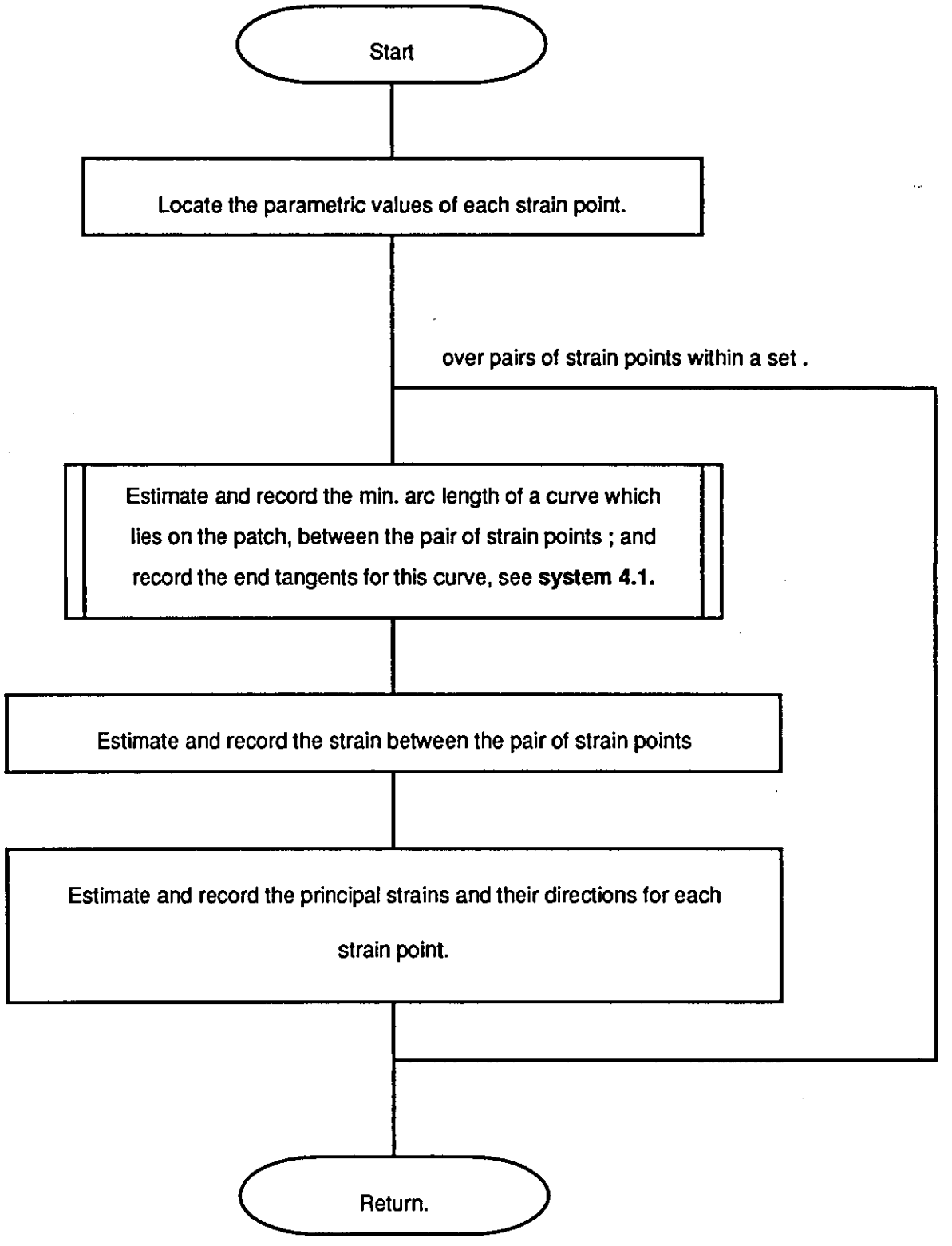

Figure(2.6) : **System 2.2** flowchart to calculate and record the principal strains and directions within a set of strain points.

CHAPTER 3

DIFFERENTIAL GEOMETRY OF CURVES AND SURFACES.

3.1 Introduction.

This chapter presents the background theory of geodesics, which is based on the differential geometry of curves and surfaces.

In section(3.2) we define for curves two invariant quantities : curvature and torsion, which determine its shape. We derive expressions for the curvature and torsion of a parametric cubic (PC) segment, widely used in CAD [Faux et al; 1983], defined in Ferguson form by :

$$r(u) = a_0 + a_1 u + a_2 u^2 + a_3 u^3 \; ; \; 0 \leq u \leq 1 \; ,$$

and we deduce that a twisted PC segment cannot have zero curvature or torsion at any point along the segment. Generalizations of these results for the rational cubic segment are presented in Appendices A and B.

In section(3.3) we define for surfaces two invariant quantities : the first and second fundamental forms, which determine its shape. The normal curvature, and principal curvatures and directions are also defined.

In section(3.4) we review the work on geodesics by Willmore [1972]. The relationships between the first and second fundamental forms of a surface, and the curvature and torsion of a geodesic on this surface, are also established. We emphasize the calculation of geodesic distance to estimate lower bounds for the average strains discussed in Chapter 2.

3.2 Space curves.

In this section we define the curvature and torsion of a space curve and state the governing differential equations, satisfied by space curves. Properties of curvature and torsion for a parametric cubic segment are featured as a by-product of this work with generalizations for the rational cubic segment presented in Appendices A and B.

A space curve is a curve in 3D. It can be defined parametrically as a function of arc length, s, such that :

$\mathbf{r} = \mathbf{r}(x(s),y(s),z(s)) = \mathbf{r}(s) \; ; \; 0 \leq s \leq s_1 \; .$

It can be also be parameterized for some general parameter, u, such that [Faux et al; 1983] :

$\mathbf{r} = \mathbf{r}(x(u),y(u),z(u)) = \mathbf{r}(u) \; ; \; 0 \leq u \leq 1 \; .$

If we assume the curve is regular, the tangent vector $\frac{d\mathbf{r}(u)}{du} = \dot{\mathbf{r}}(u) \neq 0$,

then we can evaluate arc length, s, of this curve $\mathbf{r}(u)$ by :

$$s(t) = \int_0^t |\dot{\mathbf{r}}(u)| \, du \; , \; 0 \leq t \leq 1 \; .$$

3.2.1 Curvature and torsion

The shape of a space curve is determined by two scalar quantities, called curvature and torsion, which can be defined as functions of arc length [Lipschultz; 1969]. However, we cannot determine the position of a curve in space from its curvature and torsion.

Definition of curvature

We suppose that $\mathbf{r} = \mathbf{r}(s)$ is a regular space curve of class at least C^2. Then the tangent vector $\mathbf{t} = \mathbf{t}(s) = \mathbf{r}'(s) = d\mathbf{r}/ds$ is of class C^1, and the curvature k is defined by :

$\mathbf{r}''(s) = k(s)\mathbf{n}(s)$

where $\mathbf{n}(s)$ is the unit principal normal.

Definition of torsion

We suppose that $\mathbf{r} = \mathbf{r}(s)$ is a regular space curve of class at least C^3 along which $\mathbf{n}(s)$, the principal unit normal, is of class C^1. Then the rate of change of the binormal $\mathbf{b}$, where $\mathbf{b} = \mathbf{t} \times \mathbf{n}$, with respect to arc length is :

$\mathbf{b}'(s) = -\tau(s)\mathbf{n}(s)$

where $\tau(s)$ is called the second curvature or torsion of a space curve. The three pairs of vectors $\mathbf{t},\mathbf{n}$; $\mathbf{n},\mathbf{b}$; and $\mathbf{b},\mathbf{t}$ define the : osculating, normal and rectifying planes respectively, as shown in Figure(3.1).

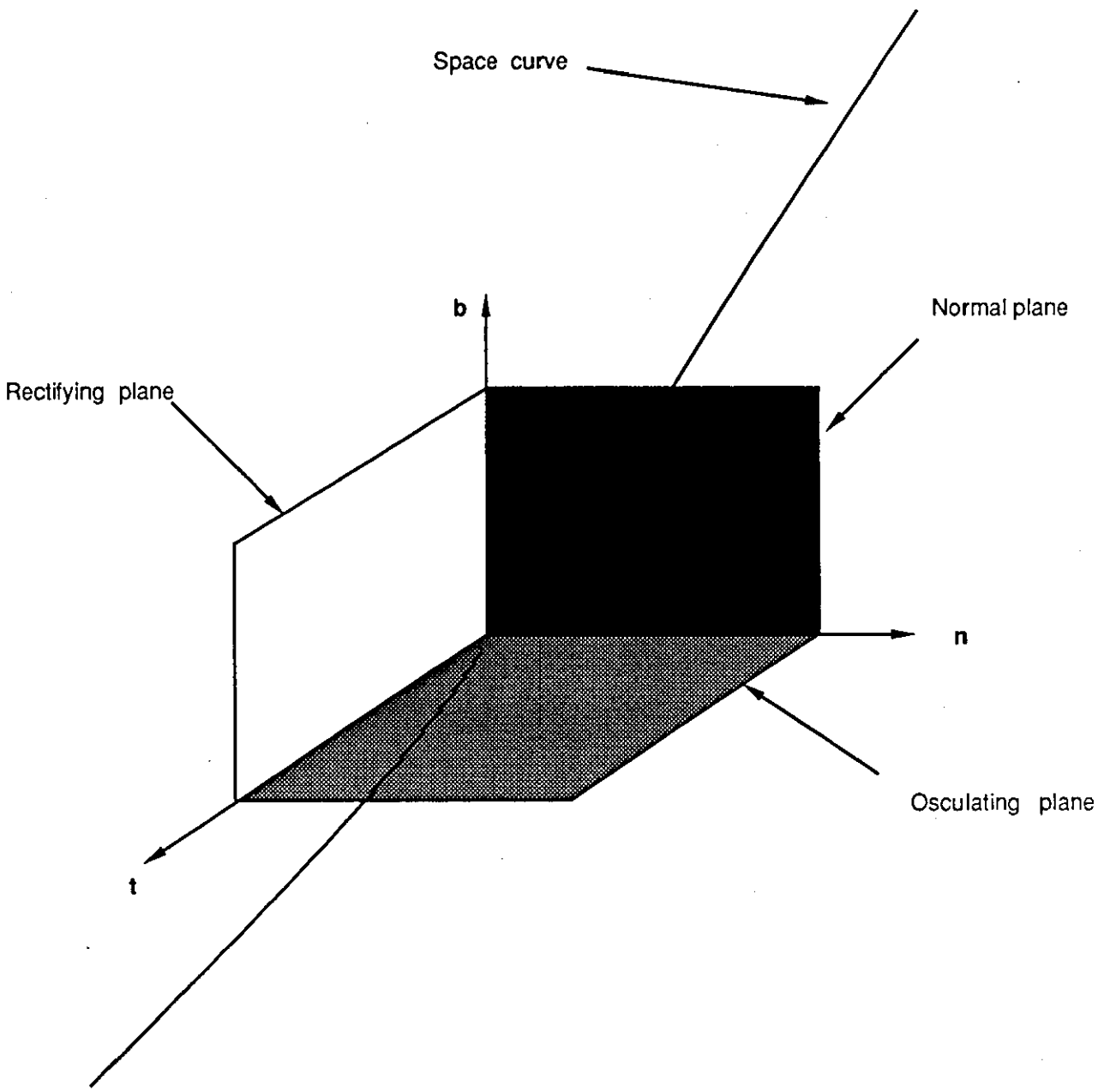

Figure (3.1) : The planes defined by the vectors **t**, **n** and **b**

3.2.2 The Serret-Frenet equations

The principal equations in differential geometry of space curves are called the Serret-Frenet equations and are :-

$$\mathbf{r}'(s) = \mathbf{t}(s) \tag{3.1}$$

$$\mathbf{t}'(s) = k(s)\mathbf{n}(s) \tag{3.2}$$

$$\mathbf{n}'(s) = \tau(s)\mathbf{b}(s) - k(s)\mathbf{t}(s) \tag{3.3}$$

$$\mathbf{b}'(s) = -\tau(s)\mathbf{n}(s) \tag{3.4}$$

When dealing with a curve $\mathbf{r} = \mathbf{r}(u)$ parameterized by an arbitrary parameter, u, not necessarily arc length, it is convenient to work in terms of the following equations :-

$$\mathbf{t}(u) = \frac{\dot{\mathbf{r}}(u)}{|\dot{\mathbf{r}}(u)|} \quad ; \ |\dot{\mathbf{r}}(u)| \neq 0$$

$$k(u)\mathbf{b}(u) = \frac{\dot{\mathbf{r}}(u) \times \ddot{\mathbf{r}}(u)}{|\dot{\mathbf{r}}(u)|^3} \quad ; \ |\dot{\mathbf{r}}(u)| \neq 0 \tag{3.5}$$

$$\tau(u) = \frac{\dot{\mathbf{r}}(u).\ddot{\mathbf{r}}(u) \times \dddot{\mathbf{r}}(u)}{|\dot{\mathbf{r}}(u)|^6 k^2(u)} \quad ; \ |\dot{\mathbf{r}}(u)| \neq 0 \text{ and } k(u) \neq 0$$

$$= \frac{\dot{\mathbf{r}}(u).\ddot{\mathbf{r}}(u) \times \dddot{\mathbf{r}}(u)}{|\dot{\mathbf{r}}(u) \times \ddot{\mathbf{r}}(u)|^2} \quad ; \ |\dot{\mathbf{r}}(u) \times \ddot{\mathbf{r}}(u)| \neq 0 \tag{3.6}$$

3.2.3 The plane curve

A plane curve is characterized by the following theorem [Willmore; 1972].

Theorem 1

Let $\mathbf{r} = \mathbf{r}(s)$, be parameterized with respect to arc length, s, which is a curve of class C^3. Then a necessary and sufficient condition that $\mathbf{r}(s)$ is a plane curve is for the value of its torsion to be zero at all points along the curve.

Proof

This is a necessary condition since the osculating plane of a planar curve is just the plane which contains the curve and is therefore fixed; the binormal is orthogonal to the osculating plane and so must be a constant vector. Conversely, if the torsion is zero at all points then $\mathbf{b}$ must be a constant vector. If we differentiate the expression :

$$(\mathbf{r}.\mathbf{b})' = \mathbf{r}'.\mathbf{b} + \mathbf{r}.\mathbf{b}'$$

Substituting equations(3.1) and (3.4) we obtain

$$(\mathbf{r}.\mathbf{b})' = \mathbf{t}.\mathbf{b} - \mathbf{r}.\tau\mathbf{n} = 0$$

and so $\mathbf{r}.\mathbf{b}$ is a constant and $\mathbf{b}(s) = \mathbf{b}(0)$, say, then the curve $\mathbf{r}(s)$ satisfies the equation for a plane curve i.e.,

$$(\mathbf{r}(s) - \mathbf{r}(0)).\mathbf{b}(0) = 0$$

3.2.4 Curvature property of the parametric cubic segment.

In Theorem 2 we deduce that the curvature of a twisted parametric cubic segment (PC) segment is non-zero at all points along the segment.

Theorem 2

If the curvature of a PC segment is zero at any point, then the segment is a plane curve.

Proof

We recall that the Ferguson PC segment is defined by the following equation

$$\mathbf{r} = \mathbf{r}(u) = \mathbf{a}_0 + \mathbf{a}_1 u + \mathbf{a}_2 u^2 + \mathbf{a}_3 u^3 \qquad (3.7)$$

where, $0 \leq u \leq 1$.

Differentiating equation(3.7) three times we have :

$$\dot{\mathbf{r}}(u) = \mathbf{a}_1 + 2\mathbf{a}_2 u + 3\mathbf{a}_3 u^2 \qquad (3.8)$$

$$\ddot{\mathbf{r}}(u) = 2\mathbf{a}_2 + 6\mathbf{a}_3 u \qquad (3.9)$$

$$\dddot{\mathbf{r}}(u) = 6\mathbf{a}_3 \qquad (3.10)$$

The first two derivatives are used in this section and all three are used in the next section.

We note if $\mathbf{r}(u)$ is not a regular curve i.e. $\dot{\mathbf{r}}(u_0) = 0$, at some point $u = u_0$, then $\mathbf{r}(u)$ is a plane curve.

The curvature k(u) of a space curve is defined in section(3.2.1) and by taking the modulus of equation(3.5) we have :

$$k(u) = \frac{|\dot{\mathbf{r}}(u) \times \ddot{\mathbf{r}}(u)|}{|\dot{\mathbf{r}}(u)|^3} ; \qquad (3.11)$$

We suppose we have a point of zero curvature at $u = u_0$, say, then

$$\dot{\mathbf{r}}(u_0) \times \ddot{\mathbf{r}}(u_0) = \mathbf{0} \qquad (3.12)$$

Substituting equations (3.8) and (3.9) into the numerator of (3.11) then :

$$\begin{aligned} \dot{\mathbf{r}}(u) \times \ddot{\mathbf{r}}(u) &= [\mathbf{a}_1 + 2\mathbf{a}_2 u + 3\mathbf{a}_3 u^2] \times [2\mathbf{a}_2 + 6\mathbf{a}_3 u] \\ &= 2\mathbf{f}_1 + 6\mathbf{f}_2 u + 6\mathbf{f}_3 u^2, \end{aligned} \qquad (3.13)$$

where $\mathbf{f}_1 = \mathbf{a}_1 \times \mathbf{a}_2$, $\mathbf{f}_2 = \mathbf{a}_1 \times \mathbf{a}_3$ and $\mathbf{f}_3 = \mathbf{a}_2 \times \mathbf{a}_3$.

Therefore for zero curvature at $u = u_0$ we have, $2\mathbf{f}_1 + 6\mathbf{f}_2 u_0 + 6\mathbf{f}_3 u_0^2 = 0$.

It follows that $\mathbf{f}_1, \mathbf{f}_2$ and $\mathbf{f}_3$ must be coplanar i.e., $\mathbf{f}_1 . \mathbf{f}_2 \times \mathbf{f}_3 = 0$

$$\begin{aligned} \mathbf{f}_1 . \mathbf{f}_2 \times \mathbf{f}_3 &= (\mathbf{a}_1 \times \mathbf{a}_2) . (\mathbf{a}_1 \times \mathbf{a}_3) \times (\mathbf{a}_2 \times \mathbf{a}_3) \\ &= (\mathbf{a}_1 \times \mathbf{a}_2) . (\mathbf{a}_1 . \mathbf{a}_2 \times \mathbf{a}_3) \mathbf{a}_3 = (\mathbf{a}_1 . \mathbf{a}_2 \times \mathbf{a}_3)^2 = 0 \end{aligned}$$

Consequently the vectors $\mathbf{a}_1, \mathbf{a}_2$ and $\mathbf{a}_3$ are coplanar, and it follows r(u) must be a plane curve. Conversely, if the PC segment is a twisted curve then it cannot have zero curvature at any point along the segment. In Appendix A we prove that this property is also exhibited by the rational cubic segment.

3.2.5 Torsion property of the parametric cubic segment.

In theorem 3 we deduce that the torsion of a twisted parametric cubic segment (PC) segment is non-zero at all points along the segment.

Theorem 3

If the curvature for the PC segment is non-zero throughout the segment and if its torsion is zero at any point, then the segment is a plane curve.

Proof

The torsion of a space curve is defined in section(3.2.1) by equation(3.6) and is :

$$\tau(u) = \frac{\dot{\mathbf{r}}(u).\ddot{\mathbf{r}}(u) \times \dddot{\mathbf{r}}(u)}{|\dot{\mathbf{r}}(u) \times \ddot{\mathbf{r}}(u)|^2} \; ; \; |\dot{\mathbf{r}}(u) \times \ddot{\mathbf{r}}(u)| \neq 0 \qquad (3.14)$$

We suppose we have a point of zero torsion at $u = u_0$, say, then

$$\dot{\mathbf{r}}(u_0).\ddot{\mathbf{r}}(u_0) \times \dddot{\mathbf{r}}(u_0) = 0$$

Now,

$$\dot{\mathbf{r}}(u).[\ \ddot{\mathbf{r}}(u) \times \dddot{\mathbf{r}}(u)\ ] = [\ \dot{\mathbf{r}}(u) \times \ddot{\mathbf{r}}(u)\ ] \cdot \dddot{\mathbf{r}}(u)$$

Substituting equations(3.13) and (3.10) then :

$$= [2f_1 + 6f_2u + 6f_3u^2]. 6a_3$$

$$= 12a_1.a_2 \times a_3 \qquad (3.15)$$

and so by substituting equation(3.15) into (3.14) we have :

$$\tau(u) = \frac{12a_1.a_2 \times a_3}{|\dot{\mathbf{r}}(u) \times \ddot{\mathbf{r}}(u)|^2} \qquad (3.16)$$

Consequently, if the torsion has zero value at some point $\mathbf{r}(u_0)$, say, then the numerator of equation(3.16) must be zero. Hence the vectors $\mathbf{a}_1, \mathbf{a}_2$ and $\mathbf{a}_3$ are coplanar, giving the result :

$$\tau(u) \equiv 0 \qquad \forall\, u \in [0,1] \qquad (3.17)$$

Thus proving the property that if the torsion of a Ferguson PC segment is zero, at any point along the curve and has non-zero curvature, then it is a plane curve, since equation(3.17) is a necessary and sufficient condition for $\mathbf{r} = \mathbf{r}(u)$ to be a plane curve, see section(3.2.3). Conversely, if the PC segment is a twisted curve then it cannot have zero torsion at any point along the segment and its value is constant in sign. In Appendix B we prove that this property is also exhibited by the rational cubic segment.

In the next section we show that higher order polynomial space curves can be constructed which do not satisfy this torsion property.

3.2.6 Higher order polynomial space curves

In this section we construct a twisted quartic polynomial space curve which has zero torsion at one point only. Consider the quartic space curve $\mathbf{r} = \mathbf{r}(u)$ defined by :

$$\mathbf{r}(u) = \mathbf{a}_0 + \mathbf{a}_1 u + \mathbf{a}_2 u^2 + \mathbf{a}_3 u^4 \tag{3.18}$$

Differentiating equation(3.18) three times we obtain :

$$\dot{\mathbf{r}}(u) = \mathbf{a}_1 + 2\mathbf{a}_2 u + 4\mathbf{a}_3 u^3 \tag{3.19}$$

$$\ddot{\mathbf{r}}(u) = 2\mathbf{a}_2 + 12\mathbf{a}_3 u^2 \tag{3.20}$$

$$\dddot{\mathbf{r}}(u) = 24\mathbf{a}_3 u \tag{3.21}$$

We recall the torsion of a space curve is defined by (3.6) :

$$\tau(u) = \frac{\dot{\mathbf{r}}(u).\ddot{\mathbf{r}}(u) \times \dddot{\mathbf{r}}(u)}{|\dot{\mathbf{r}}(u) \times \ddot{\mathbf{r}}(u)|^2} \; ; \; |\dot{\mathbf{r}}(u) \times \ddot{\mathbf{r}}(u)| \neq 0 \tag{3.22}$$

Substituting equations(3.19)-(3.21) into the numerator of (3.22) then :

$$\dot{\mathbf{r}}(u).\ddot{\mathbf{r}}(u) \times \dddot{\mathbf{r}}(u) = [\mathbf{a}_1 + 2\mathbf{a}_2 u + 4\mathbf{a}_3 u^3].[(2\mathbf{a}_2 + 12\mathbf{a}_3 u^2) \times 24\mathbf{a}_3 u]$$

$$= 48\mathbf{a}_1.\mathbf{a}_2 \times \mathbf{a}_3 u \tag{3.23}$$

We also require that,

$$\dot{\mathbf{r}}(u) \times \ddot{\mathbf{r}}(u) \neq 0 \tag{3.24}$$

Therefore we consider that,

$$\dot{\mathbf{r}}(u) \times \ddot{\mathbf{r}}(u) = 0 \tag{3.25}$$

then from (3.25) there exists non-zero scalars α, β such that ,

$$\alpha \dot{\mathbf{r}}(u) + \beta \ddot{\mathbf{r}}(u) = 0$$

i.e. $\alpha \mathbf{a}_1 + 2(\alpha u + \beta)\mathbf{a}_2 + 4u^2(\alpha u + 3\beta)\mathbf{a}_3 = 0$

So $a_1.a_2$ and a_3 must be coplanar. Hence for equation(3.24) to hold we want : $a_1.a_2 \times a_3 \neq 0$. With this assumption :

$$|\dot{r}(u) \times \ddot{r}(u)|^2 = C^2(u) \; ; \; C(u) \neq 0 \tag{3.26}$$

Hence using equation(3.23) and (3.26) :

$$\tau(u) = \frac{48 a_1.a_2 \times a_3 u}{C^2(u)} \tag{3.27}$$

Therefore from equation(3.27) we can deduce that the value of torsion is zero at $u = 0$ and is non-zero at every other point.

3.3 Surfaces.

We consider a surface patch, S, represented by a parametric equation : $\mathbf{r} = \mathbf{r}(x,y,z) = \mathbf{r}(x(u,v),y(u,v),z(u,v)) = \mathbf{r}(u,v)$, $0 \le u,v \le 1$. We assume that the parameter curves, where u or v equals a constant, satisfy,

$$\frac{\delta \mathbf{r}(u,v)}{\delta u} \neq 0, \quad \frac{\delta \mathbf{r}(u,v)}{\delta v} \neq 0, \quad 0 \le u,v \le 1$$

$$\mathbf{H} = \frac{\delta \mathbf{r}(u,v)}{\delta u} \times \frac{\delta \mathbf{r}(u,v)}{\delta v}, \quad \text{and } H = |\mathbf{H}| \neq 0, \quad 0 \le u,v \le 1.$$

Consequently, we define the unit surface normal

$\hat{\mathbf{N}}(u,v) = \dfrac{\mathbf{H}}{H}$, $0 \le u,v \le 1$. The vectors $\dfrac{\delta \mathbf{r}(u,v)}{\delta u}$, $\dfrac{\delta \mathbf{r}(u,v)}{\delta v}$ and $\hat{\mathbf{N}}$ form a right handed system, which is illustrated in Figure(3.2).

3.3.1 The first and second fundamental forms.

In section(3.2) we stated that the shape of a space curve can be determined by two functions of arc length, curvature and torsion. Similarly, the shape of a surface is determined by two local properties which are the first and second fundamental forms, [Lipschultz; 1969].

Definition of the first fundamental form

The first fundamental form I(u,v), which is interpreted physically by the squared element of arc length, ds^2, and is defined by :

$$I(u,v) = ds^2 = d\mathbf{r}(u,v).d\mathbf{r}(u,v)$$

$$= \left[\frac{\delta \mathbf{r}(u,v)}{\delta u} du + \frac{\delta \mathbf{r}(u,v)}{\delta v} dv \right] . \left[\frac{\delta \mathbf{r}(u,v)}{\delta u} du + \frac{\delta \mathbf{r}(u,v)}{\delta v} dv \right]$$

$$= E(u,v)du^2 + 2F(u,v)dudv + G(u,v)dv^2$$

where,

$$E(u,v) = \frac{\delta \mathbf{r}(u,v)}{\delta u} . \frac{\delta \mathbf{r}(u,v)}{\delta u}, \quad F(u,v) = \frac{\delta \mathbf{r}(u,v)}{\delta u} . \frac{\delta \mathbf{r}(u,v)}{\delta v}, \quad G(u,v) = \frac{\delta \mathbf{r}(u,v)}{\delta v} . \frac{\delta \mathbf{r}(u,v)}{\delta v}$$

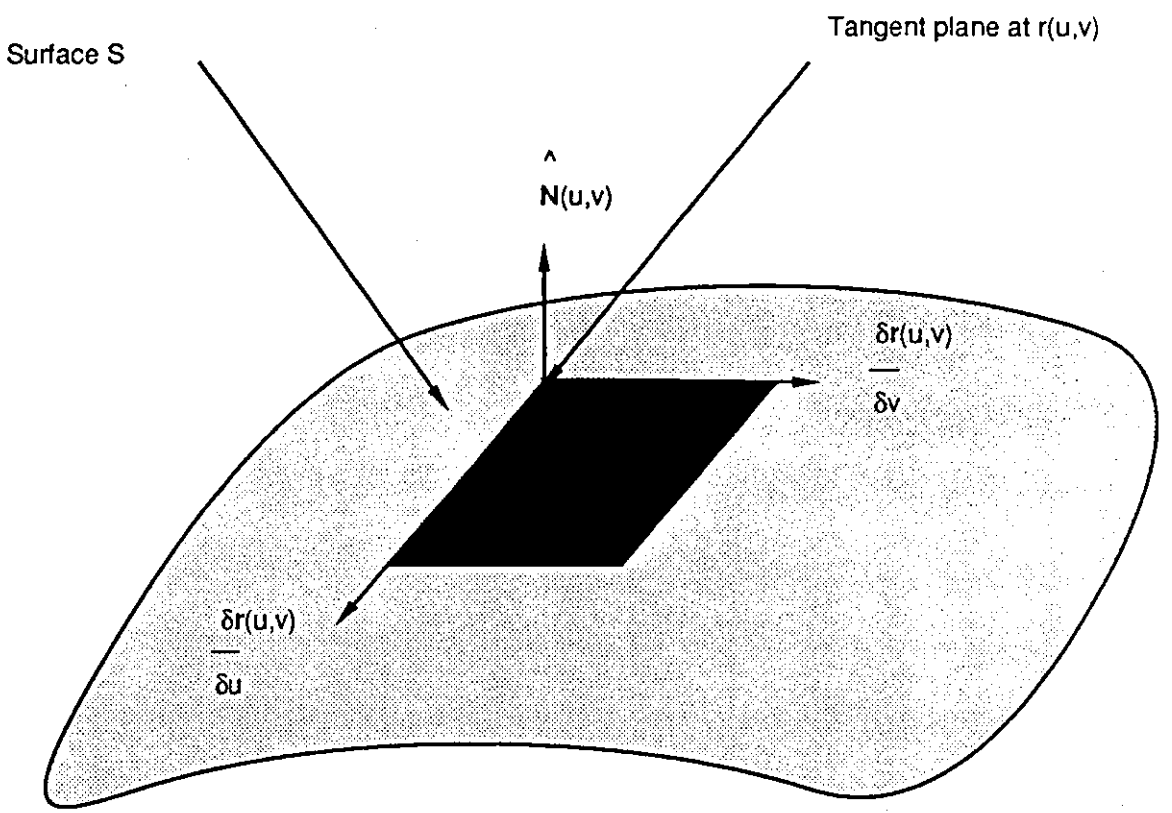

Figure (3.2) : The tangent plane defined at the point r(u,v)

The numbers E,F and G are referred to as the first fundamental coefficients.

The first fundamental form has the following properties :

a) it is independent of parameterization.

b) it is positive definite.

Definition of the second fundamental form.

The second fundamental form II(u,v), which is interpreted physically as the projection of the chord vector, the line joining two neighbouring parametric points on S, onto the unit surface normal, doubled,[Lipschultz; 1969], and is defined by :

$$\begin{aligned} II(u,v) &= -\, dr(u,v).d\hat{N}(u,v) \\ &= -\left[\frac{\delta r(u,v)}{\delta u}\,du + \frac{\delta r(u,v)}{\delta v}\,dv\right].\left[\frac{\delta \hat{N}(u,v)}{\delta u}\,du + \frac{\delta \hat{N}(u,v)}{\delta v}\,dv\right] \\ &= L(u,v)du^2 + 2M(u,v)dudv + N(u,v)dv^2 \end{aligned}$$

where,

$$L(u,v) = -\frac{\delta r(u,v)}{\delta u}.\frac{\delta \hat{N}(u,v)}{\delta u},$$

$$M(u,v) = -\tfrac{1}{2}\left[\frac{\delta r(u,v)}{\delta u}.\frac{\delta \hat{N}(u,v)}{\delta v} + \frac{\delta r(u,v)}{\delta v}.\frac{\delta \hat{N}(u,v)}{\delta u}\right],$$

$$N(u,v) = -\frac{\delta r(u,v)}{\delta v}.\frac{\delta \hat{N}(u,v)}{\delta v},$$

The numbers L,M, and N are referred to as the second fundamental coefficients.

The second fundamental form has the following properties :

a) it is independent of parameterization.

b) it can also be written $d^2r(u,v).\hat{N}(u,v)$.

3.3.2 Curves on surfaces.

Let $\mathbf{r} = \mathbf{r}(u,v)$, $0 \le u,v \le 1$, be a surface patch of class C^{n1}. Let $u = u(t)$, $v = v(t)$, $0 \le t \le 1$ be the curvilinear coordinates of a curve class C^{n2}. Then $\mathbf{r} = \mathbf{r}(u(t),v(t))$, $0 \le t \le 1$, is a curve on the surface of class C^{n3}, where $n3 = \min(n1,n2)$. The tangent vector at a parametric point P(u,v), on the surface patch is defined by :

$$\frac{d\mathbf{r}}{dt} = \frac{\delta \mathbf{r}}{\delta u}\frac{du}{dt} + \frac{\delta \mathbf{r}}{\delta v}\frac{dv}{dt}$$

which lies in the tangent plane at P.

3.3.3 Normal curvature.

Definition of normal curvature

Let $\mathbf{r}(u(s),v(s))$, $0 \le s \le s_1$, be a regular curve parameterized with respect to arc length s, of class C^2, on the surface patch S, and passing through point P. The normal curvature at P is :

$$K_n(u(s),v(s)) = \frac{d^2\mathbf{r}(s)}{ds^2} \cdot \hat{N}(s)$$

In terms of the second fundamental coefficients this can be expressed as :

$$K_n = L\left[\frac{du}{ds}\right]^2 + 2M\left[\frac{du}{ds}\frac{dv}{ds}\right] + N\left[\frac{dv}{ds}\right]^2$$

The normal curvature is independent of parameterization.

3.3.4 Principal curvatures and directions.

In general the normal curvature varies with the tangent direction at P. The principal curvatures and directions at P on the surface patch correspond to the minimum and maximum values of normal curvature with their associated tangent directions.

The normal curvature at P is :

$$K_n = L\left[\frac{du}{ds}\right]^2 + 2M\left[\frac{du}{ds}\frac{dv}{ds}\right] + N\left[\frac{dv}{ds}\right]^2 .$$

The tangent direction at P depends on the values of $\frac{du}{ds}$, $\frac{dv}{ds}$

which are subject to the constraint equation $\mathbf{r}'(s).\mathbf{r}'(s) = 1$, i.e. :

$$E\left[\frac{du}{ds}\right]^2 + 2F\left[\frac{du}{ds}\frac{dv}{ds}\right] + G\left[\frac{dv}{ds}\right]^2 = 1$$

The principal curvatures K_a, K_b are defined by the roots of the quadratic [Willmore; 1972] :

$$K^2(EG - F^2) - K(EN - 2FM + GL) + LN - M^2 = 0$$

The principal directions corresponding to the principal curvatures are obtained from the equation :

$$(EM - FL)\left[\frac{du}{ds}\right]^2 + (EN - GL)\left[\frac{du}{ds}\frac{dv}{ds}\right] + (FN - GM)\left[\frac{dv}{ds}\right]^2 = 0 \qquad (3.28)$$

If the coefficients of equation(3.28) are all zero the normal curvature is the same in all directions and the principal directions are not well defined. Otherwise the discriminant of equation(3.28) is positive definite and the roots of this equation are real and distinct, and the principal directions must be orthogonal.

3.3.5 Lines of curvature.

Definition of lines of curvature

If the tangent vector of a curve on a surface patch is parallel to a principal direction at each point along the curve, then the curve is a line of curvature.

3.4 Geodesics.

This section reviews the work on geodesics by Willmore [1972]. He regards the problem of finding the shortest distance between two points **a**,**b** on a surface S, as identifying curves of stationary distance rather than of shortest length. We present the definition of a stationary curve and from this a necessary and sufficient condition, derived by Willmore, for a curve on a surface to be a geodesic.

We also present expressions for the curvature and torsion of a geodesic curve in terms of the coefficients of the first and second fundamental forms and note their similarity with the equations associated with principal curvatures and directions at a parametric point (u,v).

3.4.1 Definition of a stationary curve.

Let **a**,**b** be two points on a surface S of class C^2. We consider the curves, **r**(t), which join **a** and **b** with curvilinear coordinates of the form $u = U(t)$, $v = V(t)$, and are continuous functions of class C^2.

Every curve **r**(t), $0 \le t \le 1$, has arc length l :

$$l = \int_0^1 f(u,v,\dot{u},\dot{v})\, dt \quad \text{where,}$$

$$f(u,v,\dot{u},\dot{v}) = |\dot{\mathbf{r}}| = \left[E\left[\frac{du}{dt}\right]^2 + 2F\left[\frac{du}{dt}\frac{dv}{dt}\right] + G\left[\frac{dv}{dt}\right]^2 \right]^{\frac{1}{2}}$$

We deform $\mathbf{r}(t)$, keeping the end points fixed, such that the new curve $R(t)$ has curvilinear coordinates $U'(t)$, $V'(t)$ defined by :

$$U'(t) = U(t) + \epsilon\,\alpha(t)$$
$$V'(t) = V(t) + \epsilon\,\beta(t)$$

where $\alpha(t),\beta(t)$ are arbitrary functions of class C^2 and also satisfy :
$\alpha(0) = 0 = \beta(0)$; $\alpha(1) = 0 = \beta(1)$

The variation in arc length $\delta l(\epsilon)$, is derived by Willmore [1972] as :

$$\delta l(\epsilon) = \int_0^1 [f(U(t,\epsilon),V(t,\epsilon),\dot{U}(t,\epsilon),\dot{V}(t,\epsilon) - f(U(t),V(t),\dot{U}(t),\dot{V}(t)]\,dt$$

By a Taylor expansion of first order in ϵ and integrating by parts the coefficients of $\dot{\alpha}(t),\dot{\beta}(t)$ gives :

$$\delta l(\epsilon) = \epsilon\int_0^1 [\alpha(t)A(U(t),V(t),\dot{U}(t),\dot{V}(t)) - \beta(t)B(U(t),V(t),\dot{U}(t),\dot{V}(t))]dt + o(\epsilon^2)$$

where,

$$A = \frac{\delta f}{\delta u} - \frac{d}{dt}\left[\frac{\delta f}{\delta \dot{u}}\right],\quad B = \frac{\delta f}{\delta v} - \frac{d}{dt}\left[\frac{\delta f}{\delta \dot{v}}\right]$$

For a variation of second order in ϵ we must have :

$$\int_0^1 [\alpha(t)A(u(t),v(t),\dot{u}(t),\dot{v}(t)) - \beta(t)B(u(t),v(t),\dot{u}(t),\dot{v}(t))]dt = 0 \qquad (3.29)$$

for all admissible functions $\alpha(t)$, $\beta(t)$.

We recall the Euler-Lagrange Lemma [Willmore; 1972] : if $g(t)$ is a continuous function over the open interval $(0,1)$ and satisfies :

$$\int_0^1 v(t)g(t)\,dt = 0$$

for all admissible function $v(t)$ with $v(0) = 0$ and $v(1) = 0$.

Then $g(t) \equiv 0 \ \forall\, t \in (0,1)$. (3.30)

By choosing, $\alpha(t) \neq 0 \ \forall\, t \in (0,1)$ and $\beta(t) \equiv 0, \ \forall\, t \in [0,1]$, we deduce from (3.29) and (3.30), with $v(t) = \alpha(t)$, $g(t) = A(t)$, that :

$A(t) \equiv 0 \ \forall\, t \in (0,1)$ and similarly $B(t) \equiv 0 \ \forall\, t \in (0,1)$ (3.31)

Hence the curvilinear coordinates $u(t), v(t)$, $0 \leq t \leq 1$, of a geodesic must satisfy the differential equations in equations(3.31) at all points on the curve.

3.4.2 The normal property of geodesics.

Willmore [1972] derives a necessary and sufficient condition for a curve on a surface to be a geodesic or stationary curve, by first substituting into equations(3.31), $f(u,v,\dot{u},\dot{v}) = (2T(u,v,\dot{u},\dot{v}))^{\frac{1}{2}}$, where $T = \frac{1}{2}\left|\dot{r}(t)\right|^2$ to give :

$$X(t) = \frac{d}{dt}\left[\frac{\delta T}{\delta \dot{u}}\right] - \frac{\delta T}{\delta u} = \frac{1}{2T}\frac{dT}{dt}\frac{\delta T}{\delta \dot{u}}$$

$$Y(t) = \frac{d}{dt}\left[\frac{\delta T}{\delta \dot{v}}\right] - \frac{\delta T}{\delta v} = \frac{1}{2T}\frac{dT}{dt}\frac{\delta T}{\delta \dot{v}}$$

Then eliminating $\dfrac{dT}{dt}$ gives :

$$X(t)\frac{\delta T}{\delta \dot{v}} - Y(t)\frac{\delta T}{\delta \dot{u}} \equiv 0 \ , \ \forall\, t \in (0,1)$$

From this equation Willmore deduces the unit principal normal at every point along a geodesic curve must be normal to the surface.

In the next two sections we highlight the relationship of curvature and torsion of a geodesic in terms of the first and second fundamental coefficients of a surface.

3.4.3 Curvature of a geodesic.

In this section we remark on the expression for the curvature k_G of a geodesic. We assume the geodesic curve $\mathbf{r}(u(s),v(s))$ is of class at least C^2. Then we have from equation(3.2) in section(3.2.2) :

$$\frac{d^2\mathbf{r}(s)}{ds^2} = k_G(s)\ \mathbf{n}(s)$$

If a geodesic is parameterized with respect to arc length and the principal normal $\mathbf{n}(s)$ is parallel to the unit surface normal $\hat{\mathbf{N}}(s)$, then

$$k_G(s) = \frac{d^2\mathbf{r}(s)}{ds^2} \cdot \hat{\mathbf{N}}(s)$$

Comparing this expression with definition of normal curvature, see section(3.3.3), it follows that :

$$k_G(s) = K_n = L\left[\frac{du}{ds}\right]^2 + 2M\left[\frac{du}{ds}\frac{dv}{ds}\right] + N\left[\frac{dv}{ds}\right]^2,$$

The curvature of a geodesic has extreme values which must correspond to the principal curvatures and directions at a parametric point (u,v).

3.4.4 Torsion of a geodesic.

In this section we state an expression for the torsion τ_G of a geodesic curve derived by Weatherburn [1927]. We assume the geodesic curve $\mathbf{r}(u(s),v(s))$ is of class at least C^2 and is parameterized with respect to arc length. We recall from section(3.2.1) the unit binormal, $\mathbf{b}(s)$, is defined by :

$$\mathbf{b}(s) = \frac{d\mathbf{r}(s)}{ds} \times \mathbf{n}(s) \tag{3.32}$$

Substituting equation(3.32) into (3.4) it follows that :

$$\hat{\mathbf{N}}(s).\mathbf{n}(s)\tau_G(s) = \hat{\mathbf{N}}(s) \cdot \frac{d\mathbf{n}(s)}{ds} \times \frac{d\mathbf{r}(s)}{ds}$$

$$\text{But } \mathbf{n}(s) = \hat{\mathbf{N}}(s), \text{ so } \tau_G(s) = \hat{\mathbf{N}}(s) \cdot \frac{d\hat{\mathbf{N}}(s)}{ds} \times \frac{d\mathbf{r}(s)}{ds} \tag{3.33}$$

Now we can write,

$$\frac{d\hat{\mathbf{N}}}{ds} = \frac{\delta\hat{\mathbf{N}}}{\delta u}\frac{du}{ds} + \frac{\delta\hat{\mathbf{N}}}{\delta v}\frac{dv}{ds} \quad \text{and} \quad \frac{d\mathbf{r}}{ds} = \frac{\delta\mathbf{r}}{\delta u}\frac{du}{ds} + \frac{\delta\mathbf{r}}{\delta v}\frac{dv}{ds},$$

Substituting these expressions into equation(3.33) we can deduce the torsion in terms of the first and second fundamental coefficients :

$$\tau_G(s) = \frac{1}{H}\left[(EM - FL)\left[\frac{du}{ds}\right]^2 + (EN - GL)\left[\frac{du}{ds}\frac{dv}{ds}\right] + (FN - GM)\left[\frac{dv}{ds}\right]^2 \right]$$

Comparing this expression with equation(3.28), we can deduce immediately that if the tangent to a geodesic is parallel to a principal direction we must have zero torsion. Further, if a line of curvature is also a geodesic curve then its torsion must be identically zero; since by definition its tangent is parallel to a principal direction at all points along the curve. Therefore this geodesic must be a plane curve, since this is a necessary and sufficient condition for a curve to be planar, (see section(3.2.3)).

CHAPTER 4

THE SHORTEST PLANAR PATH ALGORITHM.

In this chapter we present a naïve algorithm, the radial plane subdivision method, for the evaluation of the shortest planar path between two points p^a and p^b on a surface patch P. The surface patch P is represented by a parametric equation :

$$p = p(u,v) \ , \ 0 \le u,v \le 1 \tag{4.1}$$

We assume that the parametric curves, where u or v equals a constant, are at least class C^1 regular curves i.e.,

$$\frac{\delta p(u,v)}{\delta u} \neq 0 \text{ and } \frac{\delta p(u,v)}{\delta v} \neq 0; \ 0 \le u,v \le 1.$$

In addition we have,

$$H = \frac{\delta p(u,v)}{\delta u} \times \frac{\delta p(u,v)}{\delta v} \ , \ H = |H| \neq 0 \ , \ 0 \le u,v \le 1$$

Now we can define the surface normal $\hat{N}(u,v) = \frac{H}{|H|}$.

In section(4.1) we construct a surface Q, a portion of P, defined by a family of planar intersects between the points $\mathbf{p}^a$ and $\mathbf{p}^b$, and we want to find the curve with minimum arc length. We present the background mathematics for the construction of Q and highlight the underlying geometric assumptions necessary for its definition.

In section(4.2) we outline a system specification for the radial plane subdivision method. The evaluation of arc length in the algorithm is based on the faceting or lattice technique [Geisow and Pratt; 1986] and processing of facet/plane intersections is described. In section(4.3) we examine the choice of mesh parameters with bonnet and roof information.

4.1 Shortest planar path.

In section(4.1.1) we are concerned with the construction of Q. The parametrization of Q is described and in section(4.1.2) the geometric significance of the chosen parametrization is discussed. In section(4.1.3) we derive a stationary condition which the shortest planar path must satisfy.

4.1.1) Construction of surface Q

We construct a surface Q, which is a portion of P, and is defined parametrically by :

$$\mathbf{q} = \mathbf{q}(u^*,v^*) \ , \ 0 \le u^*,v^* \le 1 \ . \qquad (4.2)$$

The parametric curves, defined by constant v^*, are planar and lie between the points $\mathbf{p}^a$ and $\mathbf{p}^b$, on P, such that :
$\mathbf{q}(0,v^*) = \mathbf{p}^a$ and $\mathbf{q}(1,v^*) = \mathbf{p}^b$, $v^* \in [0,1]$.

The parametric curve, defined by constant u^*, lies in a plane with normal parallel to the chord vector $\mathbf{N}^{ba} = \mathbf{p}^b - \mathbf{p}^a$, and contains a point $\mathbf{c}(u^*)$, $u^* \in [0,1]$, on the line L^{ab} between the points $\mathbf{p}^a$ and $\mathbf{p}^b$, and $\mathbf{c}(u^*) = (1 - u^*)\mathbf{p}^a + u^* \mathbf{p}^b$, $u^* \in [0,1]$.

Let $\hat{N}_r(v^*)$ be the normal to the plane X^{v^*}, which contains the planar intersect $\mathbf{q}(u^*,v^*)$, $0 \leq u^* \leq 1$, $v^* \in [0,1]$ and is defined by,

$$\hat{N}_r(v^*) = (\sin(\theta^* - \phi^*)\, \hat{N}_r(0) + \sin(\phi^*)\hat{N}_r(1))/\sin(\theta^*)$$

where,

$v^* = \phi^*/\theta^*$, $\phi^* \in [0,\theta^*]$, $\theta^* = \cos^{-1}(\hat{N}_r(0).\hat{N}_r(1))$, $\theta^* \in (0,\pi)$ and the bounding planes X^0 and X^1, have continuous planar intersects $\mathbf{q}(u^*,0)$ and $\mathbf{q}(u^*,1)$, $0 \leq u^* \leq 1$, respectively. We refer to the family of planes X^{v^*}, $\forall$ $v^* \in [0,1]$ as radial planes. This configuration is illustrated in Figure(4.1).

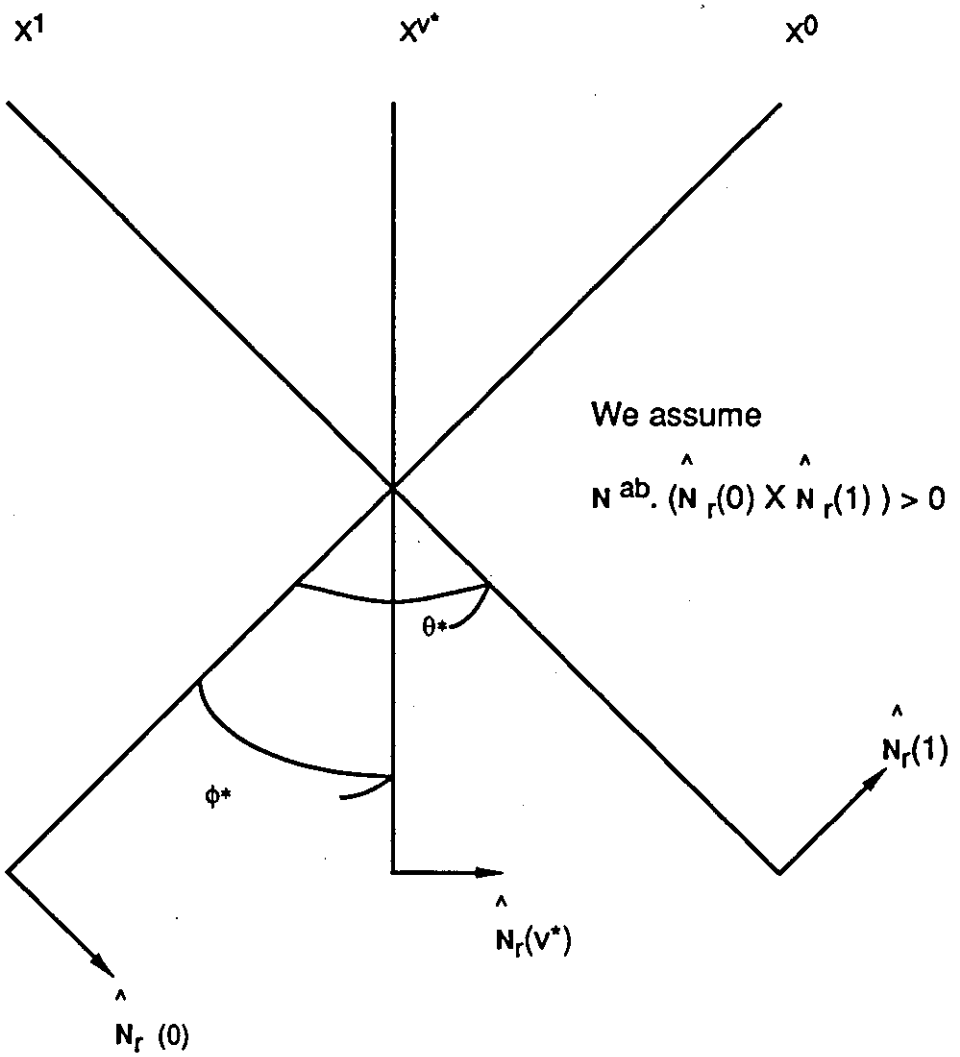

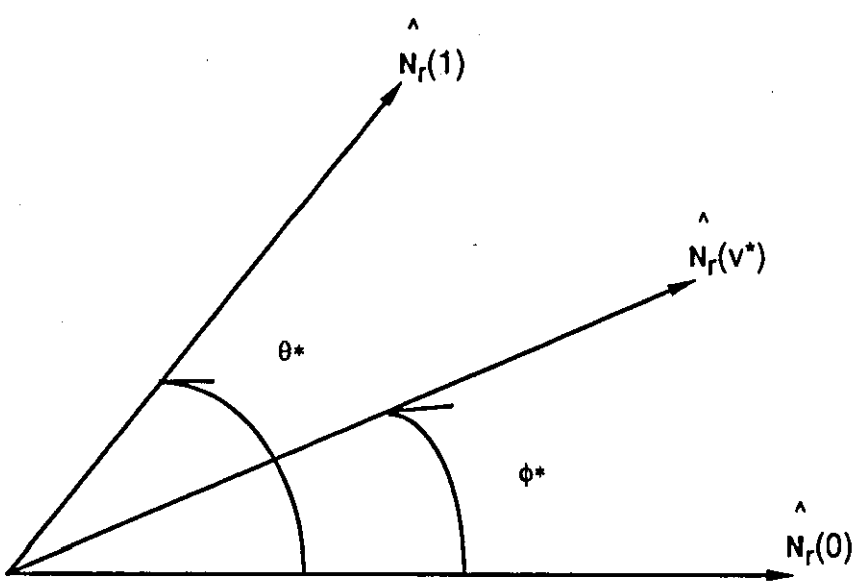

Figure (4.1) : The normal $\hat{N}_r(v^*)$ relative to $\hat{N}_r(0)$ and $\hat{N}_r(1)$.

We have parameterized the plane curve $\mathbf{q}(u^*,v^*_1)$, $0 \le u^* \le 1$, $v^*_1 \in [0,1]$ with respect to the chord between the points $\mathbf{p}^a$ and $\mathbf{p}^b$. Then, the equations,

$$(\mathbf{p}(u,v) - \mathbf{c}(u^*_1)).\mathbf{N}^{ba} = 0$$
$$(\mathbf{p}(u,v) - \mathbf{d}).\hat{\mathbf{N}}_r(v^*_1) = 0, \tag{4.3}$$

where $\mathbf{d} = \mathbf{c}(u^*_2)$, $u^*_2 \in [0,1]$,
define the parametric coordinates (u^*_1,v^*_1) of a point on the planar intersection $q(u^*,v^*_1)$, $0 \le u^* \le 1$, $v^*_1 \in [0,1]$ on the surface patch P.

We illustrate this surface/plane intersection in Figure(4.2) and the parametrization of each planar intersect $\mathbf{q}(u^*,v^*)$, $0 \le u^* \le 1$, $v^* \in [0,1]$ is illustrated in Figure(4.3). In the next section we evaluate the geometric significance of the parametrization of Q.

4.1.2) Geometric evaluation of the parametrization of Q.

If the chosen parametrization with respect to chord length is not single valued then the planar curve $\mathbf{q}(u^*,v^*)$, $0 \le u^* \le 1$, $v^* \in [0,1]$, has more than one point defined for some parametric values. The curve doubles back on itself and therefore its tangent vector must be orthogonal to the chord vector $\mathbf{N}^{ba}$ at some point $u^*_1 \in [0,1]$ on this curve i.e.,

$$\frac{\delta \mathbf{q}(u^*_1,v^*)}{\delta u^*} \cdot \mathbf{N}^{ba} = 0, \; u^*_1 \in [0,1] \tag{4.4}$$

An example of this condition is illustrated in Figure(4.4).

To ensure that the chosen parametrization with respect to the chord is single valued then a necessary condition is,

$$\frac{\delta \mathbf{q}(u^*,v^*)}{\delta u^*} \cdot \mathbf{N}^{ba} \neq 0, \; \forall \, u^*,v^* \in [0,1] \tag{4.5}$$

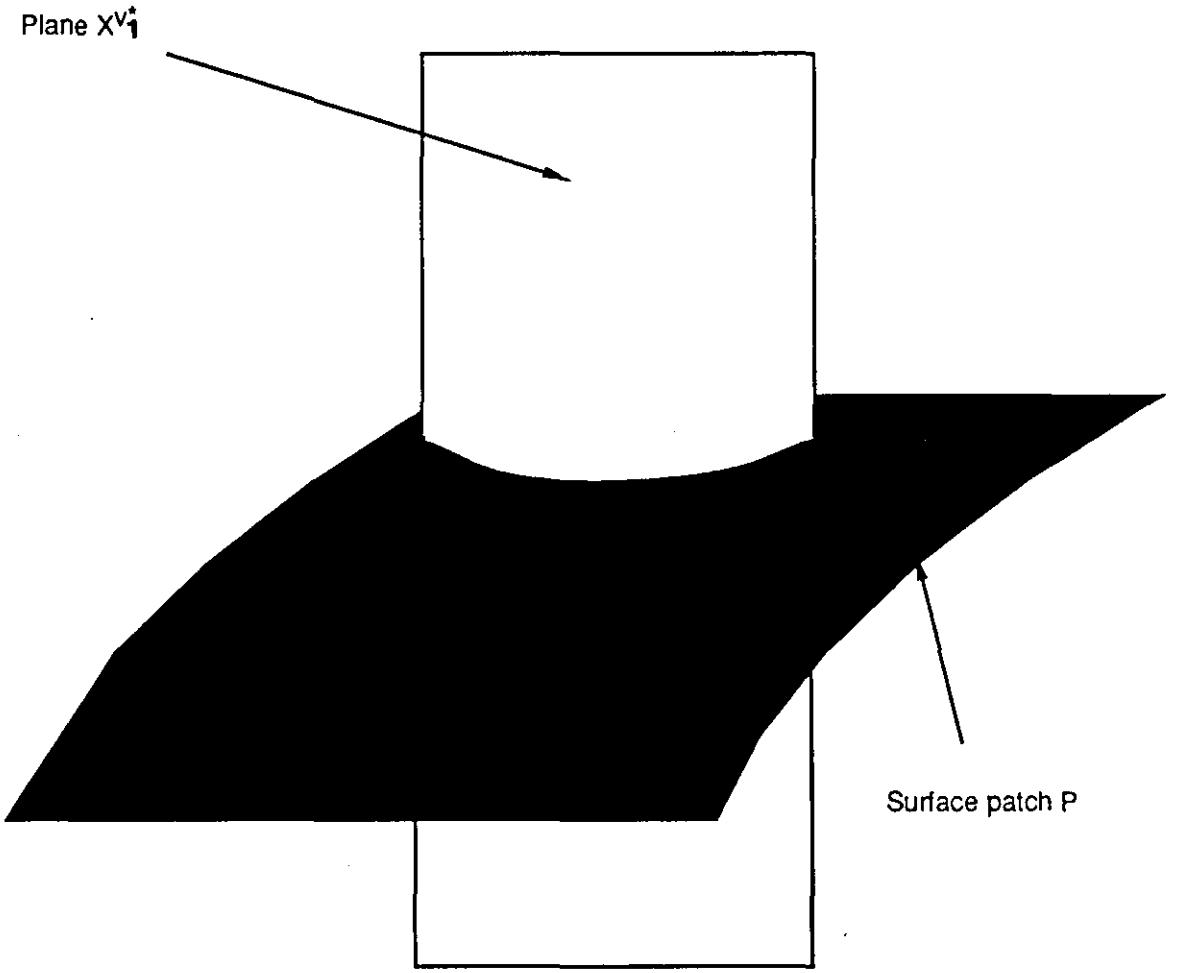

Figure (4.2) : The plane X^{v^*1} intersect with the surface patch P, and a planar intersect $\mathbf{q}(u^*,v^*)$, $0 < u^* < 1$, $v^*_1 \varepsilon [0,1]$, between the points $\mathbf{p}^a$ and $\mathbf{p}^b$.

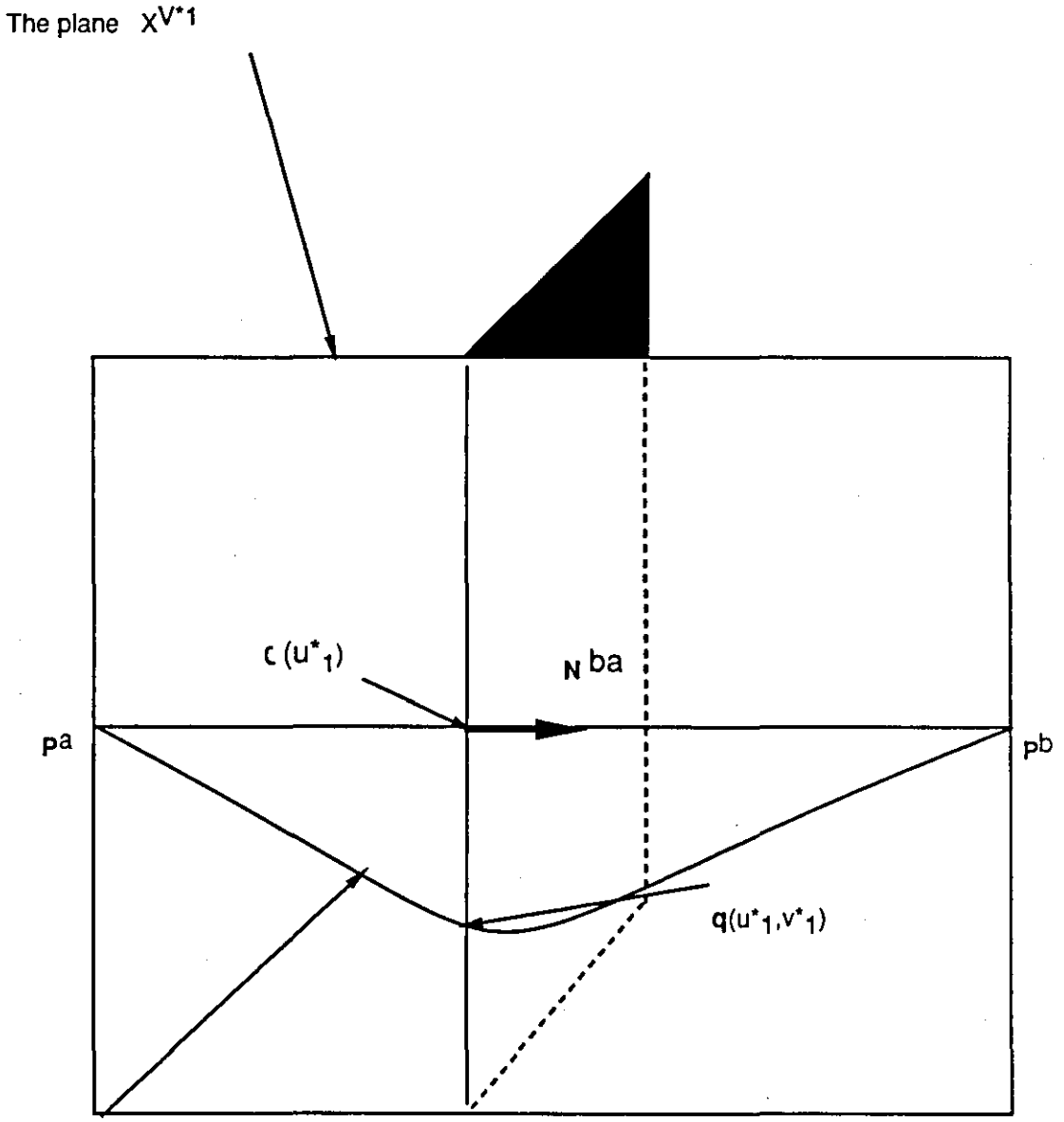

The planar intersect $q(u^*,v^*_1)$,$0 < u^* < 1$, $v^*_1 \varepsilon [0,1]$

Figure (4.3) : The parametrization of the planar intersect $q(u^*,v^*_1)$,

$0< u^* < 1$, $v^*_1 \varepsilon [0,1]$, with respect to the chord length.

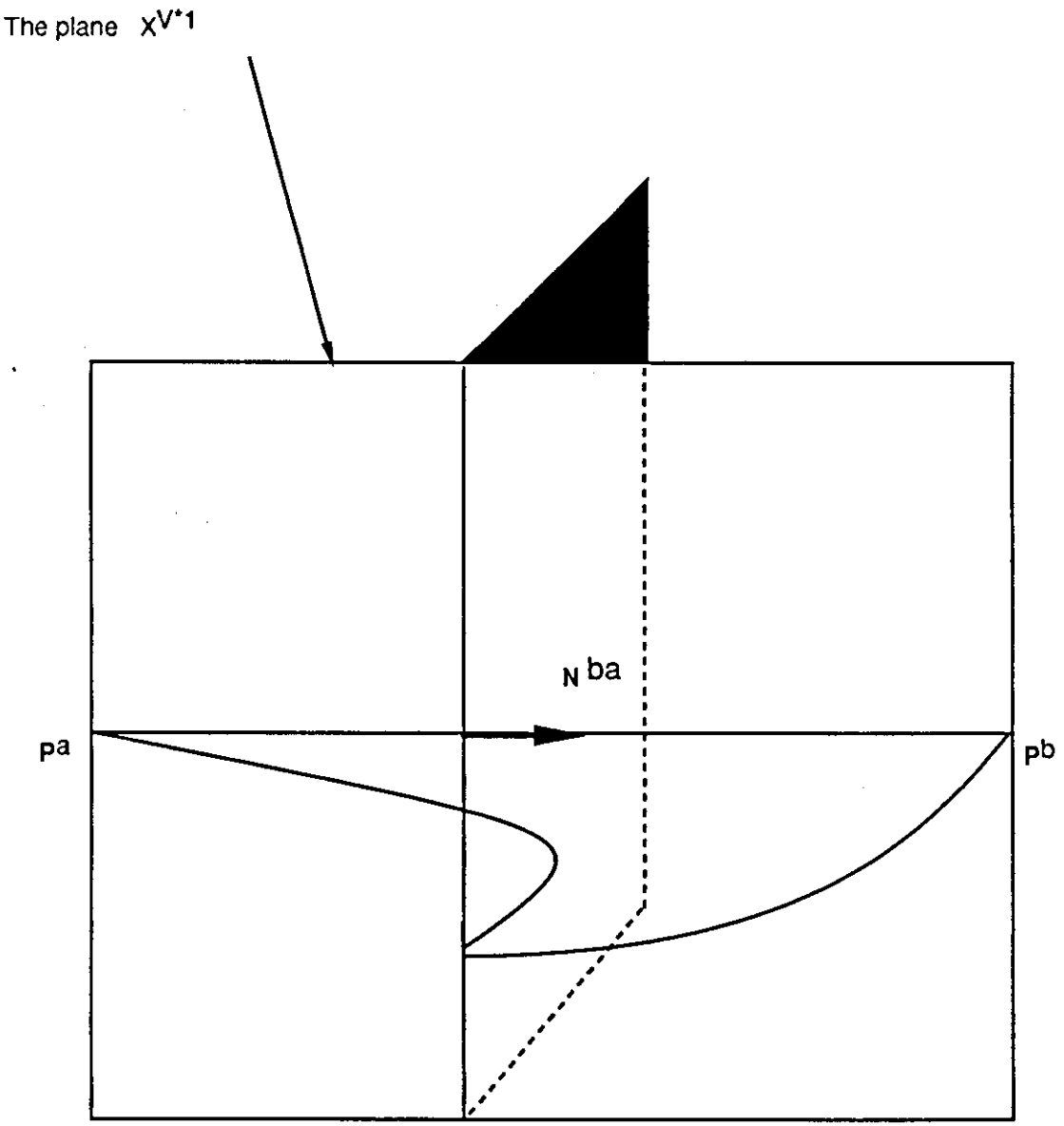

Figure (4.4) : A continuous plane / surface intersect curve, which is not single valued with respect to the chord length.

The tangent vector $\frac{\delta q(u^*,v^*)}{\delta u^*}$, at a point (u^*,v^*) must be orthogonal to the surface normal $\hat{N}(u,v)$ and plane normal $\hat{N}_r(v^*)$. Therefore,

$$\frac{\delta q(u^*,v^*)}{\delta u^*} = \alpha(u^*,v^*) \quad \hat{N}(u,v) \times \hat{N}_r(v^*)$$

where $\alpha(u^*,v^*) \neq 0, \forall\ u^*, v^* \in [0,1]$.

To accommodate the condition in equation(4.5), which ensures that the chosen parametrization for each planar curve $q(u^*,v^*)$, $0 \leq u^* \leq 1, \forall\ v^* \in [0,1]$ is single valued, we require that,

$$(\hat{N}(u,v) \times \hat{N}_r(v^*)) \cdot N^{ba} \neq 0, \forall\ u^*,v^* \in [0,1] \qquad (4.6)$$

We note that $\hat{N}_r(v^*) \cdot N^{ba} = 0$, then the surface normal $\hat{N}(u,v)$ and plane normal $\hat{N}_r(v^*)$ must not be parallel to satisfy equation(4.6) $\forall\ u^*,v^* \in [0,1]$ i.e., X^{v^*} and the tangent plane at any point on P cannot be coincident. We also require that the surface normal $\hat{N}(u,v)$ and the chord vector N^{ba} are not parallel $\forall\ u^*,v^* \in [0,1]$.

However, this condition does not rule out the possibility of a multiple intersect, as illustrated in Figure(4.5), and we need to show that parametrization of the parametric curves $q(u^*,v^*)$, $u^* \in [0,1]$, $0 \leq v^* \leq 1$, is single valued.

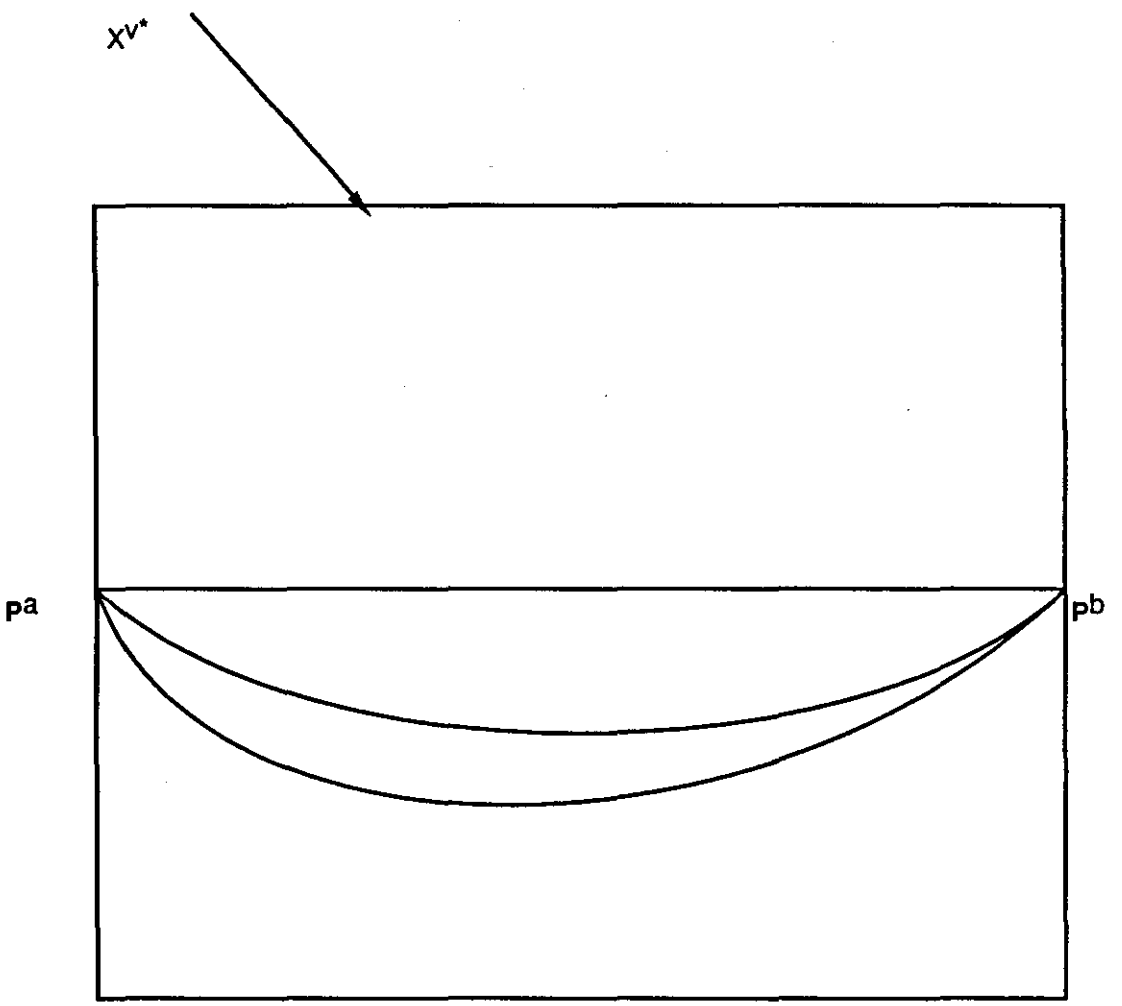

Figure (4.5) : A multiple intersect with the surface patch P and plane X^{v*}.

First we consider the surface Q as a reparametrization of a portion of the surface patch P such that :

$\mathbf{q}(u^*,v^*) = \mathbf{p}(u(u^*,v^*),v(u^*,v^*))$, $u^*,v^* \in [0,1]$.

Willmore [1972] states that if the Jacobian $\delta(u,v)/\delta(u^*,v^*)$ defined by,

$$\frac{\delta(u,v)}{\delta(u^*,v^*)} = \begin{vmatrix} \frac{\delta u}{\delta u^*} & \frac{\delta u}{\delta v^*} \\ \frac{\delta v}{\delta u^*} & \frac{\delta v}{\delta v^*} \end{vmatrix}$$

is non-zero, with $u = u(u^*,v^*)$, $v = v(u^*,v^*)$, $u^*,v^* \in (0,1)$ is locally single valued. In Appendix C from equation(C.11) we show that,

$$\delta(u,v)/\delta(u^*,v^*) = N^{ba}.\ N^{ba}\ A/B, \tag{4.7}$$

where,

$$A = (\mathbf{p}(u,v) - \mathbf{d}).\ \frac{d\hat{N}_r(v^*)}{dv^*}$$

$$B = H\ (\hat{N}(u,v)\ X\ (\hat{N}_r(v^*)).\ N^{ba}$$

We consider when $A = 0$.

We note that, $\hat{N}_r(v^*)\ .\ \hat{N}_r(v^*) = 1$

$$d(\hat{N}_r(v^*).\ \hat{N}_r(v^*))/dv^* = 0, \text{ i.e. } \frac{d\hat{N}_r(v^*)}{dv^*}\ .\ \hat{N}_r(v^*) = 0$$

Also $\hat{N}_r(v^*)\ .\ N^{ba} = 0$

$$d(\hat{N}_r(v^*).N^{ba})/dv^* = 0, \text{ i.e. } \frac{d\hat{N}_r(v^*)}{dv^*}\ .\ N^{ba} = 0$$

Hence, the vector $\frac{d\hat{N}_r(v^*)}{dv^*}$ lies in the plane X^{v^*} and is orthogonal to the chord vector and we illustrate this in Figure(4.6).

Therefore A = 0 occurs when the vector $(\mathbf{p}(u,v) - \mathbf{d})$ is parallel to the chord vector i.e. when $\mathbf{p}(u,v)$, $u,v \in [0,1]$, lies on the line L^{ab}.
In general, it would be possible for the chord to intersect the surface. The worst case of this occurs if the line L^{ab} lies in the surface. However, the surfaces of interest are low strain areas on car body panels, where the planar intersections are either convex or concave with respect to the chord length. Therefore, the only points which lie on the line L^{ab} are the end points $\mathbf{p}^a$ and $\mathbf{p}^b$.

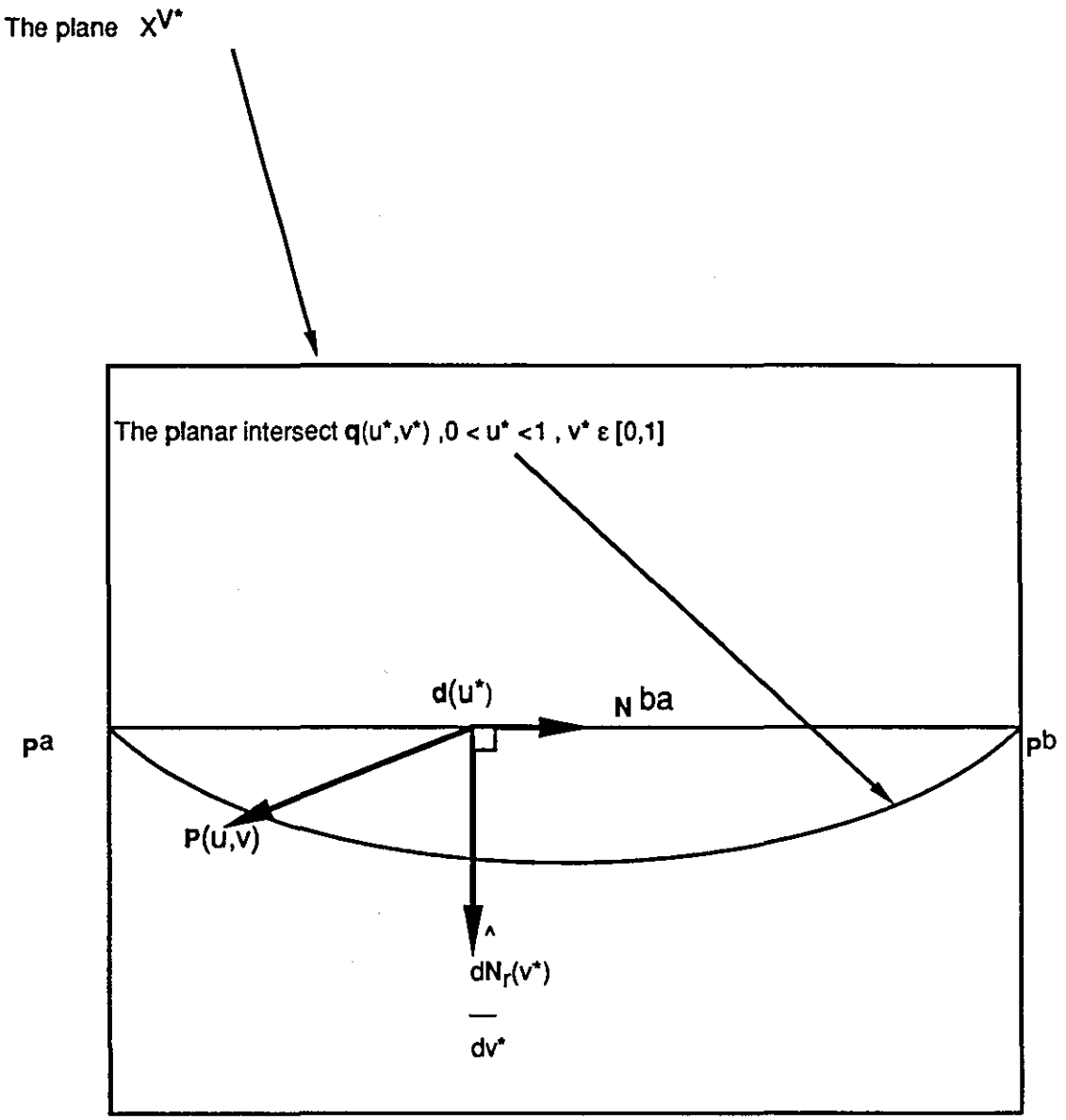

Figure (4.6) : The orientation of $\frac{\hat{dN_r(v^*)}}{dv^*}$ in the plane X^{V^*}

4.1.3) Stationary condition.

We now derive a stationary condition for the curve with minimum planar arc length. The arc lengths of each planar curve $q(u^*,v^*)$, $0 \le u^* \le 1$, $\forall\, v^* \in [0,1]$ are defined by,

$$l(v^*) = \int_0^1 [\ B(u^*,v^*)\ ]^{\frac{1}{2}}\, du^* \ ,\ v^* \in [0,1] \qquad (4.9)$$

where,

$$B(u^*,v^*) = \frac{\delta q(u^*,v^*)}{\delta u^*} \cdot \frac{\delta q(u^*,v^*)}{\delta u^*}$$

We assume that the family of radial plane intersections contains the minimum planar arc length then this curve must satisfy the condition :

$$\frac{dl(v^*)}{dv^*} = 0 \ ,\ v^* \in [0,1]$$

Since u^* and v^* are independent variables we can write :

$$\frac{dl(v^*)}{dv^*} = -\tfrac{1}{2} \int_0^1 \frac{\frac{\delta B}{\delta v^*}}{[B]^{\frac{1}{2}}}\, du^* = 0,\ v^* \in [0,1] \qquad (4.10)$$

and

$$\frac{\delta B}{\delta v^*} = 2\, \frac{\delta^2 q(u^*,v^*)}{\delta u^* \delta v^*} \cdot \frac{\delta q(u^*,v^*)}{\delta u^*} \qquad (4.11)$$

The vector nature of equation(4.10) is complex but can be solved using existing techniques for numerical integration or iteration [Sedgewick; 1984]. We adopt a geometric approach and suggest a naïve algorithm : the radial plane subdivision method and this algorithm is described in the next section.

4.2 Radial plane subdivision.

In section(4.2.1) we outline a system specification for the radial plane subdivision method. The evaluation of arc length for each planar intersect is approximated by accumulated chord length, based on the faceting technique. For each facet/plane intersect there are usually two intersect points on the facet boundary and from these points we calculate the chord length. In section(4.2.2) we describe the processing of facets and identify the possible facet/plane configurations.

4.2.1 Outline of system specification

This section outlines a system specification : **system** 4.1

System 4.1 : Shortest planar path

The system specification is illustrated in Figure(4.7); its purpose is detailed below :

To estimate and record the minimum planar arc length of a curve, from a set of radial plane/surface patch intersections on a surface patch. The curves lie between a pair of strain points defined by parametric values. The end tangents of this curve are calculated and recorded. The following information is available :

a) The numerical definition of the surface patch, represented by mesh of points.

b) The parametric values of the pair of strain points.

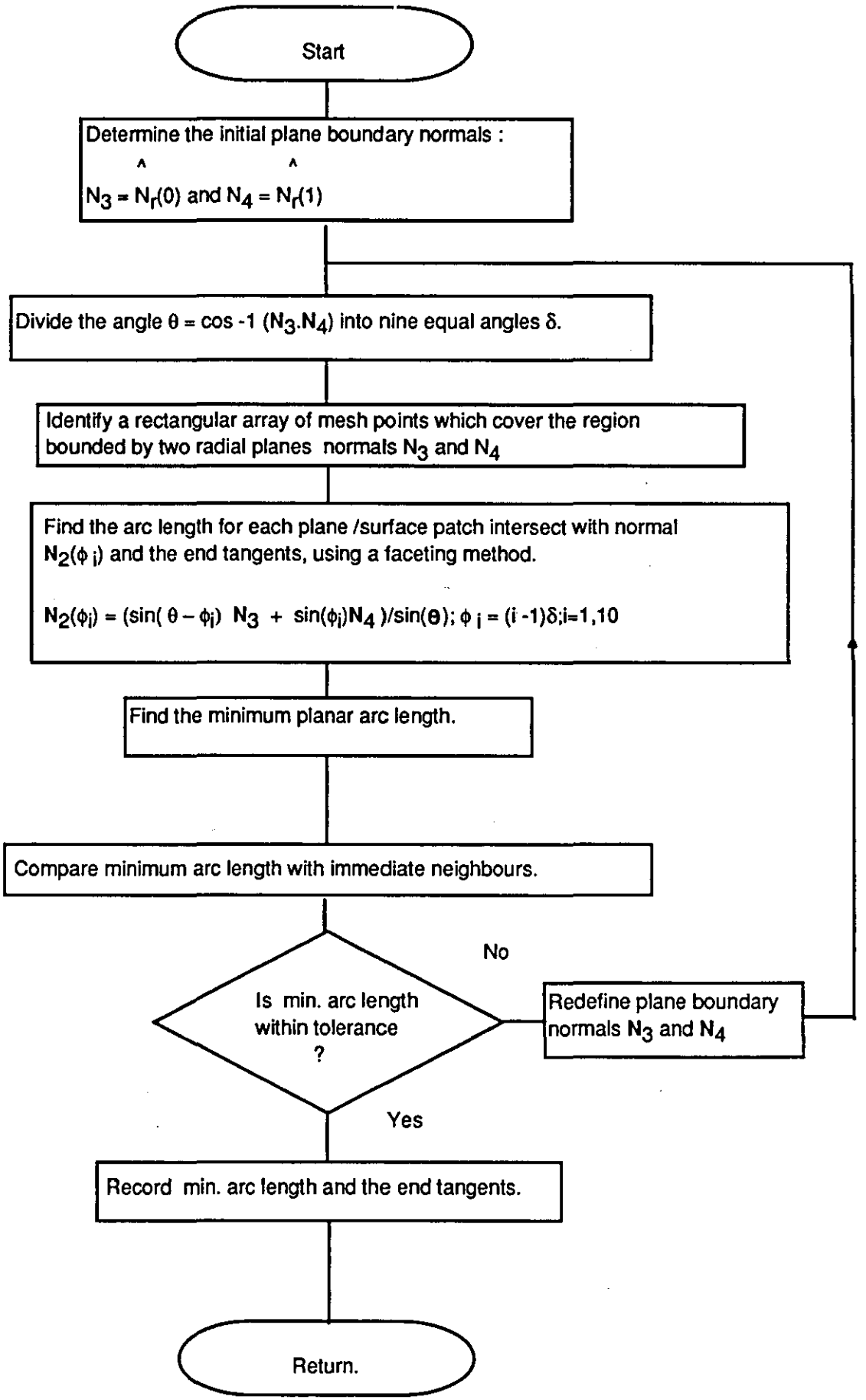

Figure(4.7) : **System 4.1** flowchart to calculate the minimum arc length between the pair of strain points defined by parametric values; from a set of radial plane/ surface patch intersections, using a faceting technique.

4.2.2) Facet/ plane intersections.

In this section we determine the possible configurations of a facet/plane intersection.

The surface patch P is represented by a rectangular mesh of points p_{ij}, i=1,...,m; j = 1,...,n defined by :

$p_{ij} = p(u_i, v_j)$,

where $u_i = (i - 1)/(m - 1)$, $i = 1,\ldots, m$ and

$v_j = (j - 1)/(n - 1)$, $j = 1,..,n$.

The k^{th} facet, $k = (j - 1)(m - 1) + i$, $j = 1,\ldots,n - 1$, $i = 1,\ldots,m - 1$ has corner points p_{ij}, p_{i+1j}, p_{ij+1} and p_{i+1j+1}, and is illustrated in Figure(4.8).

We assume that the mesh is dense so that each facet/plane intersect is connected, and the arc length between the facet boundary intersect points can be approximated by chord length.

We are only concerned with facets which lie in a region, R, bounded by two parallel planes with normals parallel to the chord vector N^{ba} and containing the points p^a and p^b, respectively. We define,

$a_{ij} = (p_{ij} - p^a).N^{ba}$,

$b_{ij} = (p_{ij} - p^b).N^{ba}$

where i = 1,...,m; j = 1,...,n .

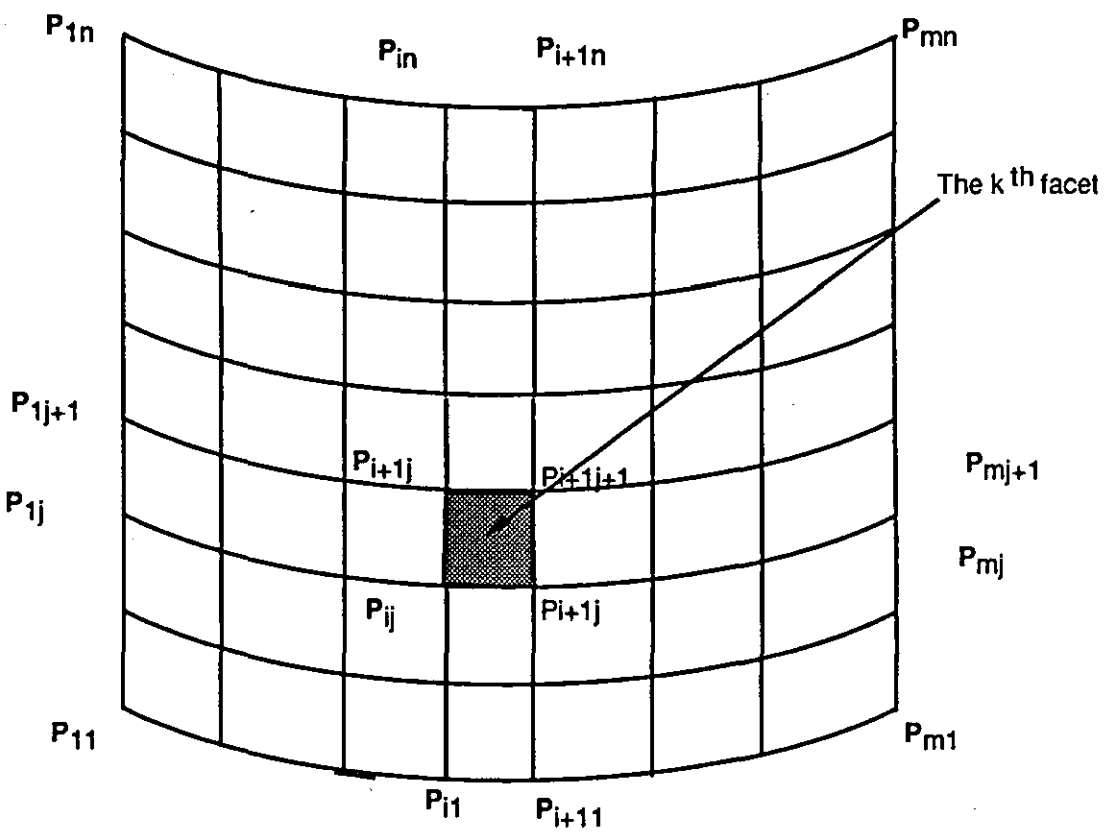

Figure (4.8) : The k th facet in an m by n mesh of points on the surface patch P.

If the k^{th} facet with the corner points: $\mathbf{p}_{ij}$, $\mathbf{p}_{i+1j}$, $\mathbf{p}_{ij+1}$ and $\mathbf{p}_{i+1j+1}$, satisfies,

$a_{ij}\, b_{ij} > 0$; $a_{i+1j}\, b_{i+1j} > 0$; $a_{ij+1}\, b_{ij+1} > 0$ and $a_{i+1j+1}\, b_{i+1j+1} > 0$;

then the facet will not lie in R. We further consider the signs of c_{ij} defined by,

$c_{ij} = (\mathbf{p}_{ij} - \mathbf{d}).\mathbf{N}_r(v^*_1)$, $v^*_1 \in [0,1]$, i= 1,...,m; j = 1,...,n

and we can determine if a facet/plane intersection occurs by considering the changes of sign of c_{ij}, c_{i+1j}, c_{ij+1} and c_{i+1j+1} at each of the corner points $\mathbf{p}_{ij}$, $\mathbf{p}_{i+1j}$, $\mathbf{p}_{ij+1}$ and $\mathbf{p}_{i+1j+1}$.

The possible sign configurations of c_{ij}, c_{ij+1}, c_{i+1j} and c_{i+1j+1} for the k^{th} facet/plane intersect are summarized in **Tables** 4.1 to 4.3. We assume that for a given facet/plane there are no intersect points or at most two intersect points, on different boundaries.

Table 4.1 : Summary of the possible signs of c_{i+1j+1}, if $c_{ij} > o$

	$c_{i+1j} > o$	$c_{i+1j} = o$	$c_{i+1j} < o$
$c_{ij+1} > o$	o/-	+/o/-	+/o/-
$c_{ij+1} = o$	+/o/-	-	-
$c_{ij+1} < o$	+/o/-	-	-

Table 4.2 : Summary of the possible signs of c_{i+1j+1}, if $c_{ij} = o$

	$c_{i+1j} > o$	$c_{i+1j} = o$	$c_{i+1j} < o$
$c_{ij+1} > o$	+	+	+/o/-
$c_{ij+1} = o$	+	#	-
$c_{ij+1} < o$	+/o/-	-	-

Table 4.3: Summary of the possible signs of c_{i+1j+1}, if $c_{ij} < o$

	$c_{i+1j} > o$	$c_{i+1j} = o$	$c_{i+1j} < o$
$c_{ij+1} > o$	+	+	+/o/-
$c_{ij+1} = o$	+	+	+/o/-
$c_{ij+1} < o$	+/o/-	+/o/-	+/o

Key

The plane normal $\hat{N}_r(v^*_1)$, $v^*_1 \in [0,1]$ cannot be orthogonal to the tangent plane.

4.3 Choice of mesh parameters.

In this section we identify the mesh size required to evaluate arc length for a surface patch/plane intersection using the faceting method. We use surface definitions for production panels at Austin Rover and the surface patches of interest, which are generally flat, are illustrated in Figure (4.9) and (4.10).

We first demonstrate convergence of the faceting method in section(4.3.1), and in section(4.3.2) we derive an error bound based on the evaluation of arc length for the estimation of strains. In section(4.3.3) we identify the best choice of mesh parameters for each surface patch.

4.3.1) Convergence of the faceting method.

To demonstrate convergence of the faceting method we consider an arbitrary, but fixed arrangement of planar intersects for each patch and evaluate arc lengths for a set of facet arrays.

We define a symmetric parametric square which has corner parametric values (0.25,0.25); (0.75,0.25); (0.25,0.75) and (0.75,0.75). For each surface patch we consider six planar intersects $\alpha_i, i = 1,\ldots,6$. The corresponding planes π_i , $i = 1,\ldots,6$ contain points which are defined by two pairs of parametric points; and are summarized in **Table** (4.4). From each pair of parametric values we determine the radial plane boundary normals for a mesh size $m = n = 9$. The normal for each plane is chosen such that the radial range θ is bisected by the plane π_i.

FRONT

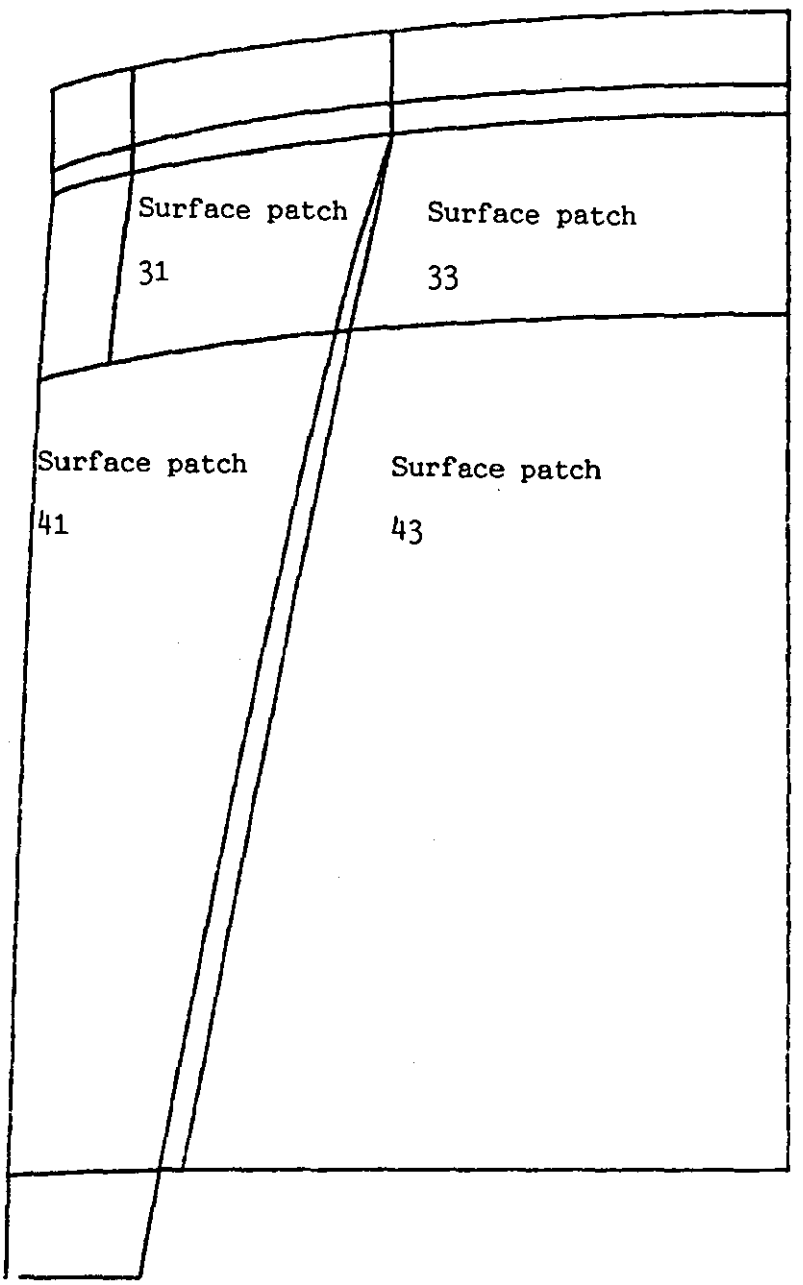

REAR

Figure(4.9) : The left hand side of the R8-bonnet with named surface patches.

FRONT

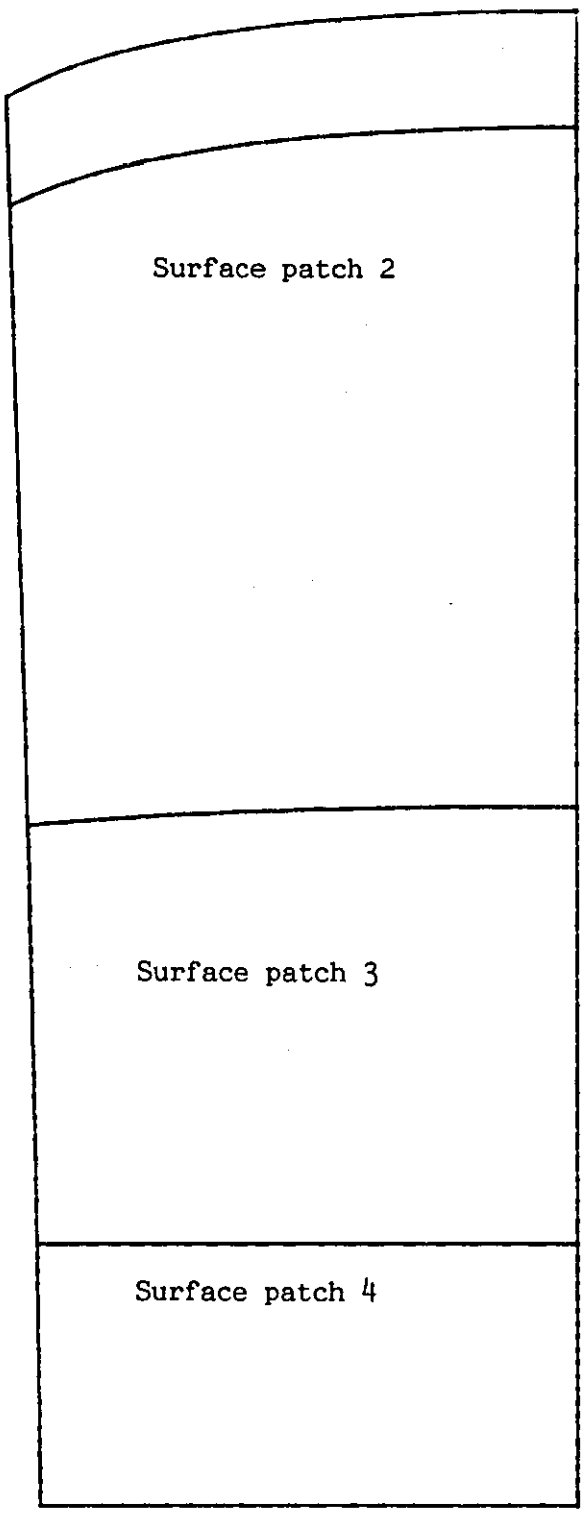

REAR

Figure(4.10) : The left hand side of the R8-roof with named surface patches.

Table (4.4) : Summary of parametric points associated with the planes π_i.

Planes	Pairs of parametric points
π_1	(0.25,0.25); (0.75,0.25)
π_2	(0.25,0.75); (0.75,0.75)
π_3	(0.25,0.25); (0.25,0.75)
π_4	(0.75,0.25); (0.75,0.75)
π_5	(0.25,0.25); (0.75,0.75)
π_6	(0.75,0.25); (0.25,0.75)

The planar intersects α_i , i = 1,...,6 are continuous and we evaluate seven arc lengths l_j, j = 1,..., 7 at the following facet arrays : $2^{(fj-1)}$ X $2^{(fj-1)}$, f_j = 1,...,7, where we term f_j the facet index. The corresponding mesh sizes are square and m,n are defined by m = n = $2^{(fj-1)}$ + 1, f_j = 1,...,7. The arc lengths calculated for each planar intersect α_i , i = 1,...,6 are presented in **Tables** (4.5) - (4.11).

Table (4.5) : Arc lengths evaluated for R8-bonnet.

R8-bonnet : Surface patch name 31						
	π_1	π_2	π_3	π_4	π_5	π_6
l^*_1	96.5333	93.7256	116.6005	108.6997	169.0162	122.0031
l^*_2	96.5527	93.7375	116.6164	108.7074	169.0445	122.0247
l^*_3	96.5607	93.7495	116.6024	108.7008	169.0460	122.0255
l^*_4	96.5676	93.7556	116.6029	108.7011	169.0541	122.0316
l^*_5	96.5694	93.7572	116.6031	108.7012	169.0563	122.0333
l^*_6	96.5698	93.7576	116.6032	108.7012	169.0569	122.0338
l^*_7	96.5699	93.7577	116.6032	108.7012	169.0571	122.0339

Table (4.6) : Arc lengths evaluated for R8-bonnet.

R8-bonnet : Surface patch name 33						
	π_1	π_2	π_3	π_4	π_5	π_6
l^*_1	96.7715	96.5047	185.1994	194.7583	226.0093	199.3301
l^*_2	96.7806	96.5123	185.2089	194.7589	226.0509	199.3685
l^*_3	96.8146	96.5419	185.2044	194.7644	226.0543	199.3693
l^*_4	96.8257	96.5514	185.2059	194.7660	226.0670	199.3791
l^*_5	96.8285	96.5538	185.2063	194.7665	226.0706	199.3816
l^*_6	96.8292	96.5544	185.2065	194.7666	226.0716	199.3823
l^*_7	96.8294	96.5546	185.2066	194.7666	226.0719	199.3825

Table (4.7) : Arc lengths evaluated for R8-bonnet.

R8-bonnet : Surface patch name 41						
	π_1	π_2	π_3	π_4	π_5	π_6
t^*_1	388.5730	374.7883	121.7240	87.8867	417.9205	371.6759
t^*_2	388.6086	374.8183	121.8960	88.0203	417.9959	371.7080
t^*_3	388.6185	374.8328	121.7266	87.8893	418.0002	371.7076
t^*_4	388.6304	374.8445	121.7275	87.8900	418.0223	371.7168
t^*_5	388.6334	374.8476	121.7277	87.8903	418.0283	371.7194
t^*_6	388.6342	374.8484	121.7278	87.8903	418.0297	371.7201
t^*_7	388.6344	374.8486	121.7278	87.8903	418.0301	371.7203

Table (4.8) : Arc lengths evaluated for R8-bonnet.

R8-bonnet : Surface patch name 43						
	π_1	π_2	π_3	π_4	π_5	π_6
t^*_1	397.7097	397.1746	217.4651	255.5524	486.1950	436.6404
t^*_2	397.7383	397.1920	217.5457	255.5918	486.2761	436.7145
t^*_3	397.7641	397.2310	217.4730	255.5635	486.2780	436.7181
t^*_4	397.7782	397.2456	217.4752	255.5666	486.3007	436.7400
t^*_5	397.7818	397.2494	217.4757	255.5674	486.3068	436.7462
t^*_6	397.7827	397.2503	217.4759	255.5676	486.3084	436.7481
t^*_7	397.7829	397.2506	217.4759	255.5676	486.3089	436.7485

Table (4.9) : Arc lengths evaluated for R8-roof.

R8-roof : Surface patch name 2						
	π_1	π_2	π_3	π_4	π_5	π_6
l^*_1	310.2613	298.3146	259.2655	254.2067	411.1020	384.6133
l^*_2	310.2629	298.3147	259.2819	254.2067	411.1567	384.6721
l^*_3	310.2892	298.3366	259.2868	254.2258	411.1643	384.6750
l^*_4	310.2971	298.3428	259.2935	254.2311	411.1837	384.6920
l^*_5	310.2992	298.3445	259.2957	254.2326	411.1897	384.6966
l^*_6	310.2997	298.3449	259.2966	254.2330	411.1915	384.6980
l^*_7	310.2999	298.3450	259.2969	254.2331	411.1919	384.6984

Table (4.10) : Arc lengths evaluated for R8-roof.

R8-roof : Surface patch name 3						
	π_1	π_2	π_3	π_4	π_5	π_6
l^*_1	199.7797	194.9902	250.4905	248.4852	318.3851	317.8482
l^*_2	199.7906	195.0205	250.5021	248.4931	318.4066	317.8711
l^*_3	199.7813	194.9917	250.5094	248.5040	318.4076	317.8716
l^*_4	199.7817	194.9921	250.5145	248.5091	318.4141	317.8779
l^*_5	199.7818	194.9923	250.5158	248.5105	318.4159	317.8796
l^*_6	199.7819	194.9923	250.5161	248.5108	318.4164	317.8800
l^*_7	199.7819	194.9923	250.5162	248.5109	318.4165	317.8801

Table (4.11) : Arc lengths evaluated for R8-roof.

R8-roof : Surface patch name 4						
	π_1	π_2	π_3	π_4	π_5	π_6
l^*_1	119.7629	119.7718	247.1580	246.3480	273.7455	274.8192
l^*_2	119.7653	119.8014	247.1673	246.3501	273.7912	274.8654
l^*_3	119.7812	119.7904	247.1776	246.3699	273.7960	274.8675
l^*_4	119.7866	119.7963	247.1830	246.3760	273.8121	274.8809
l^*_5	119.7881	119.7979	247.1843	246.3775	273.8167	274.8847
l^*_6	119.7885	119.7983	247.1847	246.3780	273.8180	274.8858
l^*_7	119.7886	119.7984	247.1848	246.3781	273.8184	274.8861

We demonstrate the convergence to the arc length of each planar intersect α_i, $i = 1,\ldots,6$ using the faceting method by plotting, for each surface patch, the percentage increase in arc length with respect to chord length against facet index f_j, $j = 1,\ldots,7$ and this is illustrated by Figures (4.11) - (4.17). We conclude that the arc lengths evaluated have a practical convergence at 64 X 64 facets i.e. with $f_7 = 7$.

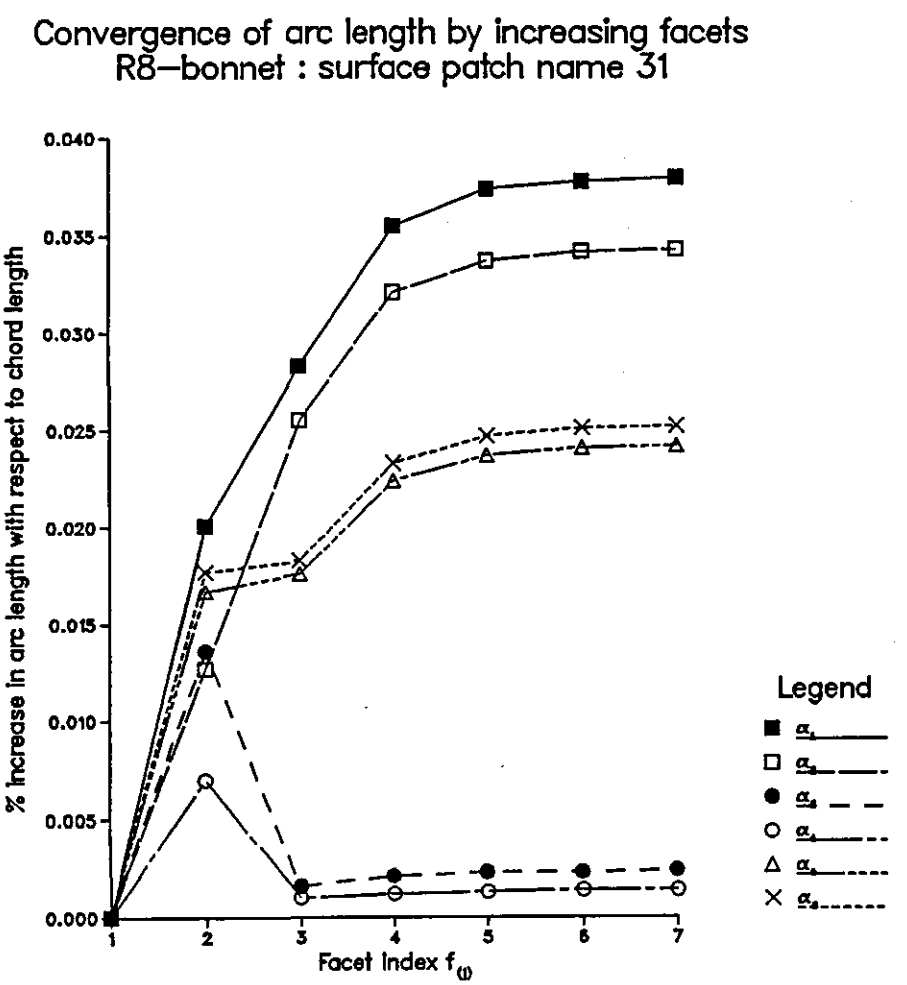

Figure(4.11) : Arc length convergence for the R8-bonnet.

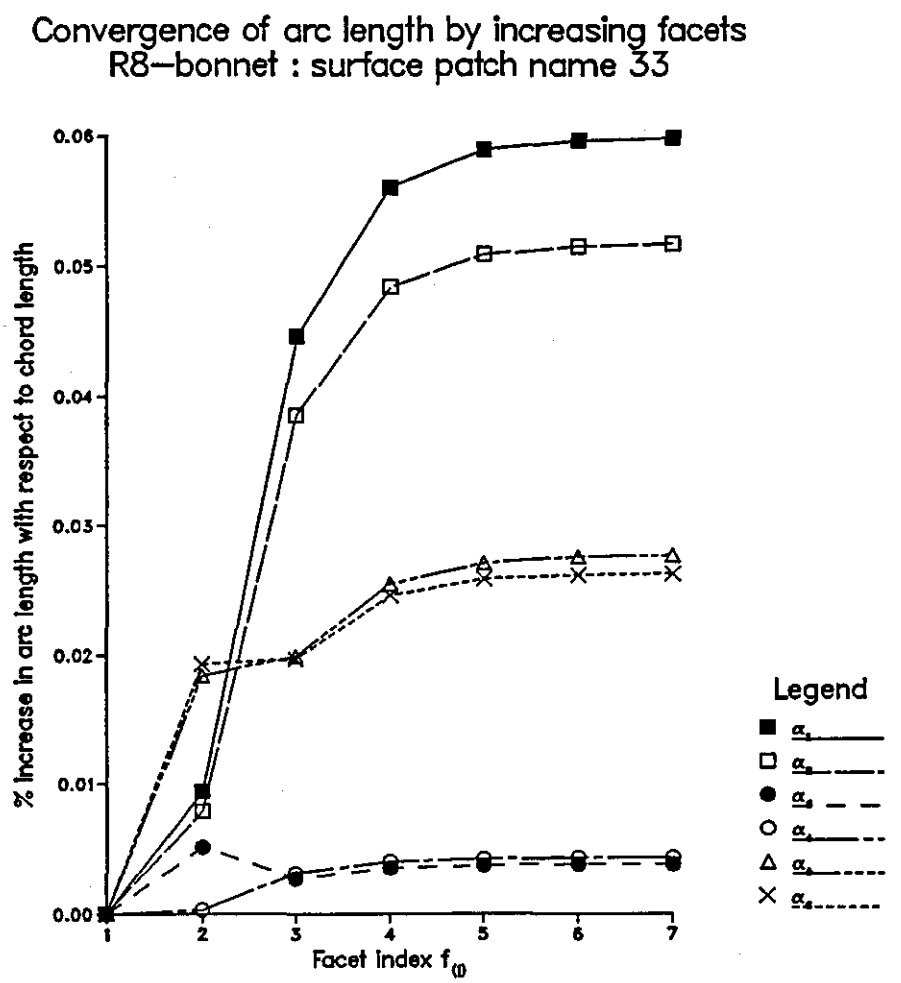

Figure(4.12) : Arc length convergence for the R8-bonnet.

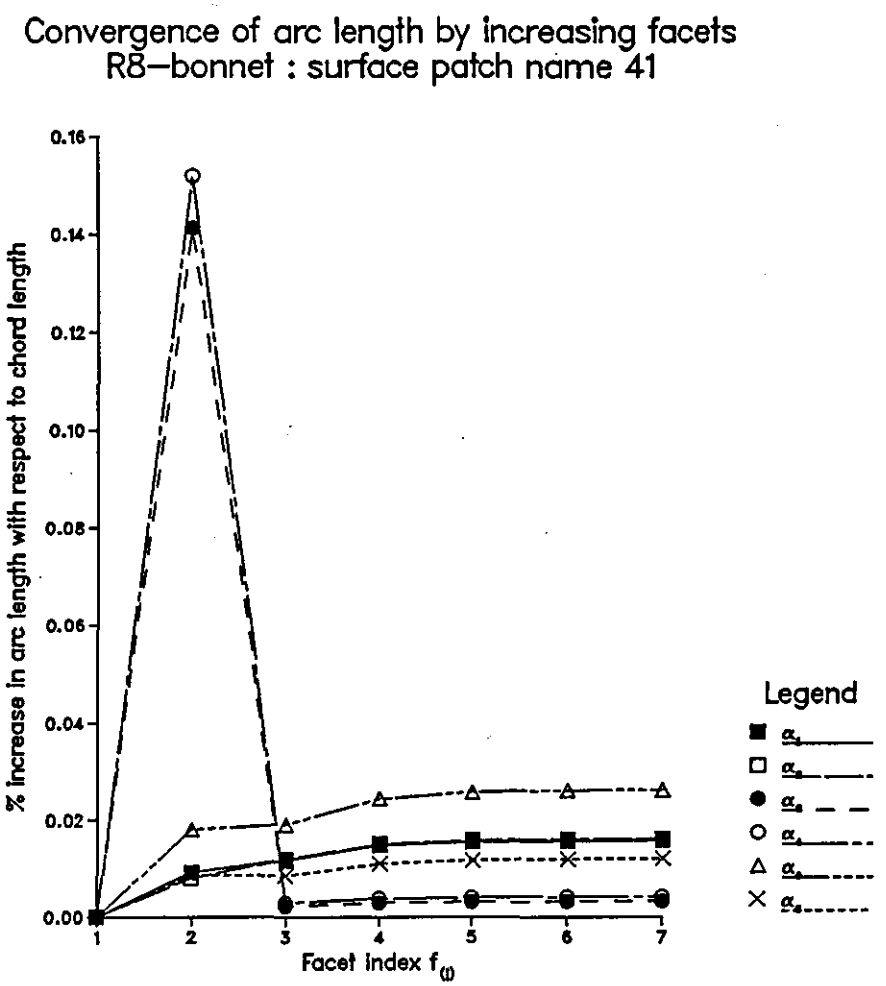

Figure(4.13) : Arc length convergence for the R8-bonnet.

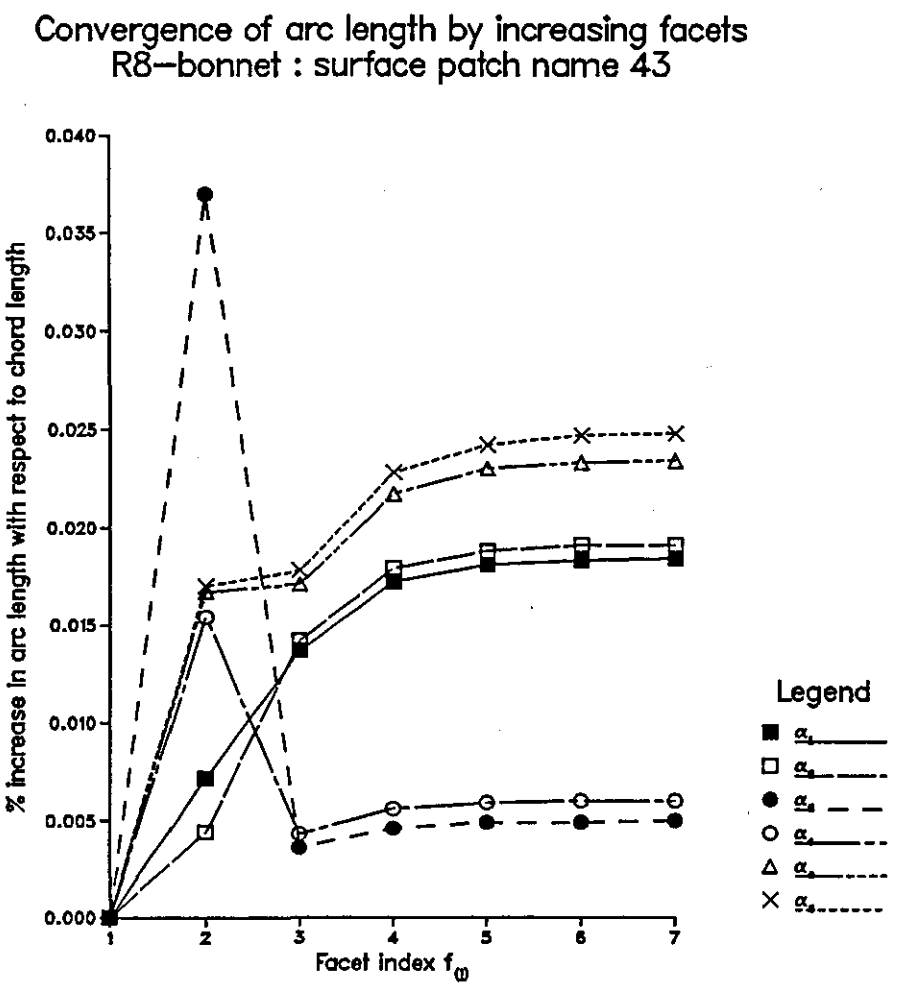

Figure(4.14) : Arc length convergence for the R8-bonnet.

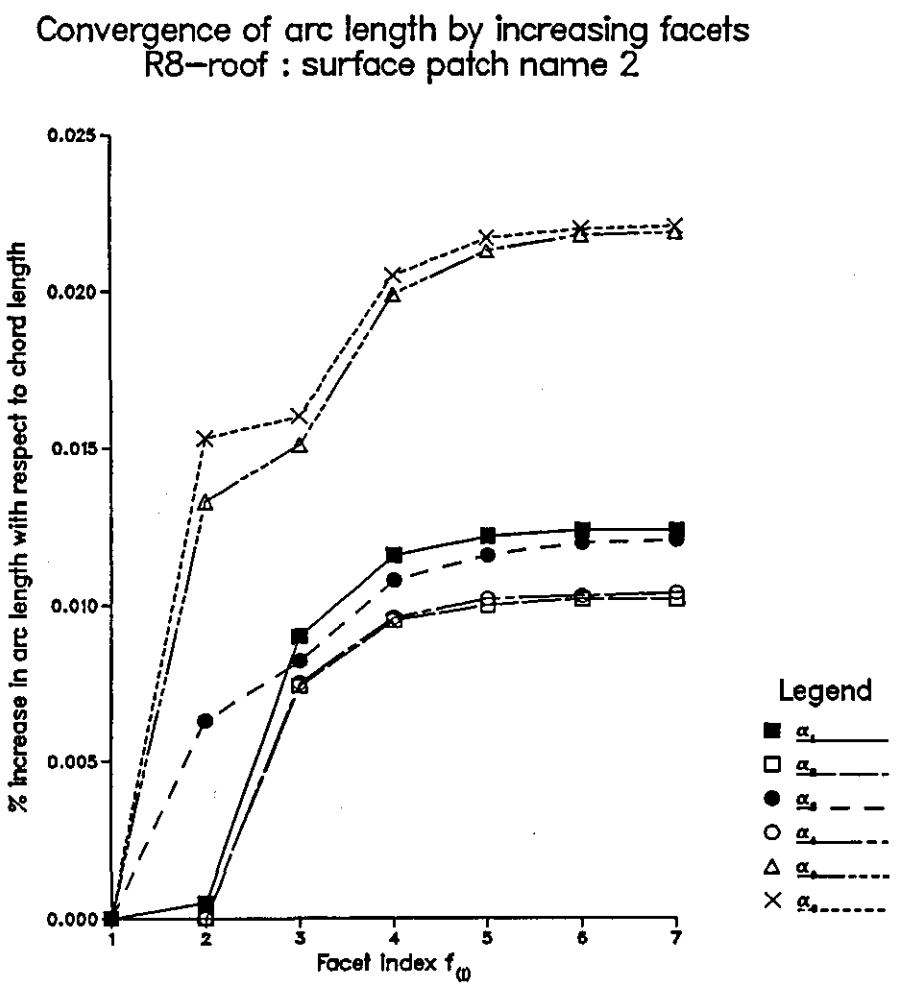

Figure(4.15) : Arc length convergence for the R8-roof.

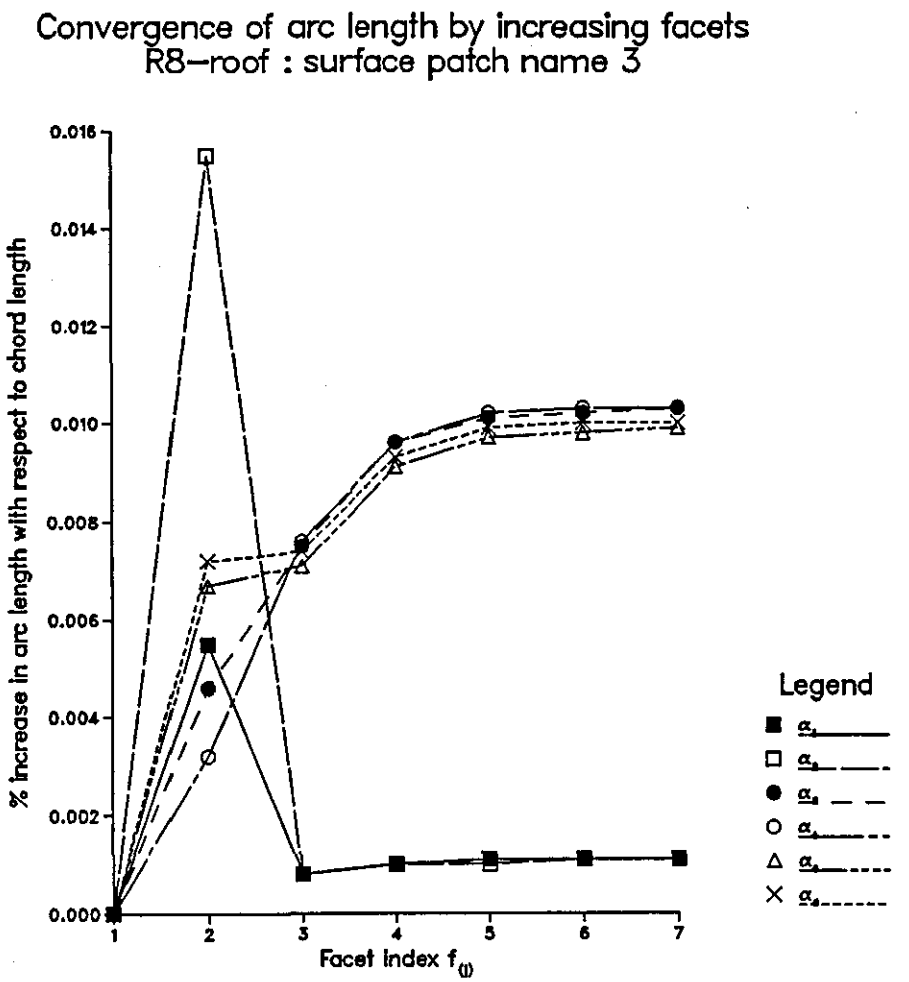

Figure(4.16) : Arc length convergence for the R8-roof.

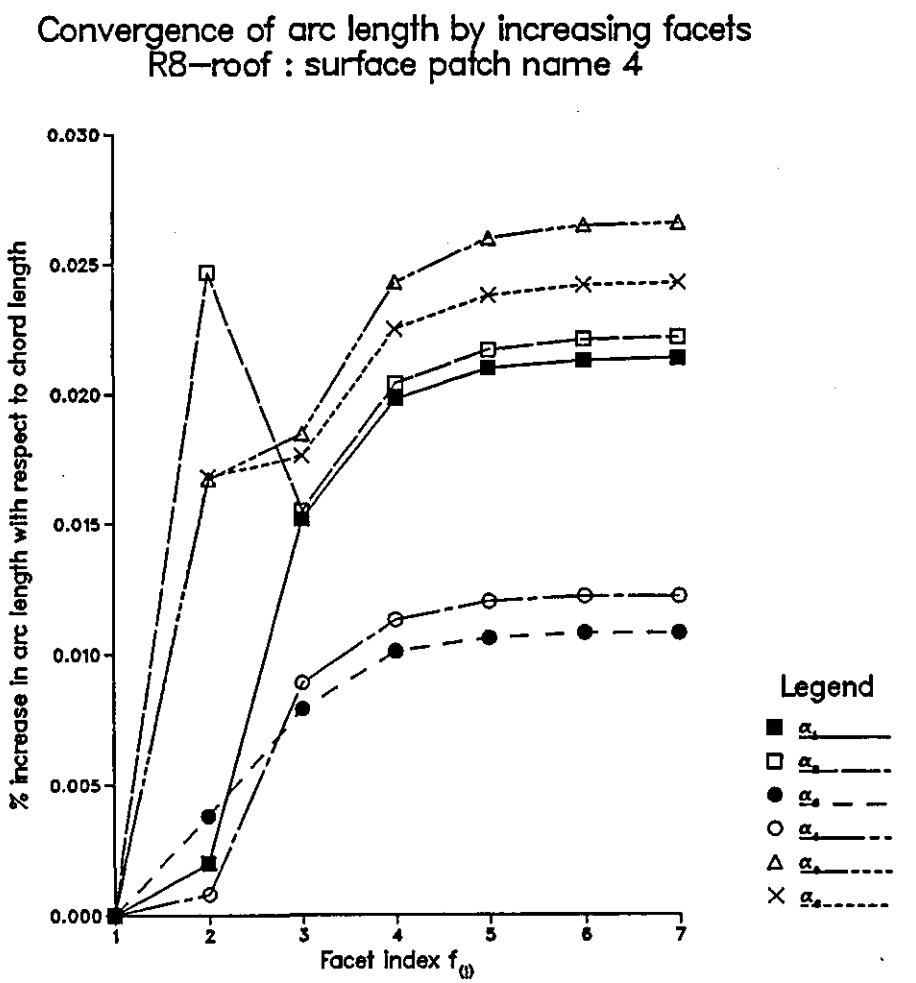

Figure(4.17) : Arc length convergence for the R8-roof.

4.3.2) Strain error based on arc length estimation.

In this section we derive an error bound based on the evaluation of arc length for the estimation of strains. We consider the deformation of the straight line L on a blank to the curve L* on a surface patch. Let l be the length of the line L and let l^* be the length of the curve L*. If we evaluate the arc length l^*_e defined by,

$$l^*_e = l^* - e, \quad e > 0 \tag{4.12}$$

and e is the associated error.

We show that the strain, S, defined by,

$$S = (l^* - l)/l \tag{4.13}$$

is bounded by the relative error E_r defined by,

$$E_r = e/l^* \tag{4.14}$$

We define the estimated strain, S_e, by :

$$S_e = (l^*_e - l)/l. \tag{4.15}$$

Now differencing equations (4.13) and (4.15),

$$S - S_e = (l^* - l^*_e) / l = e / l \tag{4.16}$$

From equation(4.12),

$$l = l^*/(S + 1) \tag{4.17}$$

Substituting equation(4.17) into (4.16) and then using equation(4.14) we obtain,

$$S - S_e = e(S + 1) /l^* = E_r (S + 1)$$

$$S = (S_e + E_r)/(1 - E_r)$$

Expanding binomially since $E_r << 1$, and ignoring small terms,

$$S = (S_e + E_r)(1 + E_r + o(E_r^2)) = S_e + E_r - S_e E_r + o(E_r^2)$$

$$\approx S_e + E_r$$

Then the error associated with the estimated strain, S_e, is approximated by the relative error, E_r. In the next section we determine the acceptable percentage error for small strain calculations.

4.3.3) Acceptable error.

The small strains are assumed to occur before the elastic limit is reached i.e. before the yield stress is reached : for mild steel the yield stress σ_y, and Youngs Modulus E are given by [Tennet; 1984],

$\sigma_y = 300 \times 10^6 \ Nm^{-2}$, $E = 210 \times 10^9 \ Nm^{-2}$

This gives a yield strain, S_y where,

$S_y = 300 \times 10^6 / 210 \times 10^9 = 1.4285 \times 10^{-3}$

We assume that an acceptable error in the strain evaluations is less than one percent. So we require that the order of relative error satisfies

$E_r \leq 1 \times 10^{-5}$.

To identify the facet index required for each planar intersect α_i, $i = 1,\ldots,6$ we plot, for each surface patch, the relative error against facet index f_j, $j = 3,\ldots,7$. We also plot the line of acceptable error, so that the values below this line correspond to the best choice of mesh parameters; this is illustrated by Figures (4.18)- (4.24).

We conclude that a facet index $f_5 = 5$, will give an acceptable tolerance for the evaluation of arc length on each surface patch considered.

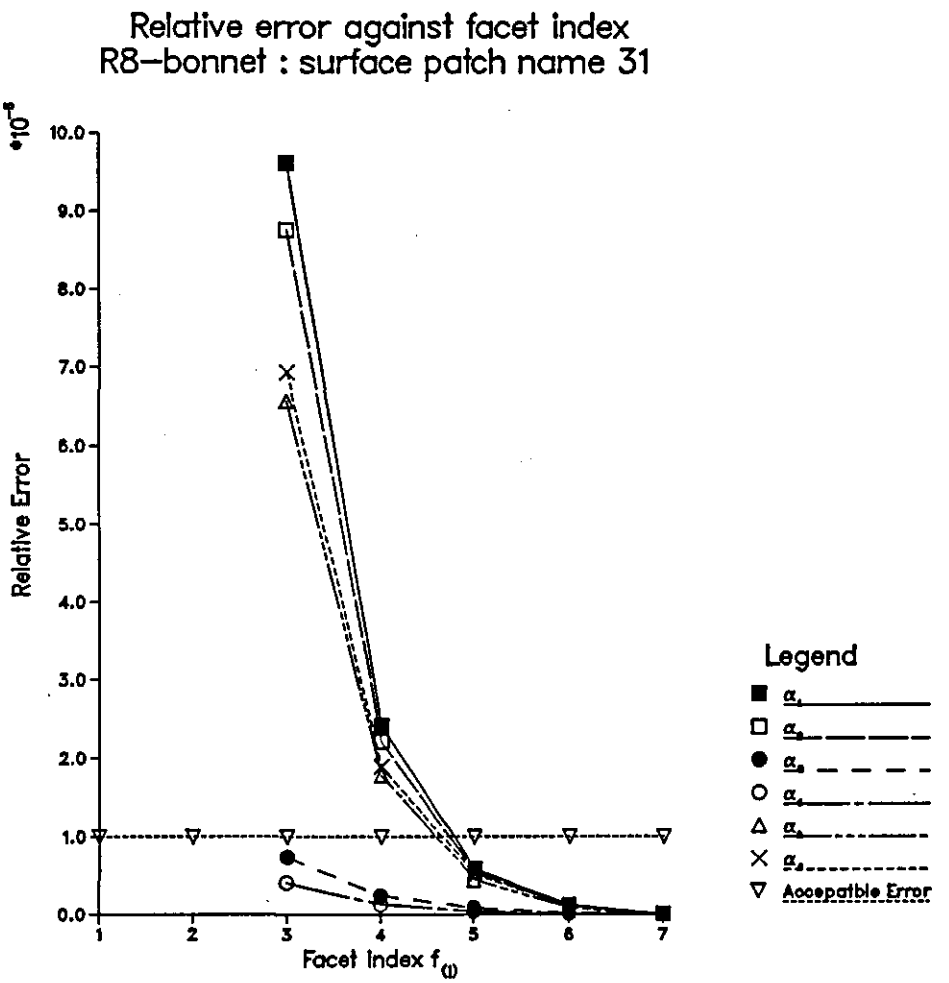

Figure(4.18) : Relative error against facet index for the R8-bonnet.

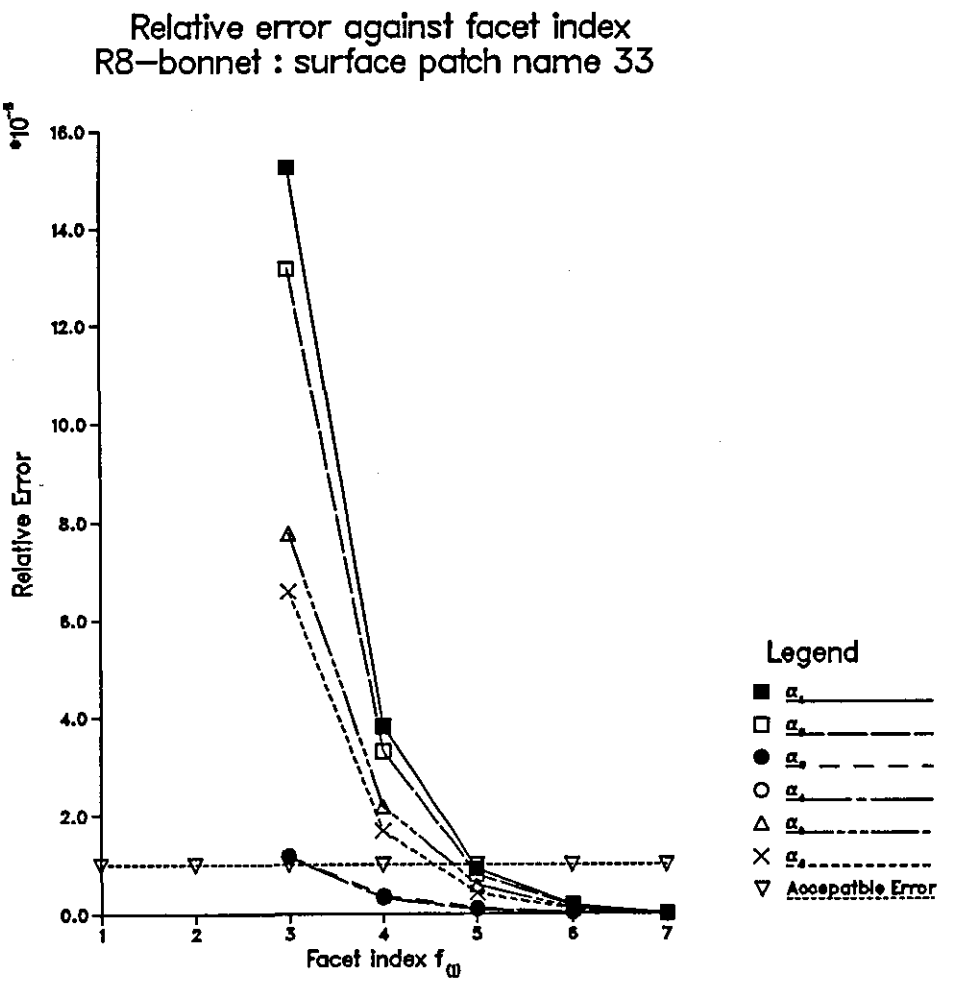

Figure(4.19) : Relative error against facet index for the R8-bonnet.

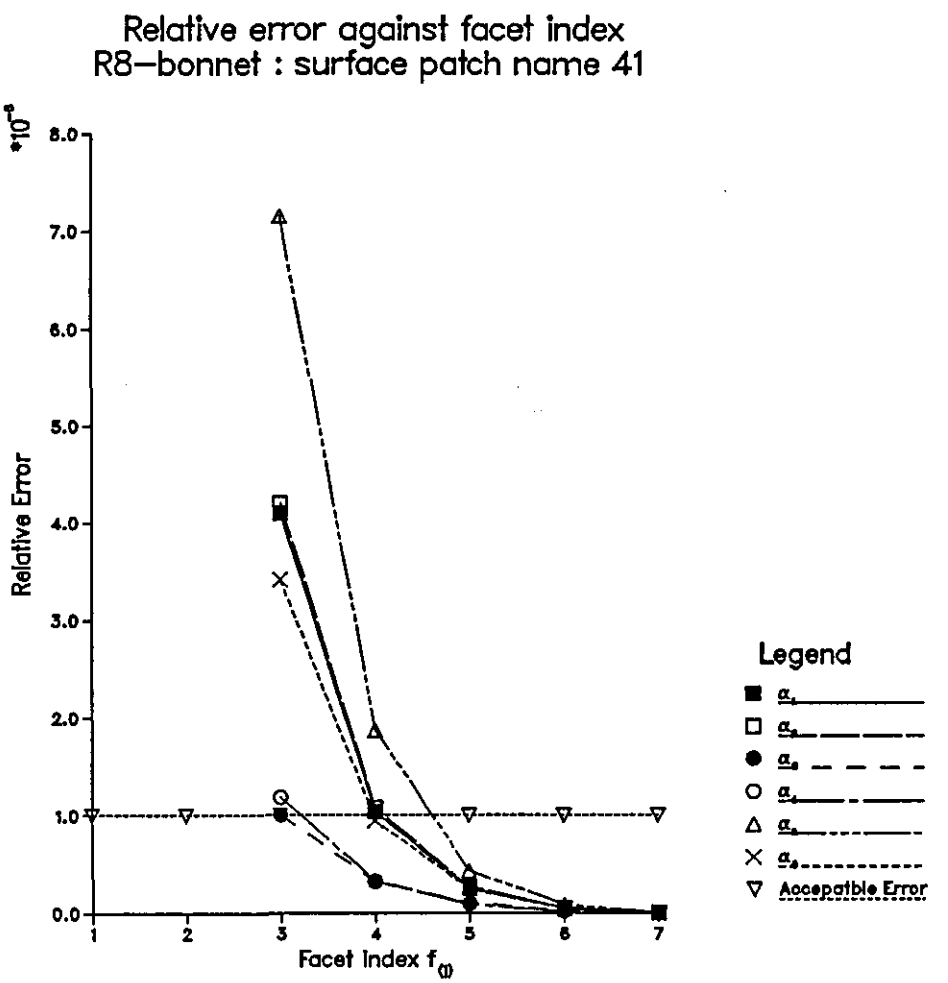

Figure(4.20) : Relative error against facet index for the R8-bonnet.

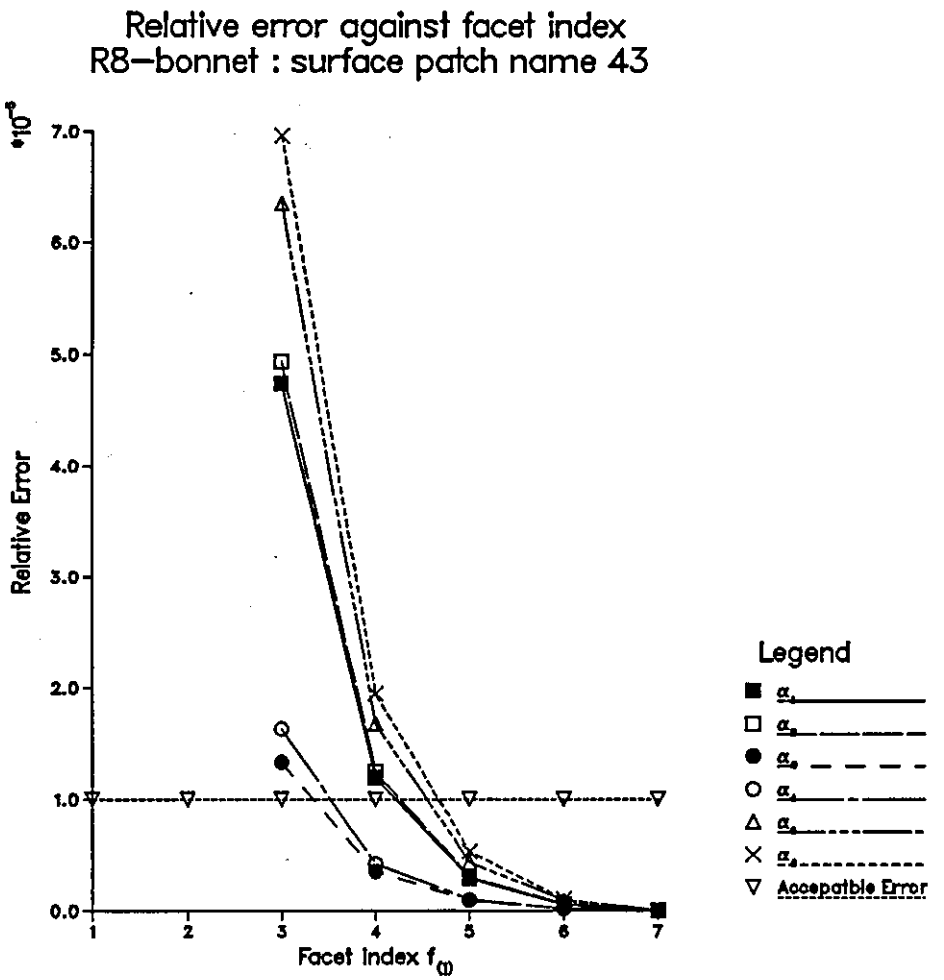

Figure(4.21) : Relative error against facet index for the R8-bonnet.

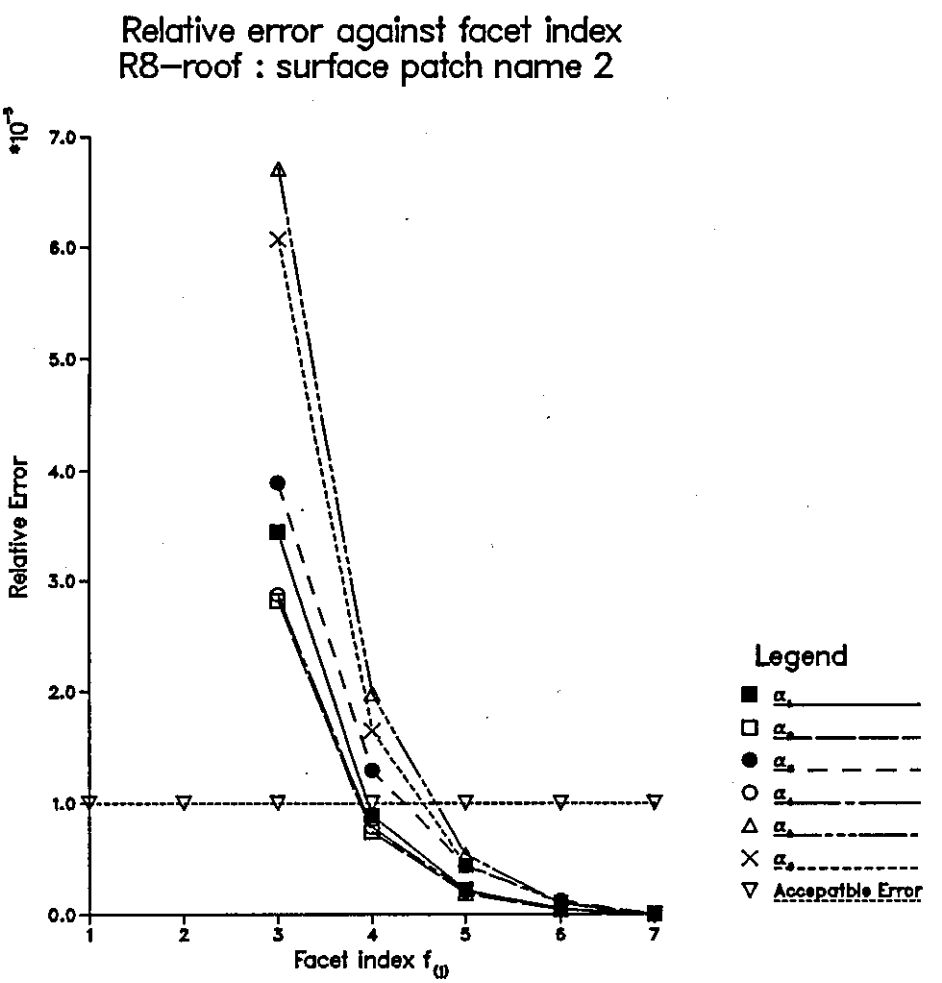

Figure(4.22) : Relative error against facet index for the R8-roof.

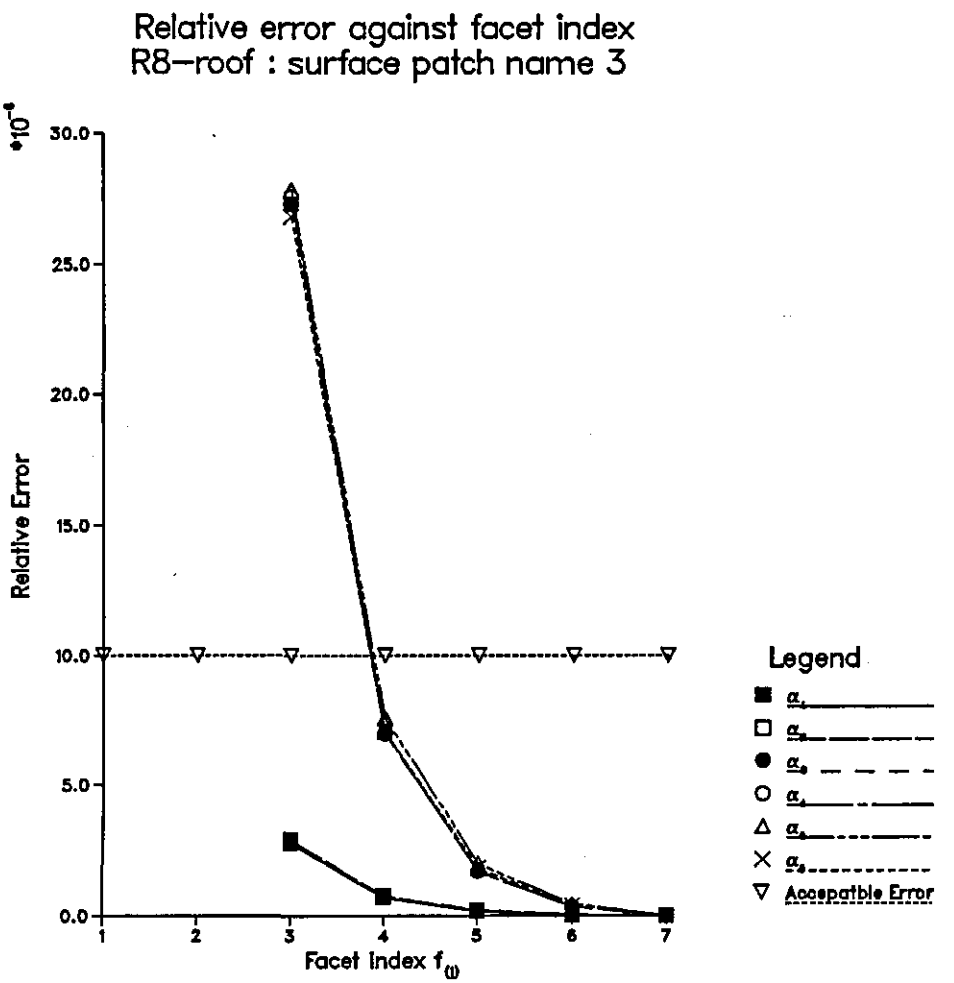

Figure(4.23) : Relative error against facet index for the R8-roof.

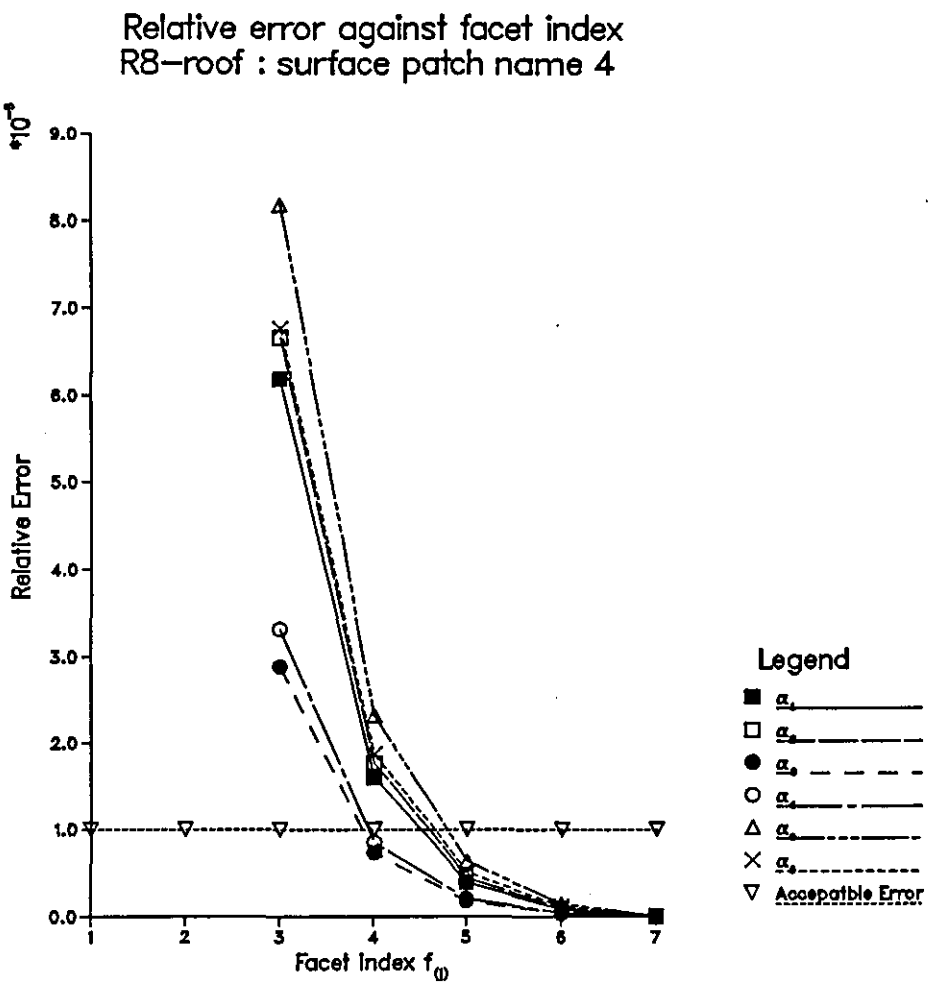

Figure(4.24) : Relative error against facet index for the R8-roof.

CHAPTER 5

ESTIMATION OF SMALL STRAINS ON TWO PRODUCTION PANELS.

In Chapter 4 we identified the best choice of mesh parameters to ensure an acceptable tolerance for the evaluation of arc length using a faceting technique, for a given surface patch/plane intersect. In this Chapter we present the results of applying the radial range subdivision method to a number of strain sets on two production panels; the R8-bonnet and R8-roof.

The number, size and orientation of the strain sets on the production blanks for the R8-bonnet and R8-roof are described in section(5.1). After pressing, strain sets are located within surface patches, which are also identified in section (5.1).

The results of the radial range subdivision method are presented in section(5.2). We identify the problem of interpreting large amounts of strain data and discuss principal strains and associated principal directions, presented graphically, in sections (5.3) and (5.4), respectively.

(5.1) Location of strain sets on production blanks.

We illustrate the location of strain sets on the production blanks for the R8-bonnet and R8-roof in Figures (5.1) and (5.2). Each strain set is etched on a blank such that after pressing it is within a single surface patch, as illustrated in Figures(5.3) and (5.4).

To ensure the strain sets are located within a single surface patch, allowance for the the sheet metal in contact with the blank holder and the deformation of the sheet metal to a doubly curved surface is made. In practice the surface patches of interest are generally flat, so a first order approximation of the arc length of the patch boundaries is sufficient to project onto the blank.

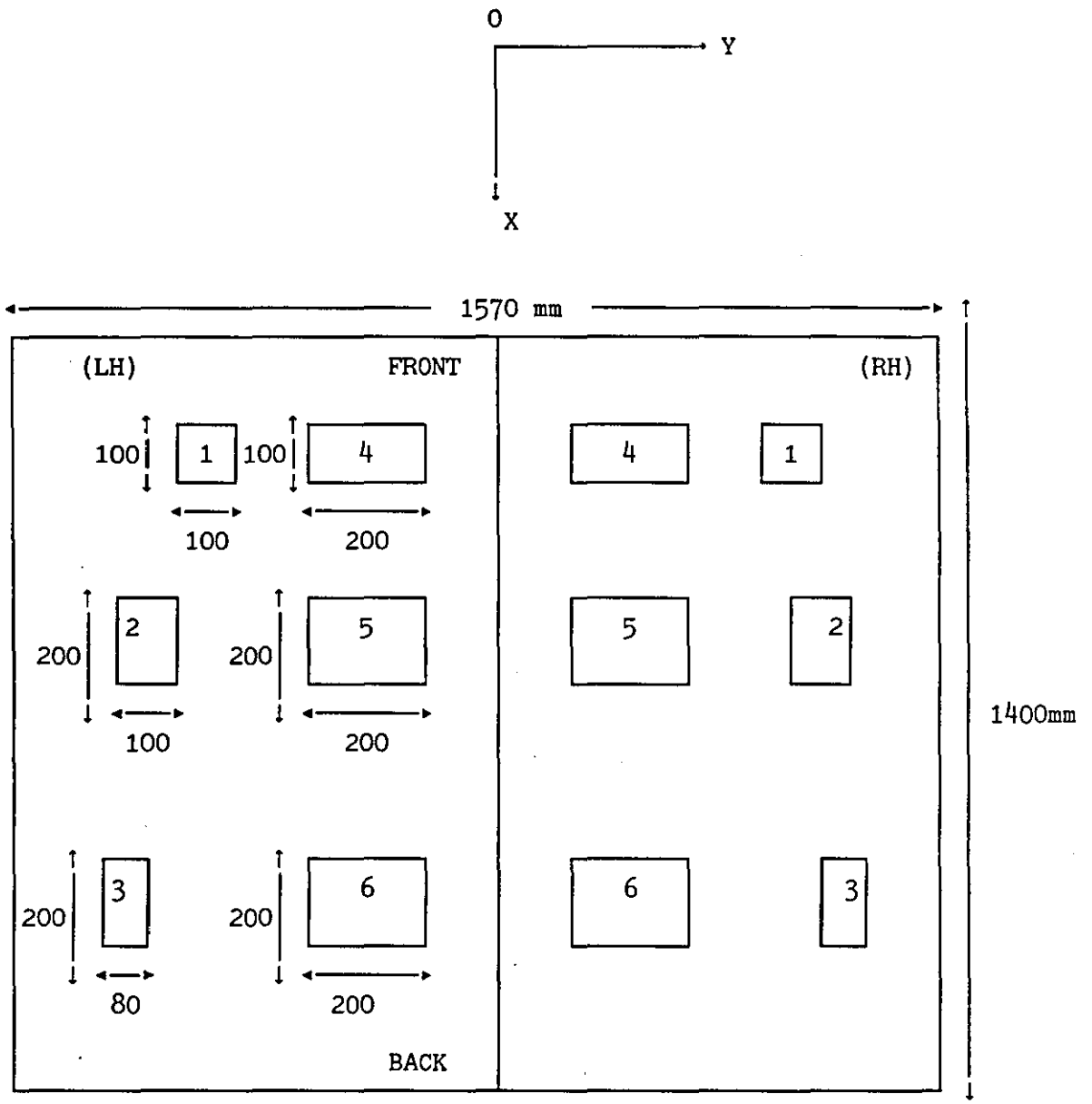

Figure (5.1) : The location, size and orientation of strain sets on the blank for the R8-bonnet.

KEY

LH - Left hand side.

RH - Right hand side.

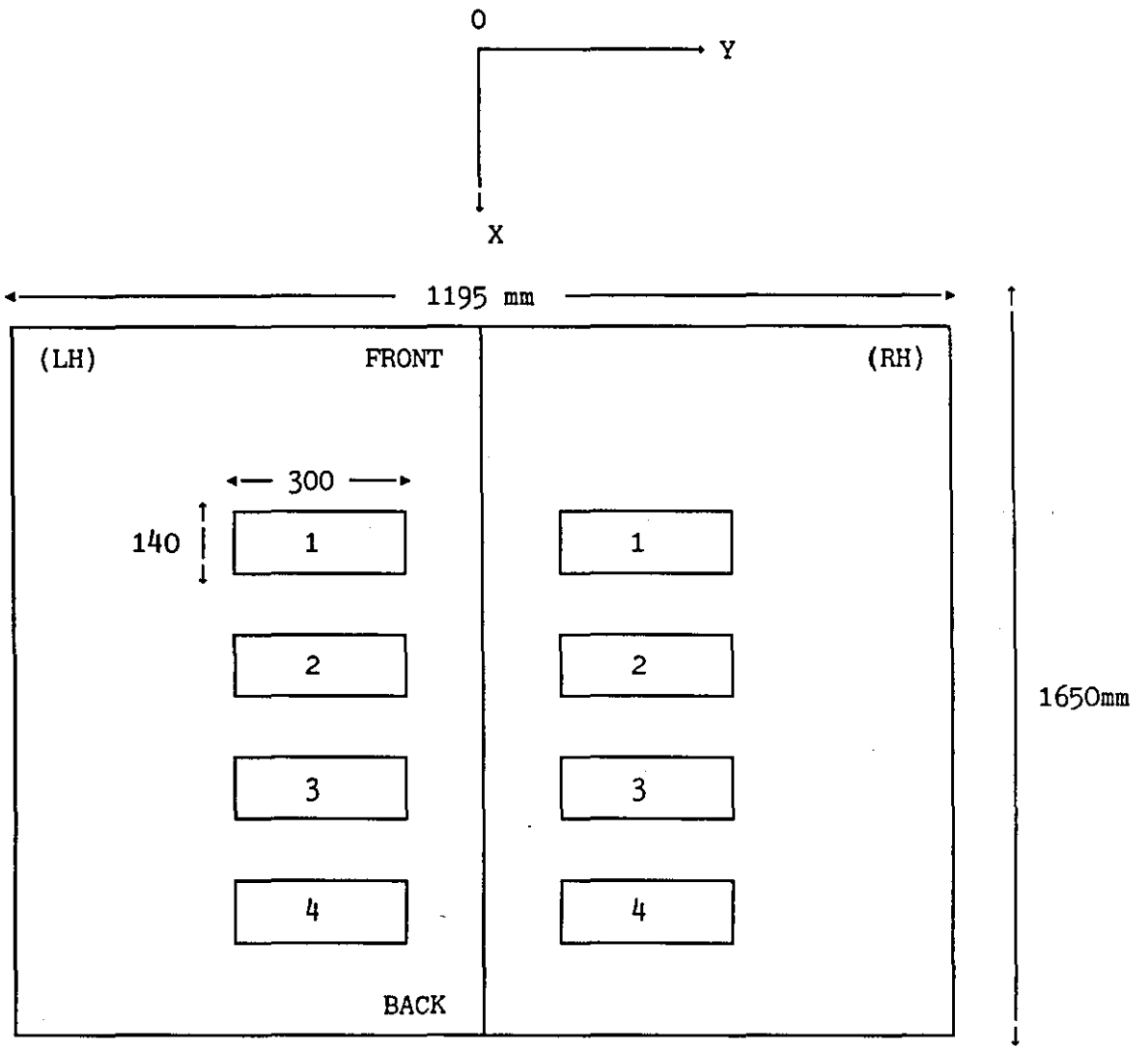

Figure (5.2) : The location, size and orientation of strain sets on the blank for the R8-roof.

KEY

LH - Left hand side.

RH - Right hand side.

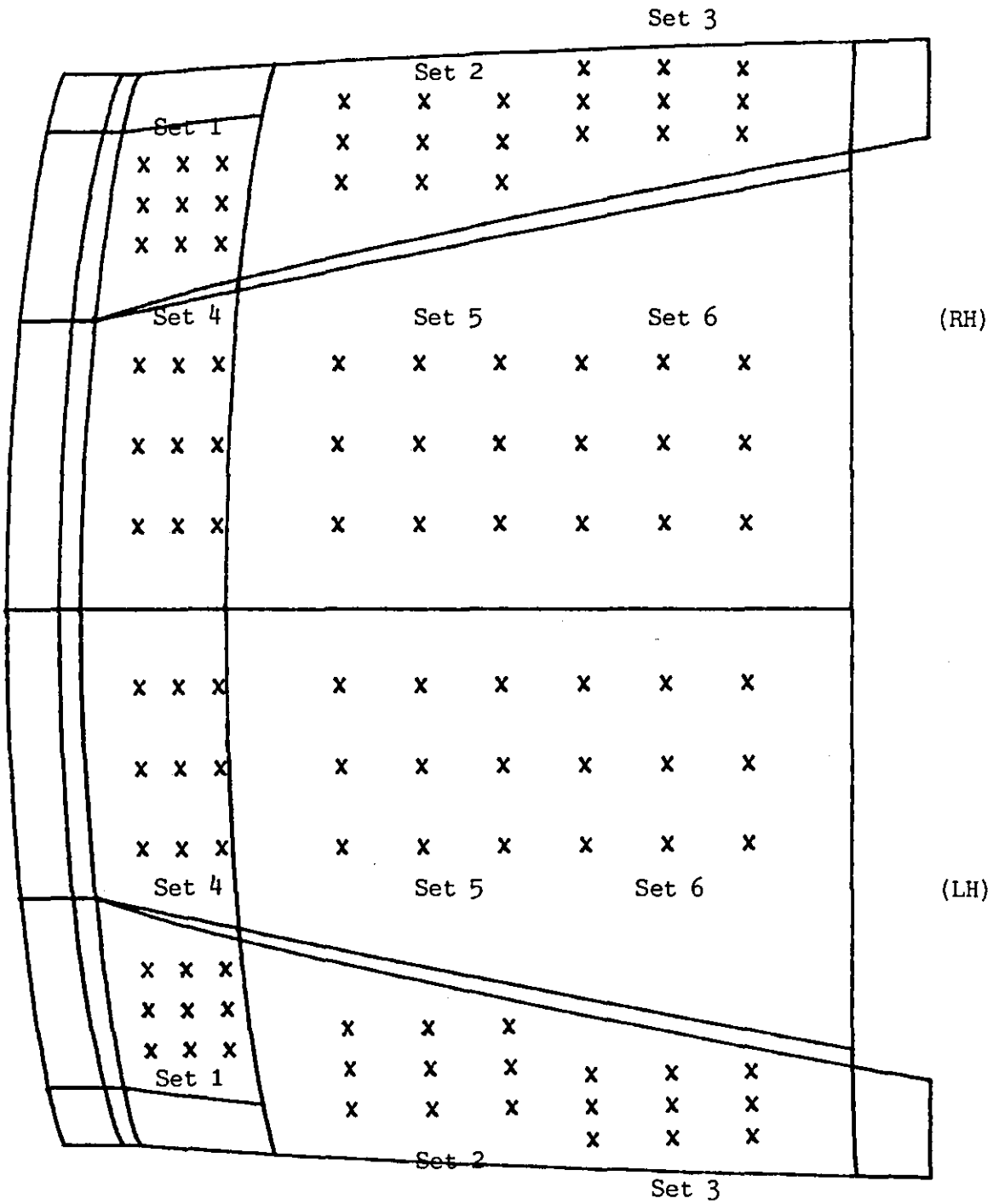

Figure (5.3) : The R8-bonnet with strain sets identified.

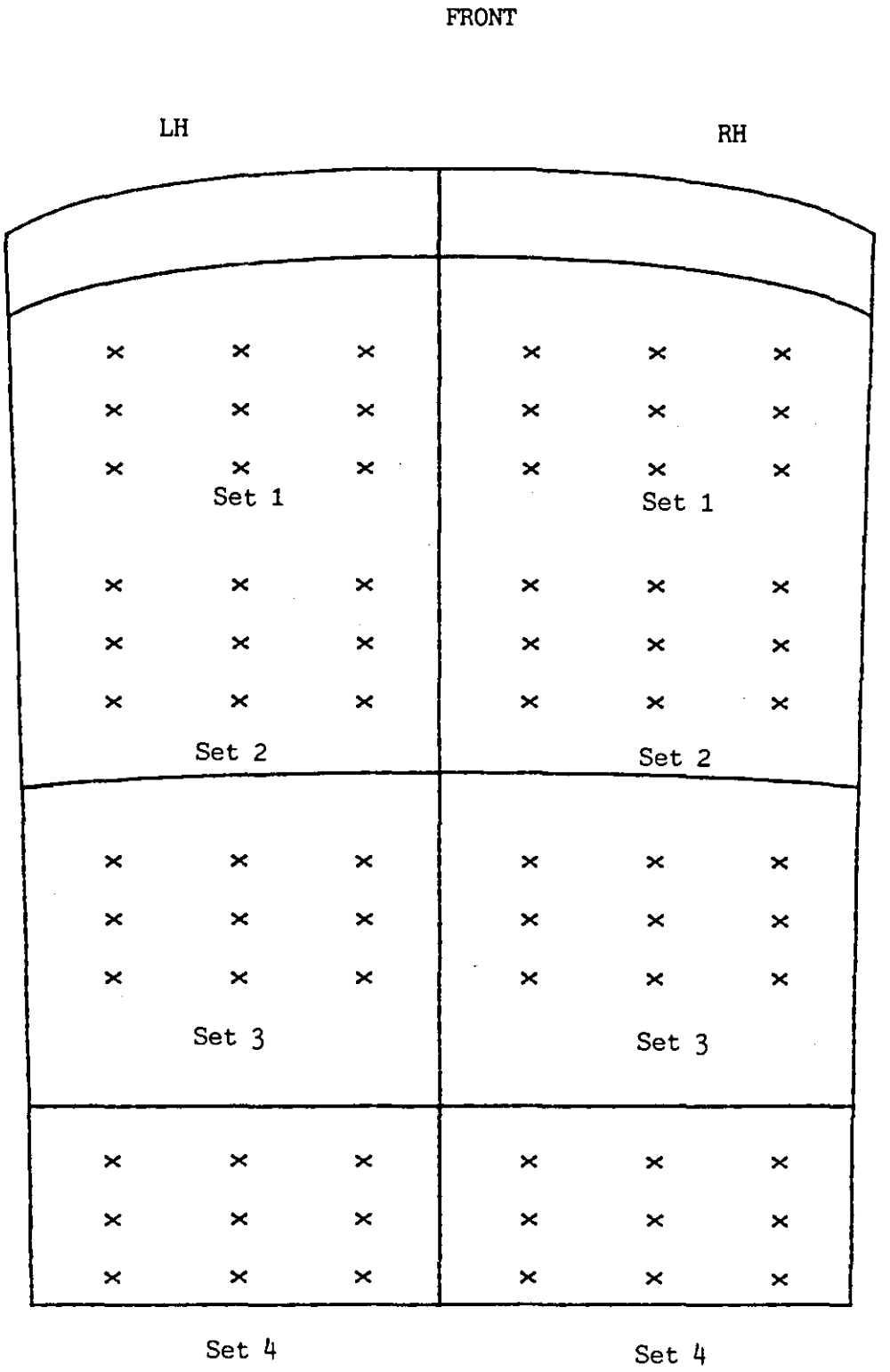

Figure (5.4) : The R8-roof with strain sets identified.

5.2) Tabulated results.

The results of applying the shortest planar path algorithm to estimate the strains on two production panels : R8-bonnet and R8-roof, are presented respectively in **Tables** (5.1) - (5.12) and **Tables** (5.13) - (5.20). Each table identifies the surface type : R8-bonnet or R8-roof, the left hand side or the right hand side of the model, the surface name of the patch and the strain set number.

We note that large amounts of strain data are to be generated, eg. for the R8-bonnet and R8-roof, it is proposed to consider 12 different material types. Clearly this indicates a problem in interpreting a large amount of strain data. In the next two sections we address this problem by considering graphical presentation of the principal strains and their principal directions in sections(5.3) and (5.4), respectively.

R8-bonnet (LH) : Surface name 31 : Strain Set 1				
STRAIN PTS.	%PRINCIPAL STRAINS	PRINCIPAL DIRECTIONS X	Y	Z
1	3.6308	0.8976	0.2711	0.3473
	2.1476	-0.2731	0.9609	-0.0444
2	3.1840	0.8856	0.3616	0.2909
	2.7182	-0.3603	0.9307	-0.0601
3	3.1757	0.8976	0.3571	0.2578
	2.6680	-0.3571	0.9326	-0.0485
4	3.8417	0.8950	0.2722	0.3530
	2.2526	-0.2771	0.9600	-0.0376
5	3.2055	0.8889	0.3492	0.2961
	2.5649	-0.3506	0.9350	-0.0501
6	2.8415	-0.4013	0.9141	-0.0550
	2.7778	-0.8783	-0.4012	-0.2595
7	4.3525	0.9051	0.2215	0.3628
	2.1062	-0.2344	0.9720	-0.0085
8	3.4764	0.8981	0.3170	0.3042
	2.3491	-0.3231	0.9457	-0.0316
9	3.2096	-0.4441	0.8937	-0.0603
	2.5105	-0.8567	-0.4434	-0.2625

Table (5.1) : Principal strains and directions for R8-bonnet.

R8-bonnet (LH) : Surface name 41 : Strain Set 2				
STRAIN PTS.	%PRINCIPAL STRAINS	PRINCIPAL DIRECTIONS X	Y	Z
1	3.2245	-0.6497	0.7541	-0.0944
	1.4449	0.7309	0.6540	0.1945
2	2.6878	-0.5918	0.8035	-0.0644
	1.7433	0.7843	0.5924	0.1839
3	2.2780	-0.4728	0.8807	-0.0271
	2.1652	0.8647	0.4697	0.1776
4	3.2860	0.7629	-0.6353	0.1190
	1.4221	0.6120	0.7692	0.1830
5	2.8737	0.7779	-0.6196	0.1038
	1.5644	0.6005	0.7819	0.1670
6	2.2126	0.8792	-0.4618	0.1168
	1.9979	0.4460	0.8842	0.1388
7	3.2906	0.8253	-0.5492	0.1303
	1.5738	0.5250	0.8317	0.1799
8	2.6810	0.8694	-0.4782	0.1233
	1.6873	0.4585	0.8744	0.1578
9	2.3532	0.0625	0.9936	0.0941
	1.3531	0.9842	-0.0770	0.1593

Table (5.2) : Principal strains and directions for R8-bonnet.

R8-bonnet (LH) : Surface name 41 : Strain Set 3				
STRAIN PTS.	%PRINCIPAL STRAINS	PRINCIPAL DIRECTIONS X	Y	Z
1	2.3824	-0.1855	0.9815	0.0465
	1.6264	0.9706	0.1756	0.1644
2	1.9570	0.9010	0.4023	0.1623
	1.9079	-0.4100	0.9119	0.0154
3	2.4302	0.8504	0.5018	0.1577
	1.5746	-0.5091	0.8606	0.0070
4	2.6503	-0.0673	0.9948	0.0767
	1.2518	0.9862	0.0546	0.1562
5	2.4054	-0.2560	0.9652	0.0530
	1.4670	0.9566	0.2450	0.1577
6	1.9684	0.8905	0.4262	0.1587
	1.6483	-0.4361	0.8992	0.0322
7	2.8519	-0.0671	0.9932	0.0956
	1.0779	0.9866	0.0517	0.1549
8	2.9223	-0.1332	0.9869	0.0914
	0.9775	0.9817	0.1187	0.1491
9	1.6382	-0.9006	-0.4031	-0.1620
	1.4959	-0.4160	0.9076	0.0543

Table (5.3) : Principal strains and directions for R8-bonnet.

R8-bonnet (LH) : Surface name 33 : Strain Set 4				
STRAIN PTS.	%PRINCIPAL STRAINS	PRINCIPAL DIRECTIONS X	Y	Z
1	4.7023	-0.9301	-0.1111	-0.3501
	1.3166	-0.1082	0.9937	-0.0278
2	4.4539	-0.9489	-0.1046	-0.2975
	1.0220	-0.1031	0.9944	-0.0210
3	4.1715	-0.9561	-0.1195	-0.2676
	1.1862	-0.1179	0.9928	-0.0224
4	4.7367	-0.9332	-0.0573	-0.3547
	1.1555	-0.0632	0.9980	0.0050
5	4.5377	-0.9493	-0.0928	-0.3004
	1.1263	-0.0960	0.9954	-0.0044
6	4.2759	-0.9523	-0.1429	-0.2696
	1.2448	-0.1439	0.9894	-0.0162
7	4.6712	0.9295	0.0838	0.3591
	1.1243	-0.0946	0.9954	0.0126
8	4.3457	0.9444	0.1228	0.3048
	1.3084	-0.1301	0.9915	0.0040
9	4.0576	-0.9522	-0.1364	-0.2733
	1.1997	-0.1426	0.9897	0.0029

Table (5.4) : Principal strains and directions for R8-bonnet.

R8-bonnet (LH) : Surface name 43 : Strain Set 5				
STRAIN PTS.	%PRINCIPAL STRAINS	PRINCIPAL DIRECTIONS X	Y	Z
1	3.8722	0.9703	0.1074	0.2168
	1.1768	-0.1067	0.9942	-0.0148
2	3.7989	0.9753	0.1050	0.1942
	0.6437	-0.1046	0.9944	-0.0124
3	3.8186	-0.9839	-0.0288	-0.1763
	0.9422	-0.0297	0.9996	0.0027
4	3.9900	-0.9740	-0.0587	-0.2186
	1.1621	-0.0618	0.9981	0.0074
5	3.6833	-0.9764	-0.0913	-0.1957
	0.9806	-0.0933	0.9956	0.0010
6	3.3559	0.9757	0.1283	0.1773
	1.0062	-0.1295	0.9916	-0.0049
7	3.6051	0.9662	0.1308	0.2222
	1.2997	-0.1358	0.9907	0.0075
8	3.4271	0.9727	0.1196	0.1990
	1.3740	-0.1240	0.9922	0.0102
9	3.2489	-0.9792	-0.0935	-0.1798
	0.8967	-0.0978	0.9951	0.0149

Table (5.5) : Principal strains and directions for R8-bonnet.

R8-bonnet (LH) : Surface name 43 : Strain Set 6				
STRAIN PTS.	%PRINCIPAL STRAINS	PRINCIPAL DIRECTIONS X	Y	Z
1	3.8799	-0.9862	-0.0399	-0.1605
	1.2008	-0.0407	0.9992	0.0013
2	4.0384	-0.9893	-0.0057	-0.1457
	0.7585	-0.0067	1.0000	0.0068
3	4.1882	-0.9913	0.0035	-0.1315
	0.6311	0.0024	1.0000	0.0082
4	3.5556	-0.9853	0.0624	-0.1590
	0.9289	0.0588	0.9979	0.0272
5	3.7893	-0.9885	0.0428	-0.1448
	0.7299	0.0399	0.9989	0.0230
6	4.0103	-0.9908	0.0359	-0.1307
	0.6000	0.0334	0.9992	0.0214
7	3.4391	-0.9842	0.0797	-0.1583
	0.6483	0.0739	0.9963	0.0426
8	3.5753	-0.9876	0.0625	-0.1439
	0.6971	0.0577	0.9976	0.0378
9	3.6637	0.9886	-0.0777	0.1288
	0.6008	0.0733	0.9966	0.0382

Table (5.6) : Principal strains and directions for R8-bonnet.

R8-bonnet (RH) : Surface name 31 : Strain Set 1				
STRAIN PTS.	%PRINCIPAL STRAINS	PRINCIPAL DIRECTIONS X	Y	Z
1	3.6084	-0.9061	0.2288	-0.3556
	1.7299	0.2330	0.9719	0.0314
2	3.2383	-0.9120	0.2800	-0.2994
	1.8547	0.2822	0.9585	0.0367
3	2.9720	-0.9114	0.3170	-0.2619
	2.0994	0.3182	0.9471	0.0390
4	3.7666	0.8991	-0.2463	0.3616
	2.0245	0.2522	0.9671	0.0314
5	3.1883	0.8909	-0.3395	0.3013
	2.6337	0.3408	0.9386	0.0500
6	2.8958	-0.9018	0.3407	-0.2653
	2.3141	0.3428	0.9384	0.0399
7	3.5262	0.8704	-0.3266	0.3677
	2.7384	0.3311	0.9419	0.0528
8	3.3240	0.4004	0.9141	0.0617
	3.1241	0.8644	-0.3992	0.3052
9	3.1752	-0.9233	0.2704	-0.2725
	1.9461	0.2775	0.9606	0.0127

Table (5.7) : Principal strains and directions for R8-bonnet.

R8-bonnet (RH) : Surface name 41 : Strain Set 2				
STRAIN PTS.	%PRINCIPAL STRAINS	PRINCIPAL DIRECTIONS X	Y	Z
1	3.2496	0.6158	0.7829	0.0875
	1.4458	-0.7591	0.6194	-0.1995
2	2.8268	0.6226	0.7790	0.0734
	1.6306	-0.7597	0.6243	-0.1818
3	2.3973	-0.7422	-0.6643	-0.0882
	1.9871	-0.6481	0.7451	-0.1576
4	3.4833	-0.7228	-0.6820	-0.1099
	1.2097	-0.6580	0.7282	-0.1907
5	2.7821	-0.7738	-0.6247	-0.1047
	1.6007	-0.6053	0.7780	-0.1679
6	2.1456	-0.9147	-0.3825	-0.1301
	2.1285	-0.3671	0.9213	-0.1277
7	3.3097	-0.8122	-0.5685	-0.1291
	1.2099	-0.5439	0.8187	-0.1828
8	2.6379	-0.8543	-0.5053	-0.1208
	1.6635	-0.4854	0.8592	-0.1612
9	2.1613	-0.9179	-0.3767	-0.1247
	2.1596	-0.3600	0.9227	-0.1377

Table (5.8) : Principal strains and directions for R8-bonnet.

R8-bonnet (RH) : Surface name 41 : Strain Set 3				
STRAIN PTS.	%PRINCIPAL STRAINS	PRINCIPAL DIRECTIONS X	Y	Z
1	2.4825	-0.1208	0.9882	-0.0940
	1.2441	-0.9806	-0.1335	-0.1435
2	2.6193	0.0651	0.9953	-0.0711
	1.0101	-0.9876	0.0541	-0.1473
3	1.8579	0.1708	0.9833	-0.0626
	0.9191	-0.9763	0.1603	-0.1454
4	2.3811	-0.0661	0.9932	-0.0962
	0.8858	0.9861	0.0797	0.1458
5	2.5908	0.0809	0.9935	-0.0796
	0.7842	0.9868	-0.0686	0.1467
6	2.1521	0.1731	0.9821	-0.0742
	0.7934	-0.9763	0.1611	-0.1444
7	2.0729	-0.1745	0.9762	-0.1290
	0.8036	0.9731	0.1910	0.1288
8	2.5716	0.0831	0.9917	-0.0979
	0.5852	0.9870	-0.0683	0.1453
9	2.4644	0.1657	0.9816	-0.0946
	0.6528	-0.9781	0.1513	-0.1431

Table (5.9) : Principal strains and directions for R8-bonnet.

R8-bonnet (RH) : Surface name 33 : Strain Set 4				
STRAIN PTS.	%PRINCIPAL STRAINS	PRINCIPAL DIRECTIONS X	Y	Z
1	4.8757	0.9302	-0.1047	0.3517
	1.3560	0.1018	0.9944	0.0268
2	4.4446	0.9505	-0.0855	0.2987
	1.3141	0.0846	0.9963	0.0162
3	4.0125	0.9623	-0.0395	0.2691
	1.2156	0.0405	0.9992	0.0017
4	4.5875	0.9231	-0.1436	0.3567
	1.3972	0.1433	0.9892	0.0275
5	4.3864	0.9514	-0.0596	0.3021
	1.1147	0.0639	0.9979	-0.0044
6	4.0012	-0.9618	0.0388	-0.2709
	1.1685	0.0434	0.9990	-0.0110
7	4.2068	0.9264	-0.0958	0.3641
	1.1754	0.1052	0.9944	-0.0060
8	4.4720	0.9499	-0.0593	0.3070
	0.9560	0.0693	0.9974	-0.0215
9	4.5852	0.9550	-0.1122	0.2746
	1.2505	0.1189	0.9929	-0.0079

Table (5.10) : Principal strains and directions for R8-bonnet.

R8-bonnet (RH) : Surface name 43 : Strain Set 5				
STRAIN PTS.	%PRINCIPAL STRAINS	PRINCIPAL DIRECTIONS X	Y	Z
1	3.8928	0.9722	-0.0873	0.2173
	1.2987	0.0870	0.9961	0.0110
2	3.7206	0.9805	-0.0243	0.1948
	1.0431	0.0254	0.9997	-0.0029
3	3.4789	0.9834	-0.0410	0.1766
	1.0266	0.0417	0.9991	-0.0003
4	3.6463	0.9734	-0.0666	0.2192
	1.1861	0.0694	0.9976	-0.0049
5	3.5869	0.9802	-0.0301	0.1959
	1.1026	0.0332	0.9994	-0.0125
6	3.5008	-0.9838	0.0249	-0.1773
	0.9547	0.0277	0.9995	-0.0131
7	3.3683	-0.9644	0.1419	-0.2231
	1.2216	0.1464	0.9892	-0.0039
8	3.1697	-0.9730	0.1159	-0.1996
	1.2395	0.1204	0.9927	-0.0102
9	2.9538	0.9811	0.0822	0.1752
	0.9233	-0.0753	0.9961	-0.0458

Table (5.11) : Principal strains and directions for R8-bonnet.

R8-bonnet (RH) : Surface name 43 : Strain Set 6				
STRAIN PTS.	%PRINCIPAL STRAINS	PRINCIPAL DIRECTIONS X	Y	Z
1	3.9468	0.9860	0.0459	0.1601
	0.8917	-0.0441	0.9989	-0.0149
2	3.9599	0.9879	0.0546	0.1453
	0.8296	-0.0529	0.9985	-0.0156
3	3.9968	0.9910	0.0251	0.1315
	0.5620	-0.0238	0.9997	-0.0111
4	3.6875	0.9859	0.0499	0.1598
	0.8844	-0.0465	0.9986	-0.0250
5	3.7690	0.9846	0.1000	0.1437
	0.8762	-0.0965	0.9948	-0.0313
6	3.9198	0.9875	0.0896	0.1298
	0.5179	-0.0866	0.9958	-0.0285
7	3.0355	0.9843	0.0761	0.1591
	0.8916	-0.0703	0.9966	-0.0419
8	3.1879	0.9747	0.1745	0.1394
	1.0107	-0.1685	0.9842	-0.0538
9	3.3524	-0.9714	-0.2022	-0.1236
	0.7379	-0.1968	0.9788	-0.0544

Table (5.12) : Principal strains and directions for R8-bonnet.

R8-roof (LH) : Surface name 2 : Strain Set 1				
STRAIN PTS.	%PRINCIPAL STRAINS	PRINCIPAL DIRECTIONS X	Y	Z
1	0.4217	0.6938	0.7166	0.0718
	0.1716	-0.7145	0.6974	-0.0556
2	0.3480	-0.9053	-0.4196	-0.0662
	0.3121	-0.4194	0.9076	-0.0167
3	0.3013	-0.8336	0.5512	-0.0366
	0.2076	0.5499	0.8343	0.0393
4	0.4724	-0.9888	-0.1153	-0.0947
	0.3351	-0.1181	0.9927	0.0250
5	0.4279	0.7013	0.7091	0.0728
	0.2803	-0.7096	0.7042	-0.0233
6	0.2883	0.1550	0.9870	0.0426
	0.2357	-0.9865	0.1569	-0.0466
7	0.4368	-0.9320	0.3570	-0.0631
	0.4162	0.3501	0.9314	0.0996
8	0.4085	-0.9662	-0.2436	-0.0846
	0.3334	-0.2483	0.9674	0.0499
9	0.3485	0.4162	0.9053	0.0847
	0.3306	-0.9077	0.4192	-0.0205

Table (5.13) : Principal strains and directions for R8-roof.

R8-roof (LH) : Surface name 2 : Strain Set 2				
STRAIN PTS.	%PRINCIPAL STRAINS	PRINCIPAL DIRECTIONS X	Y	Z
1	0.2010	-0.9489	-0.3135	-0.0353
	0.1946	-0.3137	0.9495	0.0017
2	0.2463	-0.9652	-0.2598	-0.0285
	0.1689	-0.2601	0.9656	0.0055
3	0.2643	-0.3883	0.9215	0.0039
	0.2553	-0.9213	-0.3881	-0.0235
4	0.2905	-0.7718	-0.6341	-0.0474
	0.2138	-0.6350	0.7725	0.0053
5	0.3036	-0.6002	0.7998	0.0115
	0.2365	-0.7994	-0.5994	-0.0414
6	0.3797	-0.6012	0.7989	0.0151
	0.1974	-0.7988	-0.6004	-0.0365
7	0.3676	-0.8290	0.5592	0.0097
	0.2122	0.5582	0.8263	0.0751
8	0.3366	-0.9058	0.4236	0.0047
	0.3058	0.4228	0.9033	0.0725
9	0.3123	-0.9223	-0.3838	-0.0446
	0.3102	-0.3859	0.9209	0.0550

Table (5.14) : Principal strains and directions for R8-roof.

R8-roof (LH) : Surface name 3 : Strain Set 3				
STRAIN PTS.	%PRINCIPAL STRAINS	PRINCIPAL DIRECTIONS X	Y	Z
1	0.2963	-0.8085	-0.5883	-0.0131
	0.0808	-0.5884	0.8085	0.0064
2	0.3295	0.2990	0.9542	0.0128
	0.2648	-0.9542	0.2990	0.0021
3	0.3918	-0.6130	0.7900	0.0124
	0.1313	-0.7901	-0.6130	-0.0050
4	0.3822	-0.9791	-0.2030	-0.0138
	0.2802	-0.2034	0.9786	0.0322
5	0.3330	-0.9213	0.3887	0.0115
	0.3327	0.3889	0.9207	0.0324
6	0.2739	0.5900	0.8070	0.0256
	0.2021	-0.8074	0.5896	0.0230
7	0.3156	-0.8354	0.5487	0.0325
	0.2142	0.5497	0.8331	0.0615
8	0.2981	-0.8759	-0.4812	-0.0354
	0.2061	-0.4825	0.8738	0.0601
9	0.3818	-0.7620	-0.6461	-0.0427
	-0.0007	-0.6475	0.7600	0.0558

Table (5.15) : Principal strains and directions for R8-roof.

R8-roof (LH) : Surface name 4 : Strain Set 4				
STRAIN PTS.	%PRINCIPAL STRAINS	PRINCIPAL DIRECTIONS X	Y	Z
1	0.1720	-0.0462	0.9988	0.0146
	-0.0154	-0.9983	-0.0466	0.0336
2	0.2772	0.0379	0.9992	0.0104
	0.0258	-0.9972	0.0371	0.0645
3	0.2589	-0.8185	0.5627	0.1155
	0.0026	0.5593	0.8266	-0.0634
4	0.4899	-0.7328	0.6787	0.0487
	0.0930	0.6796	0.7336	0.0026
5	0.4146	-0.8016	0.5936	0.0714
	0.1703	0.5945	0.8040	-0.0096
6	0.3878	0.0609	0.9978	0.0269
	0.2246	-0.9894	0.0568	0.1337
7	0.5827	-0.4986	0.8630	0.0811
	0.4404	-0.8661	-0.4998	-0.0063
8	0.6506	-0.6710	0.7348	0.0991
	0.1784	-0.7387	-0.6740	-0.0034
9	0.6531	-0.8332	0.5306	0.1555
	0.2206	0.5362	0.8440	-0.0068

Table (5.16) : Principal strains and directions for R8-roof.

R8-roof (RH) : Surface name 2 : Strain Set 1				
STRAIN PTS.	%PRINCIPAL STRAINS	PRINCIPAL DIRECTIONS X	Y	Z
1	0.3780	0.8186	-0.5686	0.0814
	0.1831	0.5674	0.8225	0.0399
2	0.3723	0.8006	-0.5960	0.0617
	0.2222	0.5954	0.8029	0.0292
3	0.2951	0.4390	0.8984	0.0109
	0.2816	0.8970	-0.4389	0.0526
4	0.5071	0.9430	0.3246	0.0736
	0.4340	-0.3203	0.9451	-0.0642
5	0.4080	-0.3983	0.9153	-0.0602
	0.3753	0.9148	0.4012	0.0472
6	0.3997	0.9916	0.1205	0.0477
	0.2678	-0.1186	0.9921	-0.0417
7	0.5773	-0.4028	0.9093	-0.1043
	0.5050	0.9105	0.4097	0.0555
8	0.4582	0.9679	0.2465	0.0495
	0.2960	-0.2418	0.9666	-0.0855
9	0.3728	-0.5959	0.7982	-0.0880
	0.1887	0.8013	0.5983	0.0012

Table (5.17) : Principal strains and directions for R8-roof.

R8-roof (RH) : Surface name 2 : Strain Set 2				
STRAIN PTS.	%PRINCIPAL STRAINS	PRINCIPAL DIRECTIONS X	Y	Z
1	0.3932	-0.6426	0.7655	-0.0312
	0.2931	0.7655	0.6433	0.0168
2	0.3230	0.2143	0.9767	-0.0072
	0.2114	0.9764	-0.2140	0.0282
3	0.3231	-0.1362	0.9906	-0.0157
	0.0481	0.9905	0.1365	0.0182
4	0.2679	0.9671	0.2535	0.0232
	0.2284	-0.2524	0.9667	-0.0420
5	0.2546	-0.0130	0.9993	-0.0349
	0.1902	0.9996	0.0139	0.0256
6	0.2387	-0.1471	0.9884	-0.0370
	0.1086	0.9889	0.1477	0.0147
7	0.2849	0.5248	0.8503	-0.0409
	0.0716	0.8506	-0.5218	0.0647
8	0.2136	0.8073	0.5898	-0.0194
	0.0655	-0.5896	0.8046	-0.0708
9	0.0794	0.3533	0.9337	-0.0573
	0.0413	0.9353	-0.3513	0.0426

Table (5.18) : Principal strains and directions for R8-roof.

R8-roof (RH) : Surface name 3 : Strain Set 3				
STRAIN PTS.	%PRINCIPAL STRAINS	PRINCIPAL DIRECTIONS X	Y	Z
1	0.2163	0.9513	0.3081	0.0025
	0.1609	-0.3081	0.9512	-0.0145
2	0.1821	0.2736	0.9618	-0.0120
	0.1469	0.9618	-0.2736	0.0052
3	0.2716	-0.0469	0.9988	-0.0127
	0.0019	0.9989	0.0468	-0.0043
4	0.3093	0.9803	-0.1972	0.0135
	0.2096	0.1975	0.9798	-0.0325
5	0.2352	0.5523	0.8332	-0.0277
	0.1784	0.8336	-0.5519	0.0206
6	0.1929	-0.3711	0.9281	-0.0305
	0.1859	0.9286	0.3708	-0.0161
7	0.2550	0.8901	-0.4543	0.0375
	0.2118	0.4558	0.8881	-0.0590
8	0.1639	0.3198	0.9452	-0.0657
	0.1426	0.9475	-0.3189	0.0241
9	0.1951	-0.2730	0.9597	-0.0666
	0.0994	0.9620	0.2721	-0.0228

Table (5.19) : Principal strains and directions for R8-roof.

R8-roof (RH) : Surface name 4 : Strain Set 4				
STRAIN PTS.	%PRINCIPAL STRAINS	PRINCIPAL DIRECTIONS X	Y	Z
1	0.1250	-0.3066	0.9518	-0.0017
	0.0521	0.9512	0.3063	-0.0368
2	0.1342	0.9195	0.3879	-0.0644
	0.1150	-0.3879	0.9216	0.0134
3	0.3524	0.8271	0.5496	-0.1172
	-0.1445	-0.5462	0.8353	0.0623
4	0.4656	0.4713	0.8807	-0.0469
	0.2454	0.8813	-0.4724	-0.0139
5	0.5535	0.6438	0.7621	-0.0679
	0.0464	0.7624	-0.6465	-0.0269
6	0.5446	0.7694	0.6261	-0.1263
	-0.0656	-0.6244	0.7789	0.0578
7	0.6841	0.9534	-0.3015	-0.0122
	0.3992	0.2996	0.9507	-0.0802
8	0.8538	0.9470	-0.3189	-0.0390
	0.5324	0.3144	0.9448	-0.0919
9	1.0805	0.4302	0.8932	-0.1306
	0.7023	0.8917	-0.4430	-0.0923

Table (5.20) : Principal strains and directions for R8-roof.

5.3) Principal strains.

In this section we present graphs of principal strains against strain points. This enables appreciation of the principal strain variations :

a) within a strain set.

b) between strain sets.

c) between left hand side and right hand side of a model.

For the purpose of discussion we refer to the rows within a strain set which correspond to the strain points p_1^*, p_2^*, p_3^*; p_4^*, p_5^*, p_6^* and p_7^*, p_8^*, p_9^* as rows R_1, R_2 and R_3, respectively. Hence as we travel from the front to the back of a drawn panel we can refer to the strain variation in a given row.

In section (5.3.1) and (5.3.2) we comment, briefly on the principal strains for the R8-bonnet and R8-roof, respectively. We observe that principal strain variations presented are exaggerated, but if expressed in terms of the principal stresses this would alleviate the problem.

However, we note that the onset of elastic/plastic deformation occurs at the yield point, 0.15% [Tennet;1984] and total plastic deformation occurs, in general, at a strain value, 0.65% [Dixon;1988].

5.3.1) R8-bonnet

Major strains

The graphs for the major strains against strain points for strain sets on the left hand side and the right hand side of the R8-bonnet are presented in Figures (5.5) and (5.6), respectively.

The main features identified are:

(1) The major strain variation on the left hand side and the right hand side of the R8-bonnet is between 1.5% to 5%.

(2) The rows R_1,R_2 and R_3 for the strain sets 1,2,4 and 5 show a decrease, of upto 2%, for the left hand side and right hand side of the R8-bonnet. While the rows R_1,R_2 and R_3 of strain set 6 shows an increasing magnitude.

Minor strains

The graphs for the minor strains against strain points for strain sets on the left hand side and the right hand side of the R8-bonnet are presented in Figures(5.7) and (5.8), respectively. The main features identified in these figures are :

(1) The variation of the minor strain on the left hand side and right hand side of the R8-bonnet is between 0.5% to 3.5%, and we recall the strain, 0.15%, at the yield point, used in Chapter 4 in section(4.3.3) to identify the best mesh parameters.

(2) The data set is not symmetric with respect to the left hand side and the right hand side of the R8-bonnet.

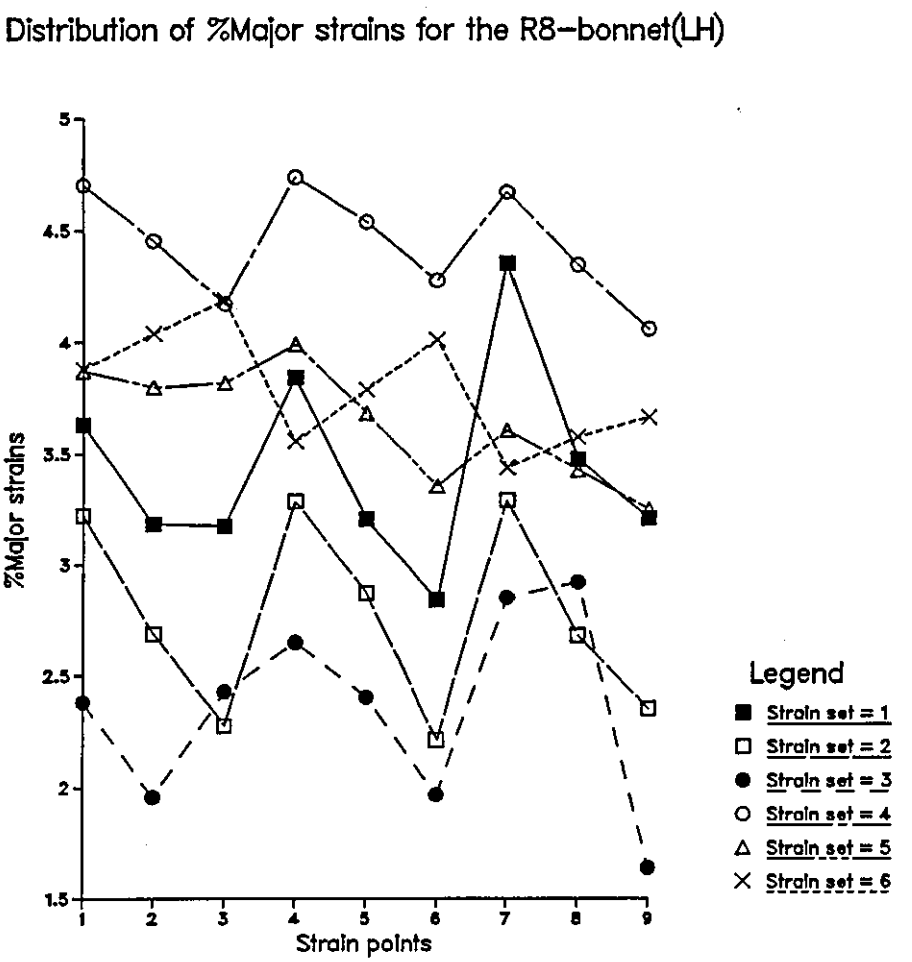

Figure(5.5) : The major strains for the R8-bonnet (LH).

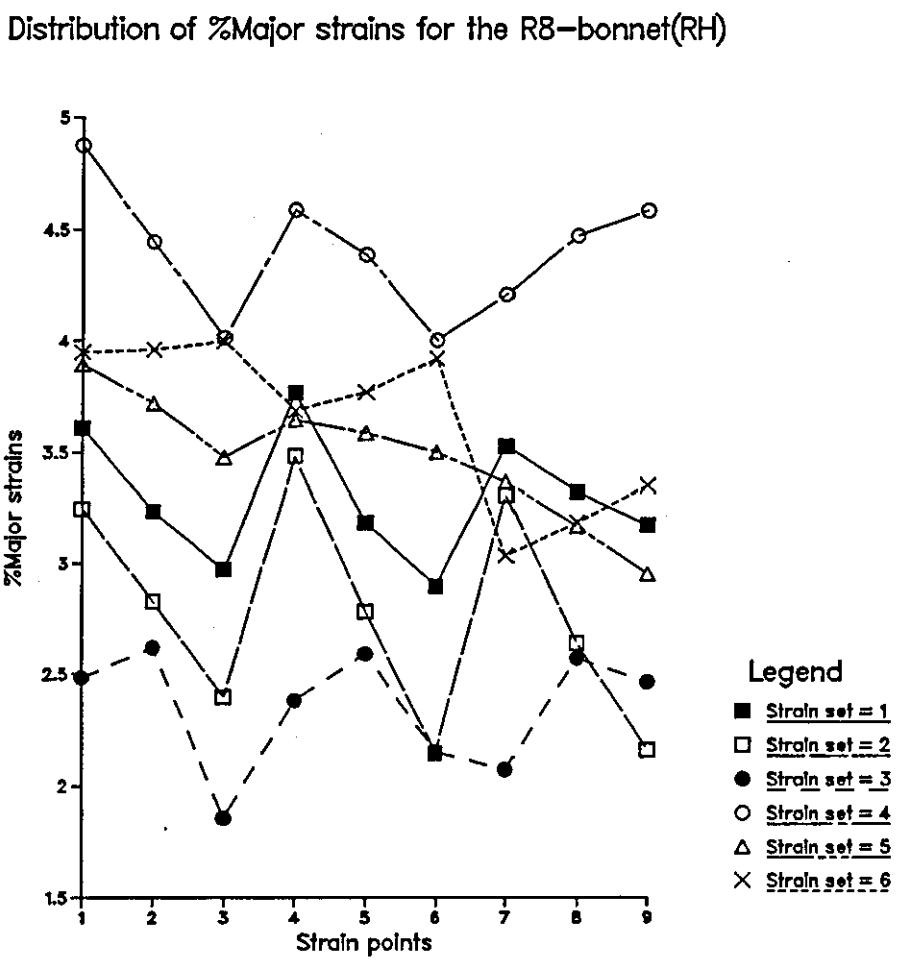

Figure(5.6) : The major strains for the R8-bonnet (RH).

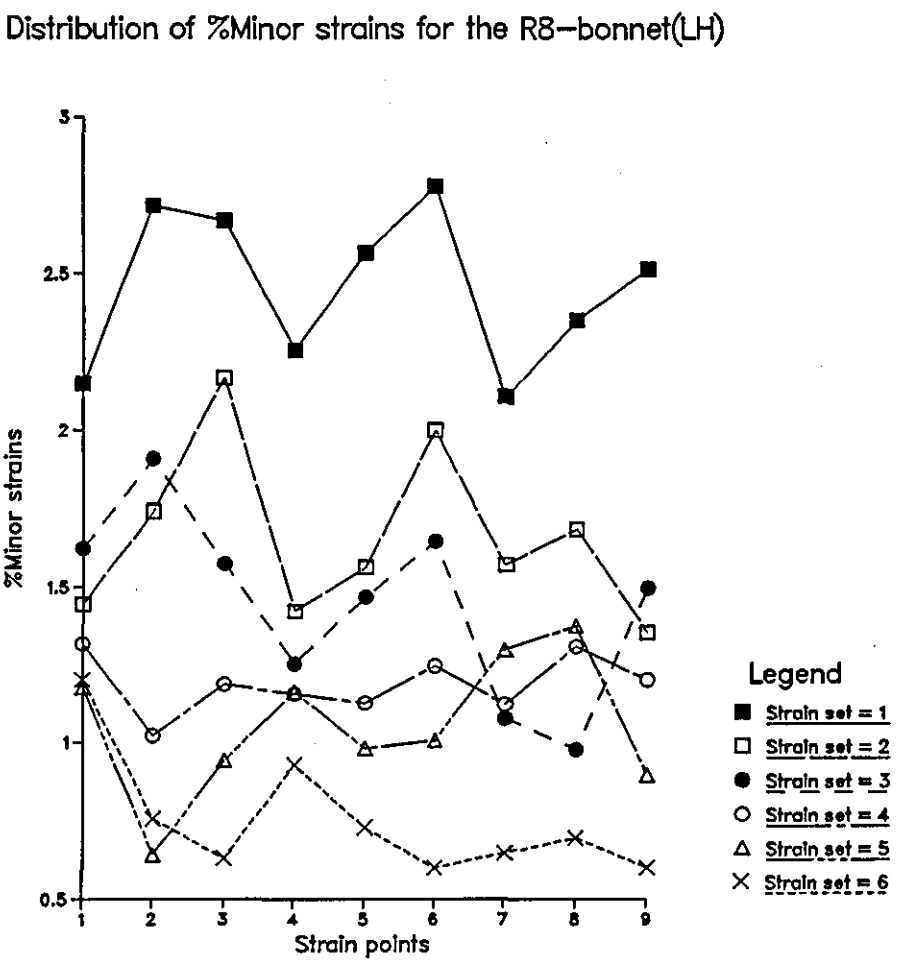

Figure(5.7) : The minor strains for the R8-bonnet (LH).

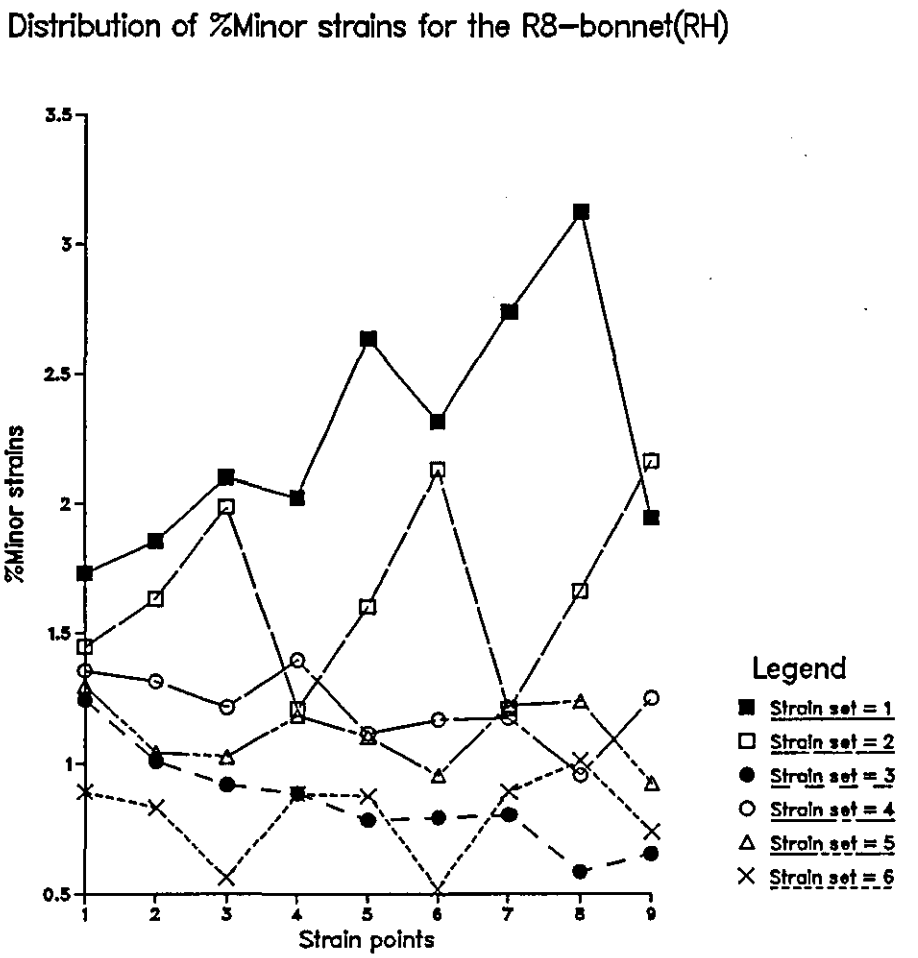

Figure(5.8) : The minor strains for the R8-bonnet (RH).

5.3.2) R8-roof

Major strains

The graphs for the major strains against strain points for the strain sets on the left hand side and right hand side of the R8-roof are presented in Figures (5.9) and (5.10), respectively. The main features identified in these figures are :

(1) The major strain varies between 0.15% to 0.7% on the left hand side of the R8-roof. The major strain varies between 0.1% to 1.1% on the right hand side of the R8-roof.

(2) The major strain variations within the rows R_1,R_2 and R_3 for strain sets 2 to 4 on the left hand side and right hand side of the R8-roof are not symmetric, while that of strain set 1 is symmetric.

Minor strains

The graphs for the minor strains against strain points for strain sets on the left hand side and the right hand side of the R8-roof are presented in Figures(5.11) and (5.12), respectively. The main features identified in these figures are :

(1) The variation of the minor strain on the left hand side of the R8-roof is between -0.05% to 0.45%. The variation of the minor strain on the right hand side of the R8-roof is -0.2% to 0.8%.

(2) The variation of the minor strain for strain sets 2 to 4 is not symmetric, while the variation of strain set 1 is symmetric.

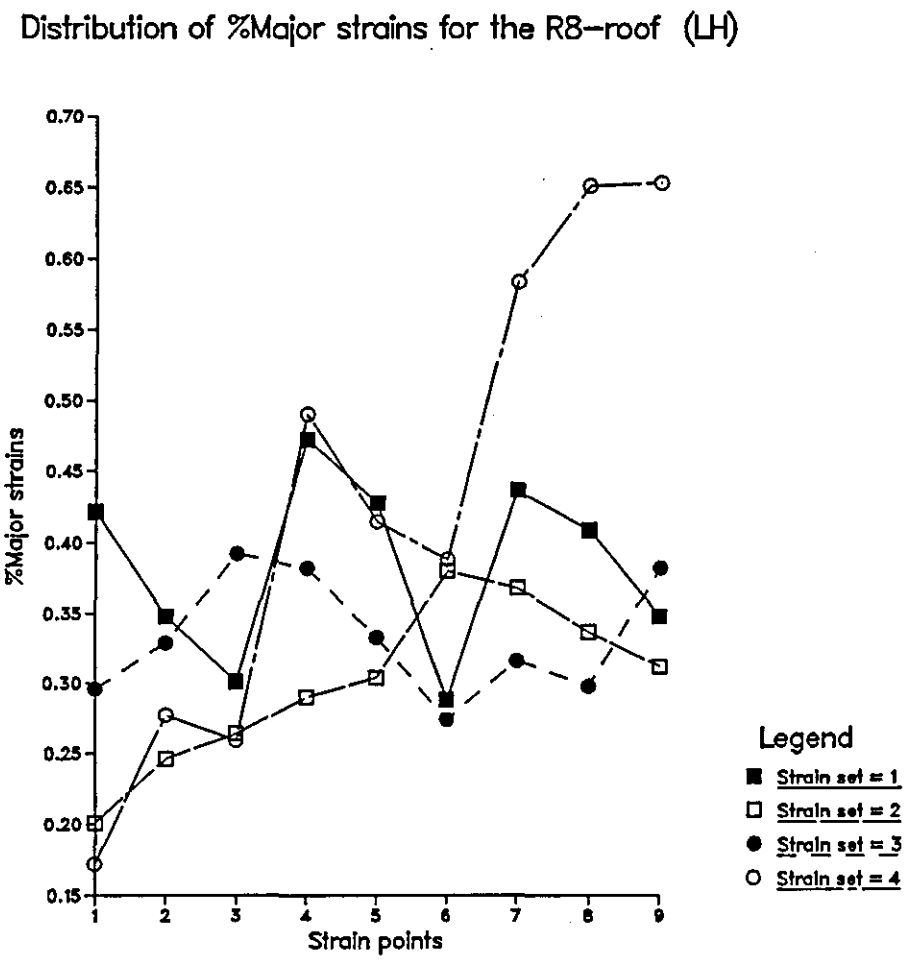

Figure(5.9) : The major strains for the R8-roof (LH).

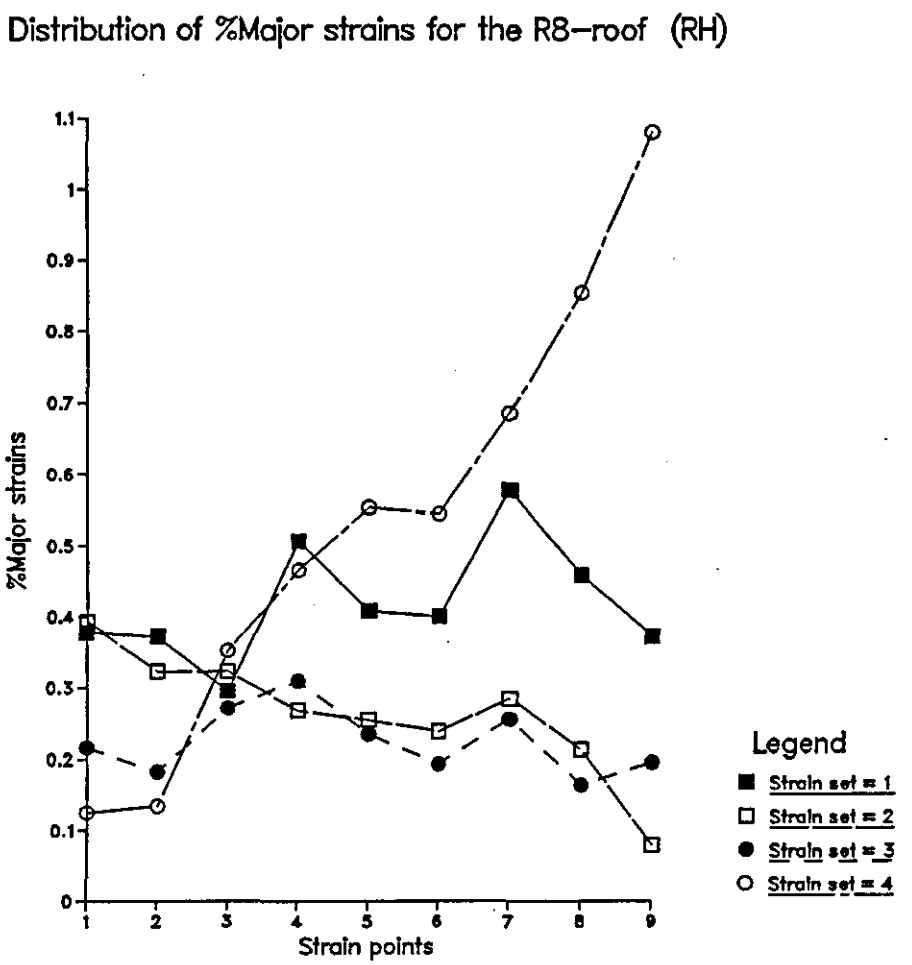

Figure(5.10) : The major strains for the R8-roof (RH).

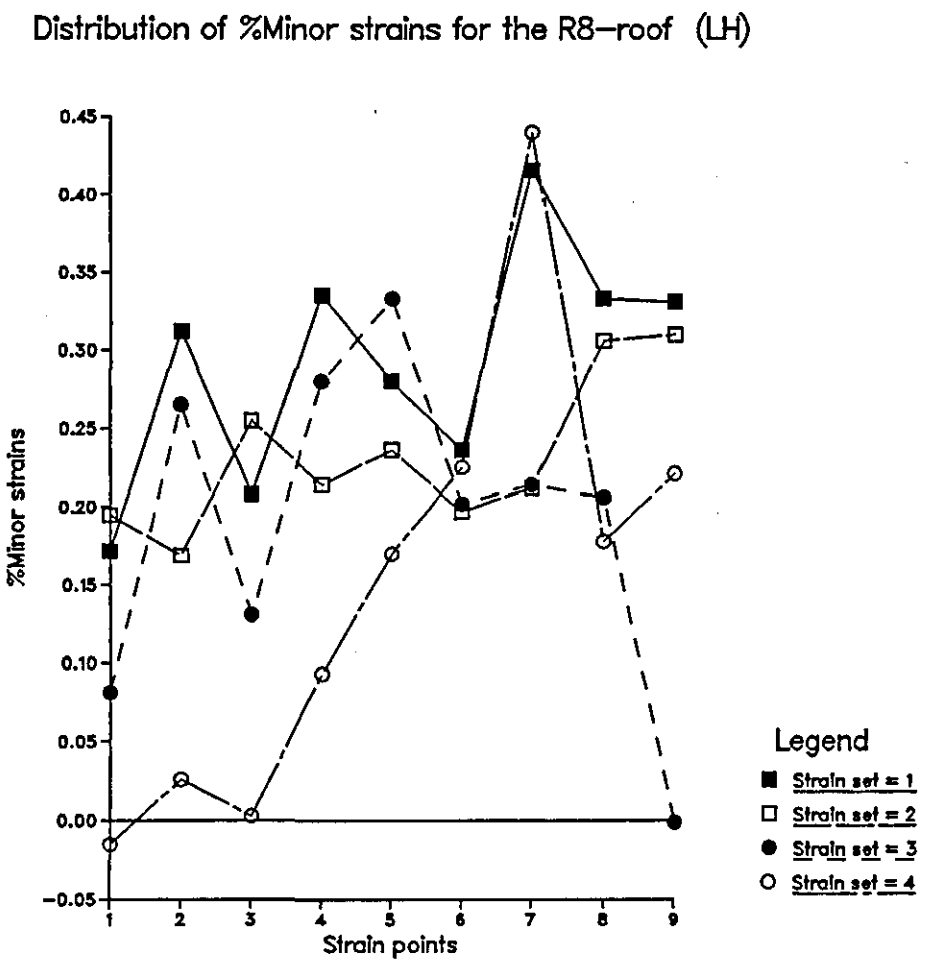

Figure(5.11) : The minor strains for the R8-roof (LH).

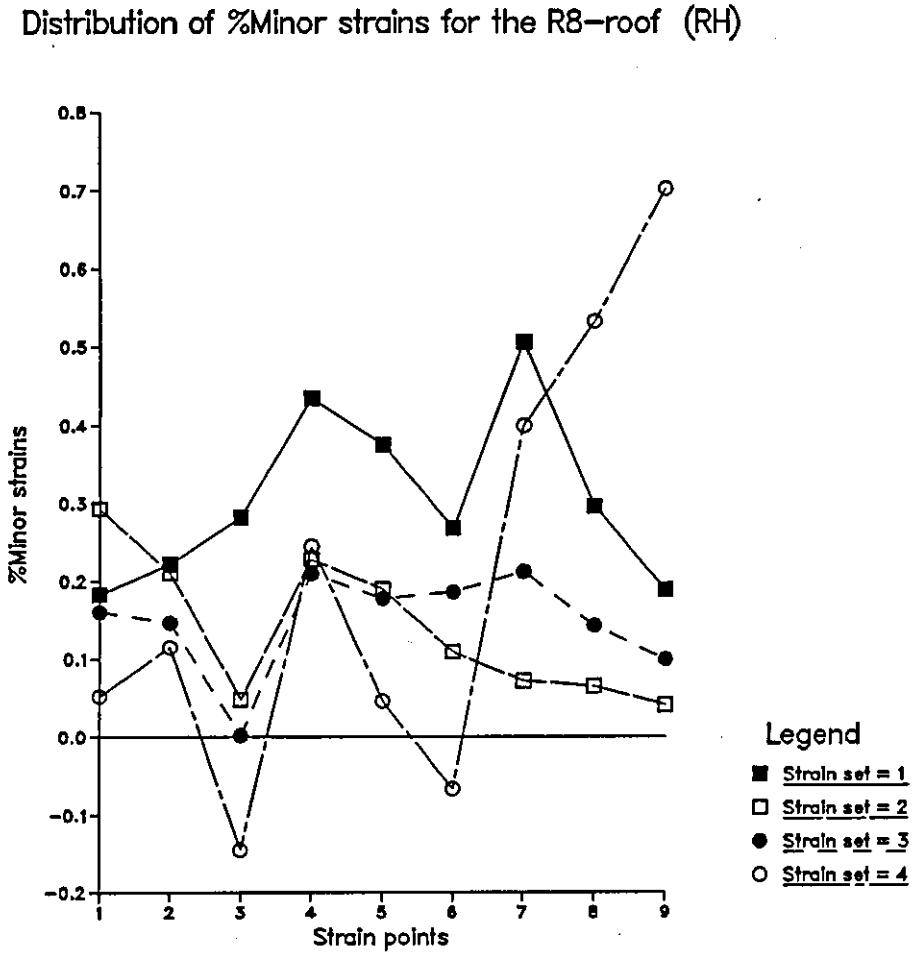

Figure(5.12) : The minor strains for the R8-roof (RH).

5.4) Principal directions

In this section we present a method of interpreting the principal directions graphically. There is a problem of interpreting the principal directions presented in **Tables** (5.1) - (5.20), since each strain point defines its own tangent plane.

To identify if the principal directions of each strain set can be characterized or follow a particular trend, we consider the angle of projection of each tangent direction onto the XY plane, of the blank, and the angle made by this projection to the X axis, the polar coordinate, $\phi \in [0^{o},180^{o}]$.

For each principal direction we plot the polar coordinate against each strain point and can determine the variation of a principal direction :

a) within a strain set.
b) between strain sets.
c) between the left hand side and the right hand side of a model.

In section (5.4.1) and (5.4.2) we comment, briefly, on the distribution of the major and minor polar coordinate for the principal directions for the R8-bonnet and R8-roof, respectively.

5.4.1) R8-bonnet.

The graphs for the variation of the major polar coordinate over the left hand side and right hand side of the R8-bonnet are presented in Figures(5.13) and (5.14), respectively. The main features identified in these figures are :

(1) The dominant directions for strain sets 1,4,5 and 6 are biased to the X axis for both the left hand side and the right hand side of the R8-bonnet.

(2) The dominant direction for strain set 2 on both sidesof the R8-bonnet is biased to 45^0 to the X axis.

(3) The dominant direction in strain set 3 on the left hand side of the R8-bonnet is not clear, while the dominant direction on the right hand side of the R8-bonnet is biased to the Y axis.

The graphs for the variation of the minor polar coordinate over the left hand side and right hand sides of the R8-bonnet are presented in Figures(5.15) and (5.16). The main features of the minor polar coordinate variation are identified in the preceding discussion regarding the distribution of the major polar coordinate. By inspection of the major and minor coordinate we conclude they are close to orthogonal.

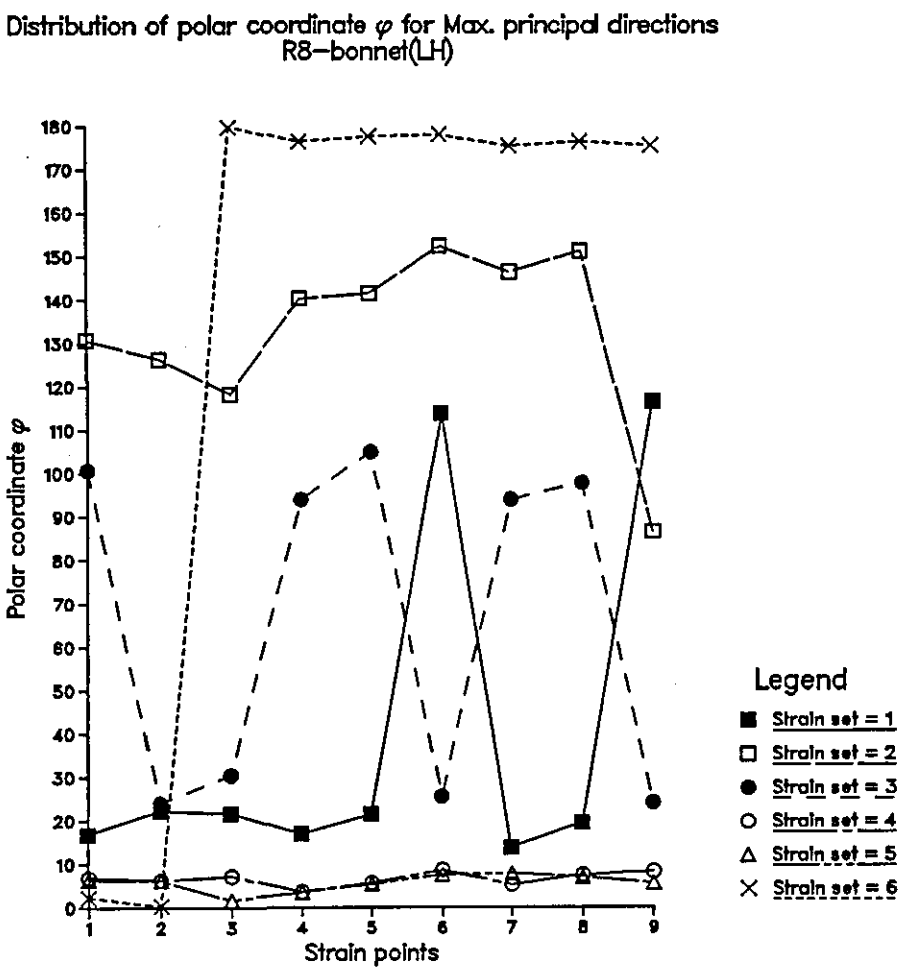

Figure(5.13) : The major directions for the R8-bonnet (LH).

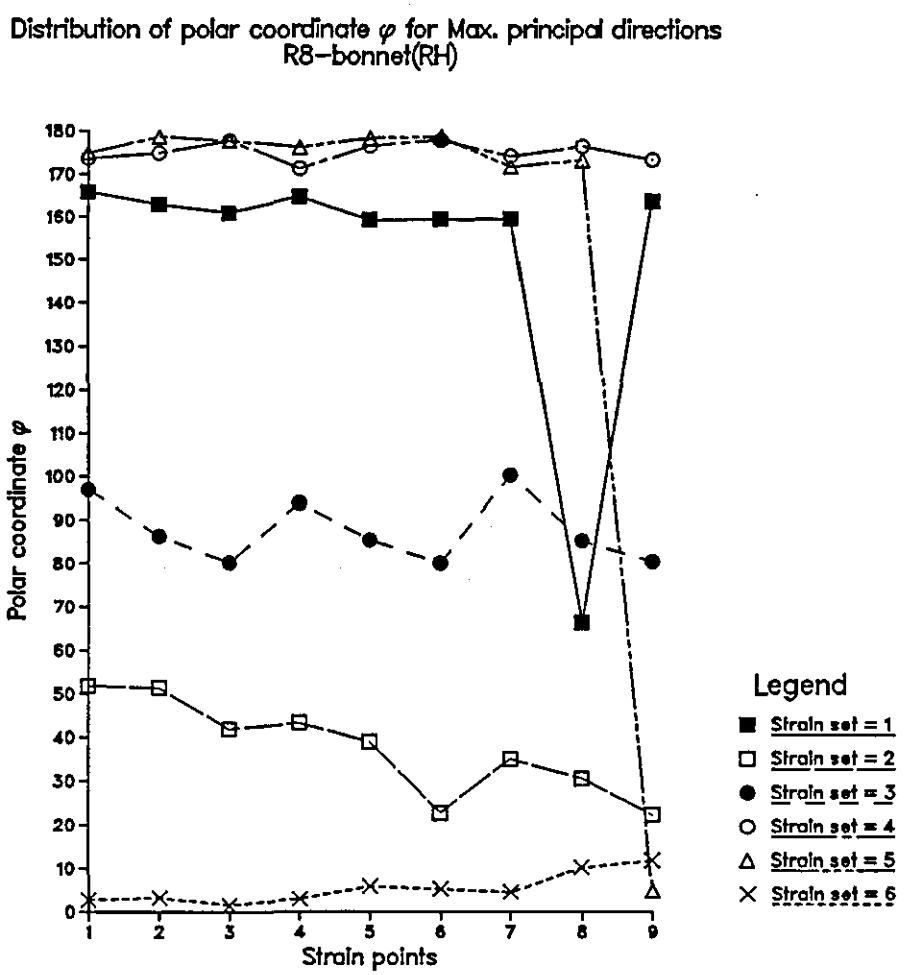

Figure(5.14) : The major directions for the R8-bonnet (RH).

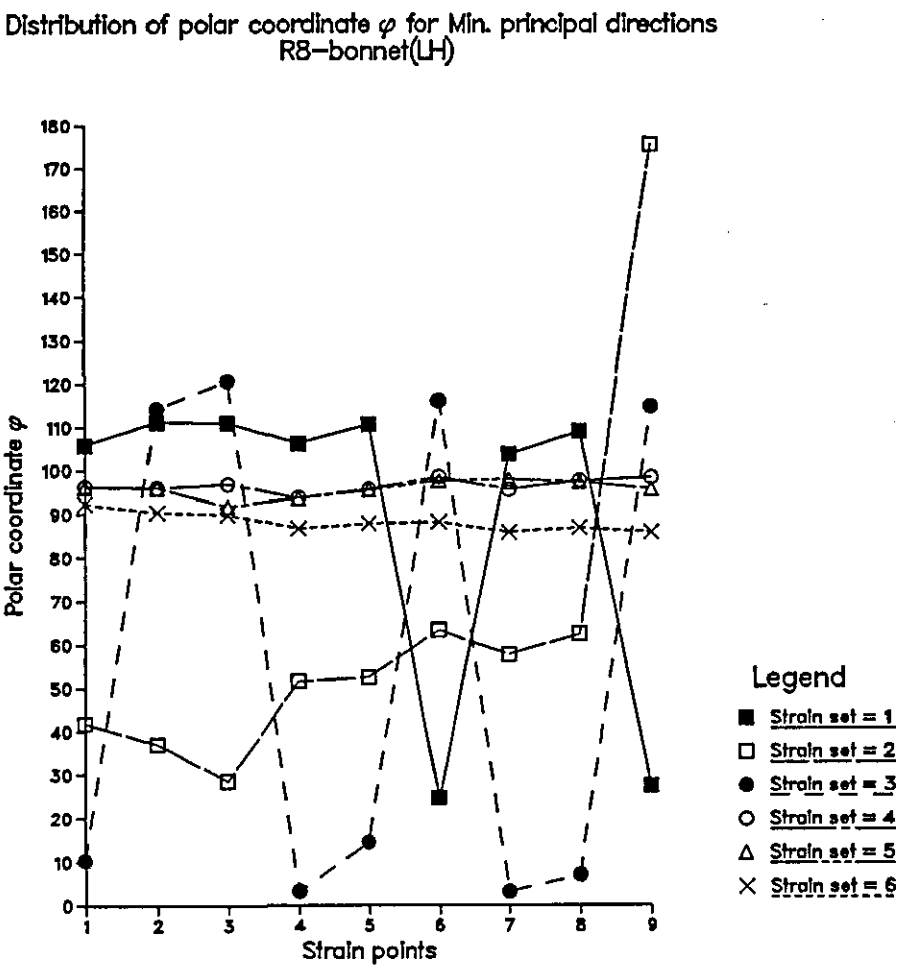

Figure(5.15) : The minor directions for the R8-bonnet (LH).

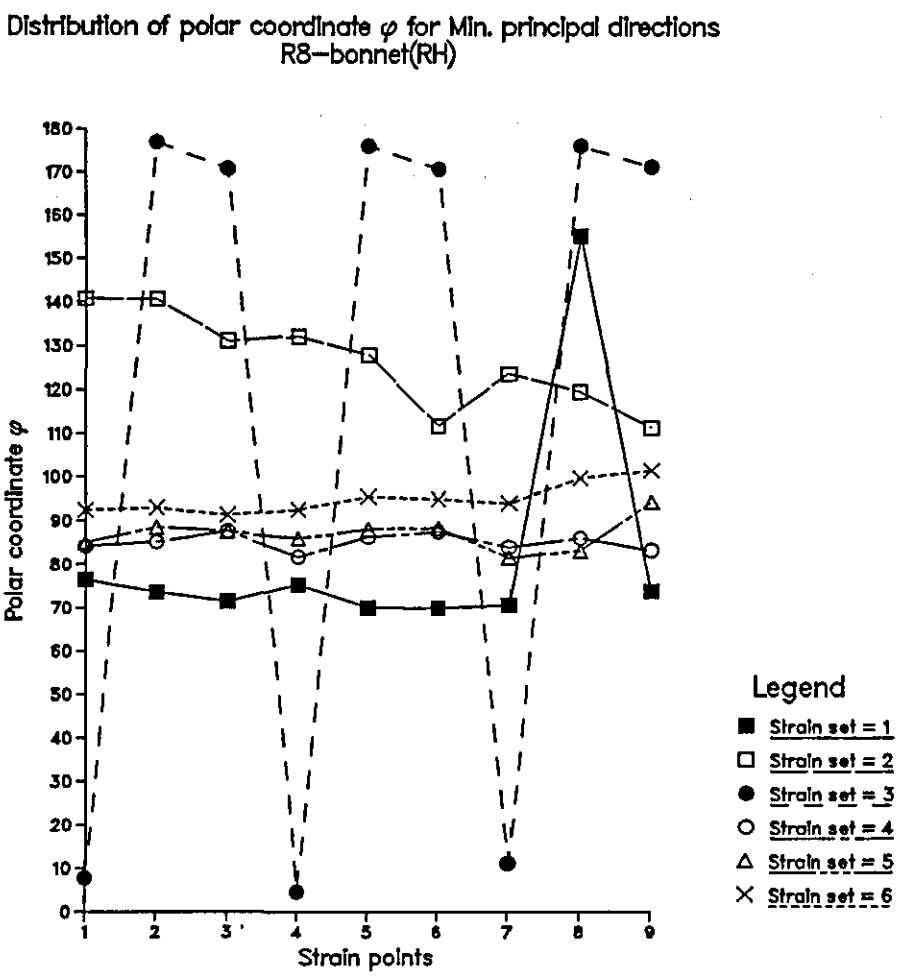

Figure(5.16) : The minor directions for the R8-bonnet (RH).

5.4.2) R8-roof.

The graphs for the principal major polar coordinate distribution over the strain sets on the left hand side and the right hand side of the R8-roof are presented in Figures(5.17) and (5.18). The main features identified in these figures are :

(1) The dominant directions are not easily determined. There are no clear trends within the rows of each set.

(2) The dominant directions vary between a bias to the X axis and through to a bias in the Y axis.

The graphs for the distribution of the minor polar coordinate over strain sets on the left hand side and the right hand side of the R8-roof are presented in Figures(5.19) and (5.20). The main features of the minor polar coordinate variation are identified in the preceding discussion regarding the distribution of the major polar coordinate. By inspection of the major and minor coordinate we conclude they are close to orthogonal.

In the next Chapter we discuss a physical interpretation for the strain data presented for the R8-bonnet and R8-roof.

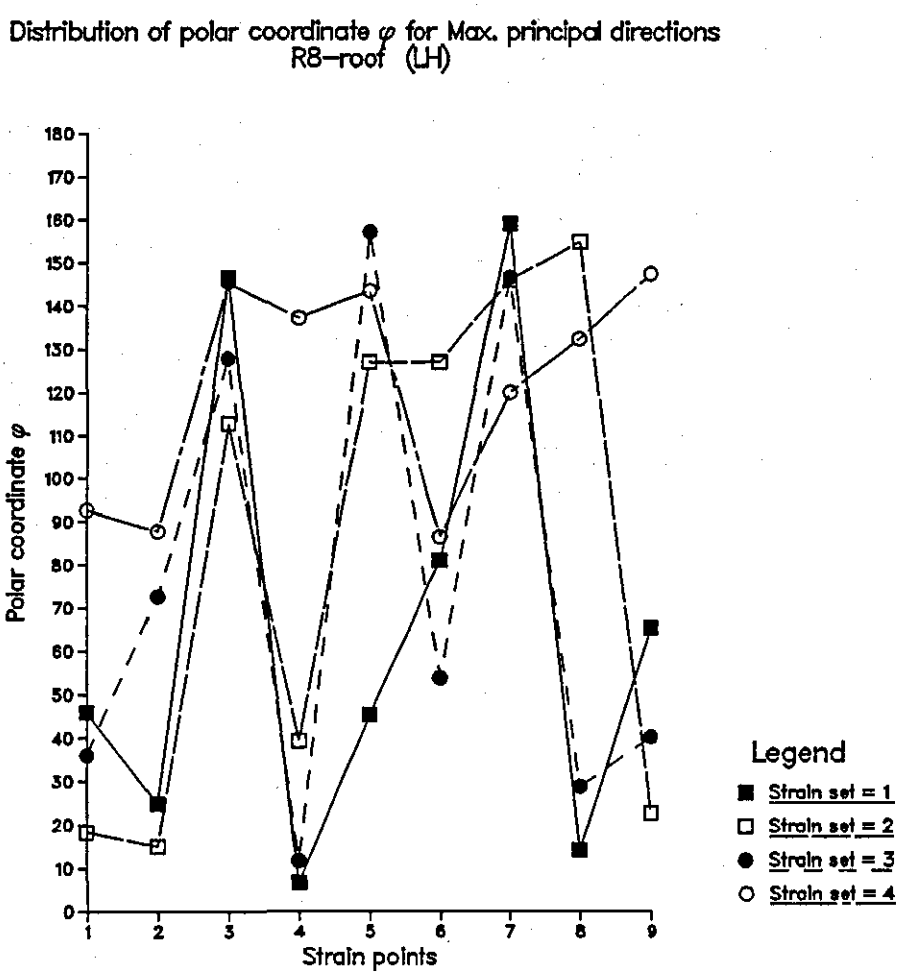

Figure(5.17) : The major directions for the R8-roof (LH).

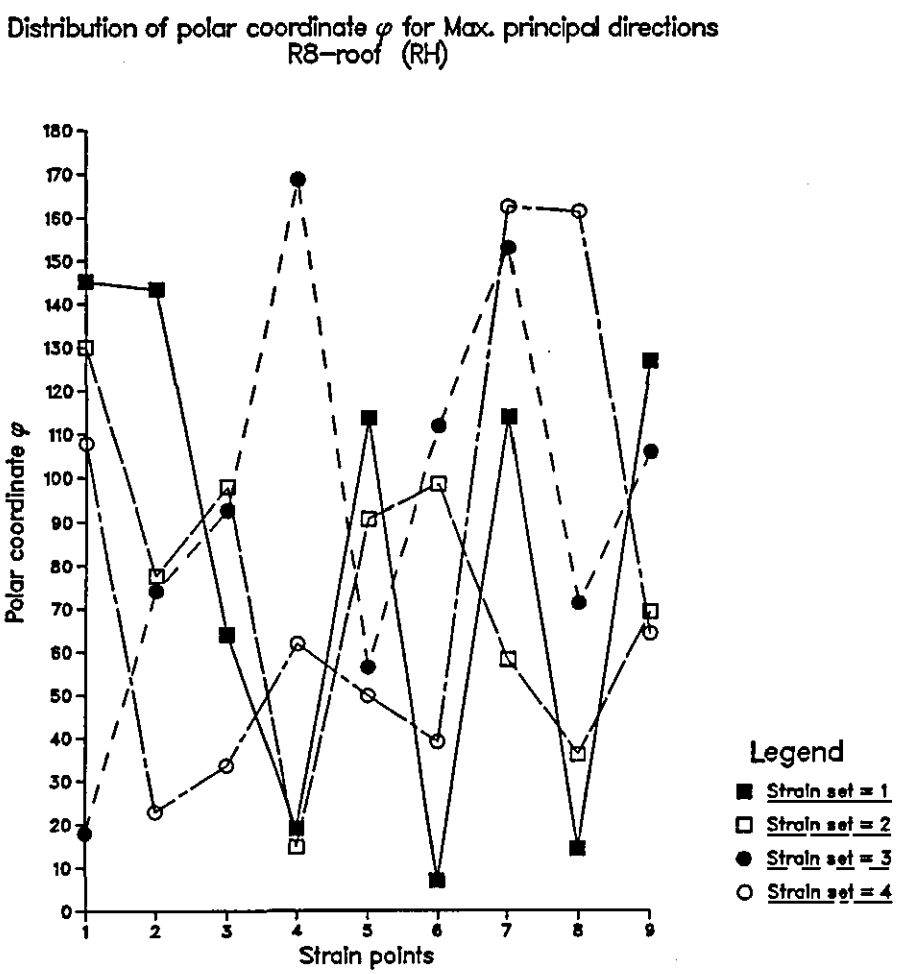

Figure(5.18) : The major directions for the R8-roof (RH).

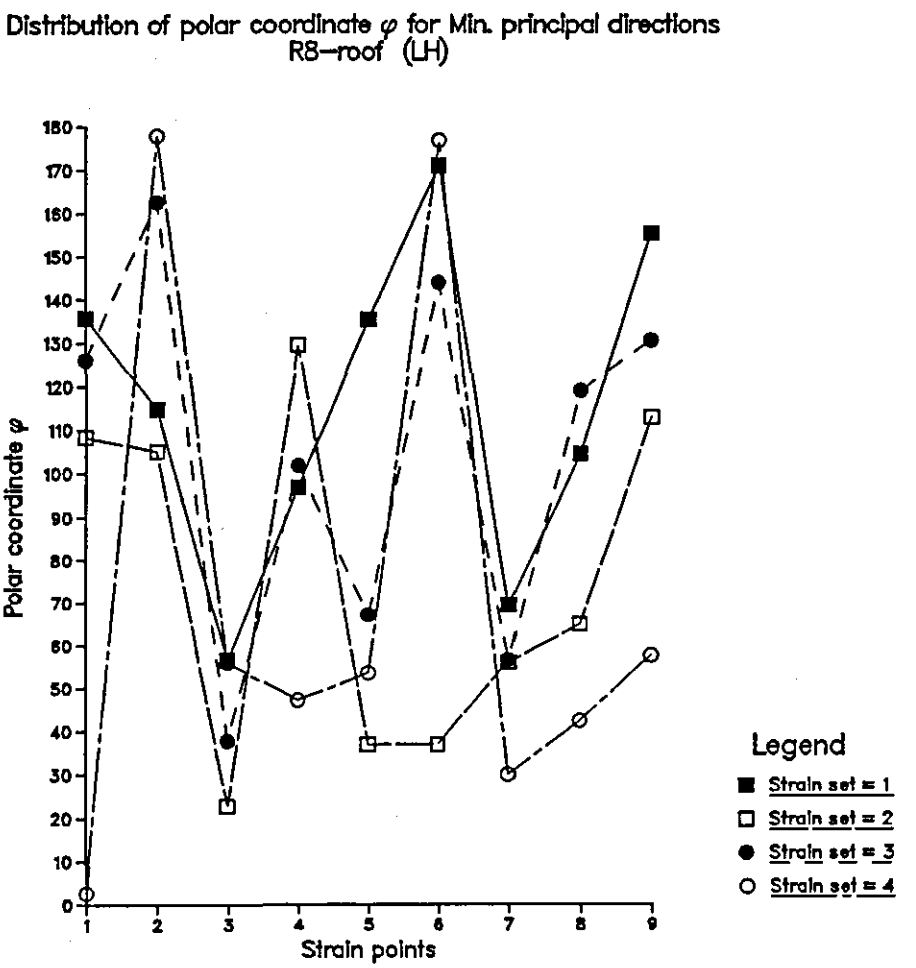

Figure(5.19) : The minor directions for the R8-roof (LH).

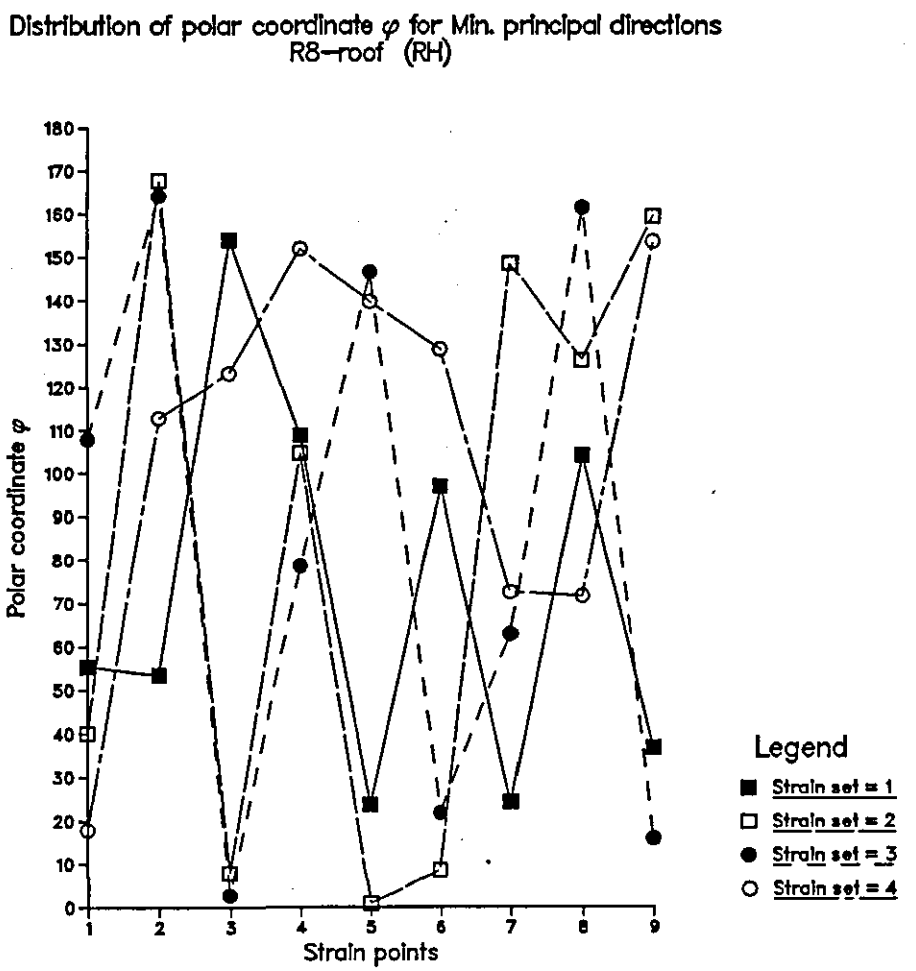

Figure(5.20) : The minor directions for the R8-roof (RH).

CHAPTER 6

DISCUSSION AND CONCLUSIONS.

The aim of the thesis has been to estimate small strains on a drawn panel and to generate a database of information which could be used in the numerical modelling of the sheet metal. In this chapter we discuss the results of Chapter 5 and identify areas for further work.

In section(6.1) we present a summary of the shortest planar path method, with a physical interpretation of the results presented in Chapter 5, identifying limitations of the method and suggesting possible improvements. The importance of estimating the shortest path between two points on a surface is identified and motivation for further work is highlighted. The development of the method is explored in section(6.2).

6.1) Summary of strain analysis.

In this thesis it has been demonstrated that a database of small strain information can be generated from a purely geometric approach, using a simple 2D model for strain analysis which is presented in Chapter 2.

In section(6.1.1) we discuss the physical significance of the strain data presented in Chapter 5. In section (6.1.2) the limitations of the radial plane subdivision method are identified and possible improvements are suggested and in section (6.1.3) we give the motivation for further work.

6.1.1) Interpretation of results.

In this section we discuss the physical significance of the results presented in Chapter 5 for the evaluation of principal strains and directions at discrete points on two production panels : the R8-bonnet and the R8-roof.

R8-bonnet

The variation of the major/minor strains correspond to the form on the panel. At the front of the bonnet there is considerably more form compared to the rear of the panel. As we travel from the front to the rear of the centre portion of the panel there is a decrease in the major strain, with direction roughly in the X axis. Also as we travel to the outer portion of the panel the major strain direction is biased in the Y axis.

R8-roof

The patterns associated to the major directions are not as clear as those identified on the R8-bonnet. We recall the discussion of errors in Chapter 2, section(2.3.4) and appreciate that the principal directions are not well defined when estimated horizontal and vertical strains are similar in value.

We note that the major/minor strains on the R8-roof are close to each other, indicating there is almost uniform strain on the roof. The little form on the roof is not significant, but the variation of form can be identified from the major strain direction biased to the X axis in the centre of the panel to a bias in the Y axis at the outer edge of the panel.

We suggest a more detailed investigation to establish the relationship between the form on a panel and its strain variations can be undertaken.

6.1.2) Limitations of the radial plane subdivision method.

The radial plane subdivision method which is described in Chapter 4, section(4.2), has the main advantage that convergence to a lower bound for the calculation of the minimum planar arc length is guaranteed where the bounding planes are defined. However there are a number of limitations:

a) accuracy is dependent on the mesh size, closeness of strain points and the evaluation of continuous planar intersects for bounding planes : X^0 and X^1.

b) the cpu time used in the algorithm is dependent on the total number of planar intersectsevaluated. The function evaluations for the calculation of arc length are dependent on the number of facets. So increasing the mesh size will increase the cpu time required for convergence.

c) the mesh size is chosen for a surface patch and not the respective pairs of strain points within a given strain set. This restricts the possibility for local mesh refinement without expensive increases in cpu time and increased storage demands.

It is assumed that the region covered by the family of radial planes on 'flat' surface patches will contain the geodesic curve. We also assume that the geodesic curve is single valued with respect to the chord direction. These assumptions are used in section(6.2), for the development of a shortest path method.

We suggest that faceting a portion of the surface patch P, which contains the surface patch Q, defined in section (4.1.1), will reduce storage and will allow the potential for increased accuracy.

6.1.3) Motivation for future work.

The results presented in Chapter 5, for the estimation of small strains on two production panels show that without any material assumptions about a drawn panel, significant modelling results can be established.

The radial range subdivision method, even though it does not give the lowest value of arc length between two points on a surface, does give significant results. The strains evaluated for both the R8-bonnet and the R8-roof are sufficiently close to the elastic, elastic/plastic region, to warrant a deeper investigation. In particular :

a) to evaluate the errors involved in the measurement of the strain points; including the etching, digitizing and location of points on the model.

b) to improve the estimation of the geodesic distance, between two points on a surface patch.

c) to provide more detailed information of the elastic, elastic/plastic region for each material considered in the overcrown prediction program [Ball and Cripps; 1987].

Finally, the results of the radial planar subdivision method need to be compared with other numerical methods used for the modelling of the drawing process.

6.2) Development of shortest path algorithms.

The recent interest in the shortest path or geodesic curve between two points on a surface is noted by Barnhill et al. [1988] and Farouki [1987]. There are three main areas of research :

1) the appreciation of free form surfaces by plotting geodesic curves from an initial point and tangent information [Barnhill et al.;1988], [Farouki;1987] and [Munchmeyer and Haw;1982].

2) Nutbourne [1986] has used the relationship between the curvature and torsion of a geodesic for a given tangent direction, and expresses these quantities in a '*circle diagram*' and gives an appreciation of Gauss curvature at points on a surface.

3) Farouki [1987] also identifies the potential uses of geodesic curves in the optimization of numerical control cutter paths, the motion of a robot arm and the windings of a solenoid.

In the next three sections we discuss methods of solving the boundary value problem : given two points **a** and **b**, on a surface calculate the shortest path between them. Let $\mathbf{r} = \mathbf{r}(u,v)$, $0 \le u,v \le 1$, be a surface of class at least C^3. Let $u = u(t)$, $v = v(t)$, $0 \le t \le 1$, be the curvilinear coordinates of a curve at least class C^3. Then the curve, $\mathbf{r}(t) = \mathbf{r}(u(t),v(t))$, $0 \le t \le 1$, is a curve on the surface of at least class C^3, and satisfies, $\mathbf{r}(0) = \mathbf{a}$, $\mathbf{r}(1) = \mathbf{b}$. We wish to minimize the arc length, l, of this curve defined by,

$$l = \int_0^1 | \dot{\mathbf{r}}(t) | \, dt \qquad (6.1)$$

In the following sections we require the first and second derivatives r(t), with respect to t.

$$\frac{dr(t)}{dt} = \frac{\delta r(u,v)}{\delta u}\frac{du(t)}{dt} + \frac{\delta r(u,v)}{\delta v}\frac{dv(t)}{dt} \tag{6.2}$$

$$\frac{d^2r(t)}{dt^2} = \frac{\delta^2 r}{\delta u^2}\left[\frac{du}{dt}\right]^2 + 2\frac{\delta^2 r}{\delta u \delta v}\frac{du}{dt}\frac{dv}{dt} + \frac{\delta^2 r}{\delta v^2}\left[\frac{dv}{dt}\right]^2 + \frac{\delta r}{\delta u}\frac{d^2u}{dt^2} + \frac{\delta r}{\delta v}\frac{d^2v}{dt^2} \tag{6.3}$$

6.2.1) Variational approach.

Clarke [1986] states that, in some circumstances, the solution of equation(6.1), is equivalent to minimizing the energy integral defined by,

$$E = \int_0^1 \dot{\mathbf{r}}(t) \cdot \dot{\mathbf{r}}(t)dt \tag{6.4}$$

He considers numerical solution of equation(6.4) and suggests that the geodesic can be characterized by a finite number of points,

$\mathbf{r}(u_0,v_0) = \mathbf{a}$, $\mathbf{r}(u_{N+1},v_{N+1}) = \mathbf{b}$,

$\mathbf{r}(u_i,v_i)$, $u_i = u_i(t_i)$, $v_i = v_i(t_i)$, $i = 1,\ldots,N$

where the t_i are chosen for Gaussian integration.

Then equation(6.4) can be approximated by finite differences, and the u_i,v_i, $i = 1,\ldots,N$, are varied to minimize E using a least squares method.

6.2.2) Differential equations approach.

This approach involves solving the differential equations which are derived using the fact that the principal normal of the geodesic curve is normal to the surface $\mathbf{r}(u,v)$, $0 \le u,v \le 1$, as discussed in section(3.4.2). We assume that the curve $\mathbf{r}(t)$, $0 \le t \le 1$ can be parameterized with respect to its arc length. The we write that $\mathbf{r} = \mathbf{r}(s)$, $0 \le s \le s_1$ is a curve of at least class C^2. We have defined in section (3.2.1),

$$\frac{d^2\mathbf{r}(s)}{ds^2} = k(s)\, \mathbf{n}(s)$$

For a geodesic curve we require that,

$$\frac{d^2\mathbf{r}(s)}{ds^2} \cdot \frac{\delta \mathbf{r}(u,v)}{\delta u} = 0 \quad \text{and} \quad \frac{d^2\mathbf{r}(s)}{ds^2} \cdot \frac{\delta \mathbf{r}(u,v)}{\delta v} = 0$$

where $u = u(s)$, $v = v(s)$, $0 \le s \le s_1$.

We can expand these equations using equation(6.3) and for convenience we write,

$$\mathbf{r}' = \frac{d\mathbf{r}}{ds}, \quad \mathbf{r}_u = \frac{\delta \mathbf{r}}{\delta u}, \quad \mathbf{r}_v = \frac{\delta \mathbf{r}}{\delta v}, \quad u' = \frac{du}{ds} \text{ and } v' = \frac{dv}{ds}$$

Then

$$\begin{aligned} \mathbf{r}''.\mathbf{r}_u &= \mathbf{r}_{uu}.\mathbf{r}_u[u']^2 + 2\,\mathbf{r}_{uv}.\,\mathbf{r}_u\,u'v' + \mathbf{r}_{vv}.\mathbf{r}_u[v']^2 + \mathbf{r}_u.\mathbf{r}_u\,u'' + \mathbf{r}_v.\mathbf{r}_u v'' \\ &= 0 \end{aligned} \qquad (6.5)$$

$$\begin{aligned} \mathbf{r}''.\mathbf{r}_v &= \mathbf{r}_{uu}.\mathbf{r}_v[u']^2 + 2\,\mathbf{r}_{uv}.\,\mathbf{r}_v\,u'v' + \mathbf{r}_{vv}.\mathbf{r}_v[v']^2 + \mathbf{r}_u.\mathbf{r}_v\,u'' + \mathbf{r}_v.\mathbf{r}_v v'' \\ &= 0 \end{aligned}$$

Usually these equations are considered as two non-linear differential equations in u and v.

The problem has been approached by Farouki [1987] using a shooting method which is described in detail by Dahliquist and Bjorck [1974]. Essentially an initial guess is made for the starting tangent direction, at one point **a**. The path of the geodesic is generated and the nearest point to b is calculated. An improved estimate of the starting direction for the geodesic at **a** is made, until the point **b** is hit. Farouki comments that this method is usually quick, but convergence cannot be guaranteed.

Clarke [1986] suggests representing the surface $\mathbf{r}(u,v)$, $0 \leq u,v \leq 1$, by a mesh of points and defining dot products of equations (6.5) over the mesh. The second order non-linear differential equations can then be considered as a system of second-order ordinary differential equations in the dependent variables u and v. Alternatively, they could be considered as a system of first-order ordinary differential equations in u, v, du/ds and dv/ds.

6.2.3) Geometric approach.

In this section we describe a simple geometric method for determining a point on a twisted geodesic curve between two points $\mathbf{p}^a$ and $\mathbf{p}^b$ on the surface patch $\mathbf{p}(u,v)$, $0 \leq u,v \leq 1$. We note that the application of the method is for 'flat' surface patches.

We assume that the geodesic curve $\mathbf{p}_G(u^*)$, $0 \leq u^* \leq 1$, is parameterized with respect to the chord direction, N^{ba} and a point, $\mathbf{c}(u^*)$, $u^* \in [0,1]$ on the chord, where, $N^{ba} = \mathbf{p}^b - \mathbf{p}^a$ and $\mathbf{c}(u^*) = (1 - u^*)\,\mathbf{p}^a + u^*\,\mathbf{p}^b$.

We also assume that the family of radial planes, X^{v^*}, $0 \leq v^* \leq 1$, as discussed in section (4.1.1), defines a portion of the surface patch $\mathbf{p}(u,v)$, $0 \leq u,v \leq 1$, which contains the geodesic curve $\mathbf{p}_G(u^*)$, $0 \leq u^* \leq 1$.

We consider the case when $\mathbf{p}_G(u^*)$, $0 \leq u^* \leq 1$, is a twisted curve and suggest a geometric method for determining a point on the curve.

To determine a point on the geodesic $\mathbf{p}_G(u^*)$, $0 \leq u^* \leq 1$, we assume that the curve meets a radial plane intersect, $\mathbf{q}(u^*,v^*)$, $0 \leq u^* \leq 1$, $v^* \in (0,1)$, defined in section(4.1.1), at a point $\mathbf{p}_G(u^*_1)$, $u^*_1 \in (0,1)$. The arc lengths l_G and $l(v^*)$, $v^* \in (0,1)$ of the geodesic curve and planar intersect are defined respectively by,

$$l_G = \int_0^1 \left| \frac{d\mathbf{p}_G(u^*)}{du^*} \right| du^*$$

$$l(v^*) = \int_0^1 \left| \frac{\delta \mathbf{q}(u^*,v^*)}{du^*} \right| du^*, \quad v^* \in (0,1) \tag{6.6}$$

and $l_G < l(v^*)$, $\forall\, v^* \in [0,1]$.

Now we can split these integrals such that,

$$l_G = \int_0^{u^*_1} \left| \frac{dp_G(u^*)}{du^*} \right| du^* + \int_{u^*_1}^{1} \left| \frac{dp_G(u^*)}{du^*} \right| du^*$$

$$l(v^*) = \int_0^{u^*_1} \left| \frac{\delta q(u^*,v^*)}{\delta u^*} \right| du^* + \int_{u^*_1}^{1} \left| \frac{\delta q(u^*,v^*)}{\delta u^*} \right| du^*, \; v^* \in (0,1)$$

The curve $p_G(u^*)$, $0 \le u^* \le u^*_1$, must be a geodesic of minimum arc length between the points $p_G(0)$ and $p_G(u^*_1)$, so we can write,

$$\int_0^{u^*_1} \left| \frac{dp_G(u^*)}{du^*} \right| du^* \le \int_0^{u^*_1} \left| \frac{\delta q(u^*,v^*)}{\delta u^*} \right| du^*$$

For $u^*_1 = \delta u^* << 1$ the above integrals can be approximated by,

$$|p_G(\delta u^*) - p_G(0)| \, \delta u^* \le |q(\delta u^*,v^*) - q(0,v^*)| \delta u^*$$

So,

$$|p_G(\delta u^*) - p_G(0)| \le |q(\delta u^*,v^*) - q(0,v^*)| \tag{6.7}$$

where, $\delta u^* \in (0,1)$, $\delta u^* << 1$, $v^* \in (0,1)$

So by evaluating the right hand side of equation(6.7), for a number of points on the planar intersect $\mathbf{q}(\delta u^*, v^*)$, $\delta u^* \in (0,1)$, $0 \leq v^* \leq 1$ we can determine a point on the geodesic near to the point $\mathbf{p}^a$. Similarly, we can repeat this process at $\mathbf{p}^b$. Hence we can build the geodesic from a finite number of points and approximate its arc length by accumulated chord length.

We note that if the geodesic curve is a planar intersect then it is uniquely defined by the plane that contains a point off the chord, and the surface normals at $\mathbf{p}^a$ and $\mathbf{p}^b$. We require that principal normal of a geodesic curve must be normal to the surface at all points along the curve. This must be satisfied at the end points of the planar geodesic curve and this condition defines the plane of the geodesic uniquely.

We conclude that a number of significant geometric results for the modelling of the drawing process are presented in the thesis. This will provide a basis for the understanding of a complex industrial problem by the comparison of a materials modelling method to a purely geometric approach.

APPENDIX A

Curvature property of the rational cubic segment.

In Theorem 4 we deduce that the curvature of a twisted rational cubic segment is non-zero at all points along the segment.

Theorem 4

If the curvature of a rational cubic segment is zero at any point, then the segment is a plane curve.

Proof

We recall that the rational cubic segment is defined by the following equations [Faux et al.; 1983] :

$$\mathbf{P}(u) = \mathbf{r}(u)W(u),\ 0 \le u \le 1 \tag{A.1}$$

where,

$$\mathbf{P}(u) = \mathbf{a}_0 + \mathbf{a}_1 u + \mathbf{a}_2 u^2 + \mathbf{a}_3 u^3 \tag{A.2}$$

$$W(u) = w_0 + w_1 u + w_2 u^2 + w_3 u^3 \tag{A.3}$$

We differentiate equation(A.1) three times to obtain :

$$\dot{\mathbf{P}}(u) = \dot{\mathbf{r}}(u)W(u) + \mathbf{r}(u)\dot{W}(u) \tag{A.4}$$

$$\ddot{\mathbf{P}}(u) = \ddot{\mathbf{r}}(u)W(u) + 2\dot{\mathbf{r}}(u)\dot{W}(u) + \mathbf{r}(u)\ddot{W}(u) \tag{A.5}$$

$$\dddot{\mathbf{P}}(u) = \dddot{\mathbf{r}}(u)W(u) + 3\ddot{\mathbf{r}}(u)\dot{W}(u) + 3\dot{\mathbf{r}}(u)\ddot{W}(u) + \mathbf{r}(u)\dddot{W}(u) \tag{A.6}$$

Now we want expressions for $\dot{\mathbf{r}}(u)$ and $\ddot{\mathbf{r}}(u)$ in terms of the vector P(u) and scalar W(u), and their derivatives. We also require the triple scalar product of the vectors $\dot{\mathbf{r}}(u)$, $\ddot{\mathbf{r}}(u)$ and $\dddot{\mathbf{r}}(u)$ for the calculation of torsion in Appendix B.

Then we first multiply equations(A.4)-(A.6) by W(u) and after substituting equation(A.1) we can express these equations in matrix form :

$$\begin{bmatrix} Q_1 \\ Q_2 \\ Q_3 \end{bmatrix} = \begin{bmatrix} W & 0 & 0 \\ 2\dot{W} & W & 0 \\ 3\ddot{W} & 3\dot{W} & W \end{bmatrix} \begin{bmatrix} W\dot{\mathbf{r}} \\ W\ddot{\mathbf{r}} \\ W\dddot{\mathbf{r}} \end{bmatrix} \qquad (A.7)$$

where, $Q_1 = W\dot{P} - P\dot{W}$, $Q_2 = W\ddot{P} - P\ddot{W}$ and $Q_3 = W\dddot{P} - P\dddot{W}$

and so,

$$\begin{bmatrix} W\dot{\mathbf{r}} \\ W\ddot{\mathbf{r}} \\ W\dddot{\mathbf{r}} \end{bmatrix} = \begin{bmatrix} 1/W & 0 & 0 \\ -2\dot{W}/W^2 & 1/W & 0 \\ (6\dot{W}^2 - 3W\ddot{W})/W^3 & -3\dot{W}/W^2 & 1/W \end{bmatrix} \begin{bmatrix} Q_1 \\ Q_2 \\ Q_3 \end{bmatrix} \qquad (A.8)$$

We note if $\mathbf{r}(u)$ is not a regular curve i.e. $\dot{\mathbf{r}}(u_0) = 0$, at some point $u = u_0$, then $\mathbf{r}(u)$ is a plane curve.

The curvature k(u) of a space curve is defined in chapter 3, section(3.2.1) and by taking the modulus of equation(3.5) we have :

$$k(u) = \frac{|\dot{\mathbf{r}}(u) \times \ddot{\mathbf{r}}(u)|}{|\dot{\mathbf{r}}(u)|^3} \; ; \quad |\dot{\mathbf{r}}(u)| \neq 0$$

We suppose we have a point of zero curvature at u then

$$\dot{\mathbf{r}}(u) \times \ddot{\mathbf{r}}(u) = \mathbf{0}$$

By inspection of equations (A.8) there exists a non-zero scalar α, such that,

$$\begin{aligned} Q_1 + \alpha Q_2 &= 0 \\ W\dot{P} - P\dot{W} + \alpha [\, W\ddot{P} - P\ddot{W} \,] &= 0 \end{aligned}$$

This implies that non-zero scalars exist α_1 , β_1

$$\dot{P} + \alpha_1 \ddot{P} + \beta_1 P = 0 \qquad \text{(A.9)}$$

Differentiating equation(A.2) twice we have :

$$\dot{P}(u) = a_1 + 2a_2u + 3a_3u^2 \qquad \text{(A.10)}$$

$$\ddot{P}(u) = 2a_2 + 6a_3u \qquad \text{(A.11)}$$

Without loss of generality we assume that a_0 is located at the origin of our co-ordinate system. Substituting in equations (A.2), (A.10) and (A.11) into equation(A.9),

$$a_1 + 2a_2u + 3a_3u^2 + \alpha_1 (2a_2 + 6a_3u) + \beta_1 (a_1u + a_2u^2 + a_3u^3) = 0$$

Then,

$$a_1(1 + \beta_1u) + a_2(2\alpha_1 + 2u + \beta_1u^2) + a_3(6\alpha_1 u + 3u^2 + \beta_1u^3) = 0$$

By comparing coefficients of a_1,a_2 and a_3 we deduce that they cannot be simultaneously zero, consequently the vectors a_1,a_2 and a_3 must be linearly dependent and $\mathbf{r}(u)$ must be a plane curve. Conversely, if the rational cubic segment is a twisted curve then it cannot have zero curvature at any point along the segment.

APPENDIX B

Torsion property of the rational cubic segment.

In Theorem 5 we deduce that the torsion of a twisted rational cubic segment is non-zero at all points along the segment.

Theorem 5

If the curvature for the rational cubic segment is non-zero throughout the segment and if its torsion is zero at any point, then the segment is a plane curve.

Proof

The torsion of a space curve is defined in chapter 3, in section(3.2.1) by equation(3.6) and is :

$$\tau(u) = \frac{\dot{\mathbf{r}}(u).\ddot{\mathbf{r}}(u) \times \dddot{\mathbf{r}}(u)}{|\dot{\mathbf{r}}(u) \times \ddot{\mathbf{r}}(u)|^2} \; ; \; |\dot{\mathbf{r}}(u) \times \ddot{\mathbf{r}}(u)| \neq 0 \qquad (B.1)$$

We suppose we have a point of zero torsion then

$$\dot{\mathbf{r}}(u).\ddot{\mathbf{r}}(u) \times \dddot{\mathbf{r}}(u) = 0$$

Then by inspection of equations (A.8) we must have non-zero scalars α, β where,

$$\mathbf{Q}_1 + \alpha \mathbf{Q}_2 + \beta \mathbf{Q}_3 = 0$$

Hence,

$$\dot{W}\dot{P} - P\dot{W} + \alpha (W\ddot{P} - P\ddot{W}) + \beta (W\dddot{P} - P\dddot{W}) = 0$$

$$W\dot{P} + \alpha W\ddot{P} + \beta W\dddot{P} - P (\dot{W} + \alpha \ddot{W} + \beta \dddot{W}) = 0 \qquad \text{(B.2)}$$

We recall from equation(A.2),

$$P(u) = a_0 + a_1 u + a_2 u^2 + a_3 u^3, \; 0 \le u \le 1.$$

and differentiating three times,

$$\dot{P}(u) = a_1 + 2a_2 u + 3a_3 u^2 \qquad \text{(B.3)}$$

$$\ddot{P}(u) = 2a_2 + 6a_3 u \qquad \text{(B.4)}$$

$$\dddot{P}(u) = 6a_3 \qquad \text{(B.5)}$$

Without loss of generality we can assume that a_0 is located at the origin of our coordinate system and substituting equations(A.2), and (B.3) - (B.5) into equation(B.2) we obtain,

$$W [a_1 + 2a_2 u + 3a_3 u^2] + \alpha W [2a_2 + 6a_3 u] + 6 \beta W a_3$$

$$- (a_1 u + a_2 u^2 + a_3 u^3) (\dot{W} + \alpha \ddot{W} + \beta \dddot{W}) = 0$$

$$a_1 [W - (\dot{W} + \alpha \ddot{W} + \beta \dddot{W})u] + a_2 [2Wu - (\dot{W} + \alpha \ddot{W} + \beta \dddot{W})u^2]$$

$$+ a_3 [3Wu^2 - (\dot{W} + \alpha \ddot{W} + \beta \dddot{W})u^3] = 0$$

By comparing the coefficients of a_1, a_2 and a_3 we deduce that they cannot be simultaneously zero, therefore a_1, a_2 and a_3 are linearly dependent and the rational cubic segment $r(u)$, $0 \le u \le 1$, must be a plane curve. Conversely, if the rational cubic segment is a twisted curve then it cannot have zero torsion at any point along the segment and its value is constant in sign. An important corollary to Theorem 5 is proved in Theorem 6.

Theorem 6

The sign of torsion is uniquely determined by the end points and end tangents for the rational cubic segment, $P(u)$, $0 \leq u \leq 1$ defined in Appendix A.

Proof

We first derive an expression for the sign of torsion and then we link this expression to the end tangents and end points of the rational cubic segment.

The numerator in equation(B.1) determines the sign of torsion,

$$\text{sgn}(\tau(u)) = \text{sgn}\ (\dot{\mathbf{r}}(u).\ddot{\mathbf{r}}(u) \times \dddot{\mathbf{r}}(u))$$

By Theorem 5 the sign of torsion for a rational cubic segment is constant. So,

$$\text{sgn}(\tau) = \text{sgn}\ (\dot{\mathbf{r}}(0).\ddot{\mathbf{r}}(0) \times \dddot{\mathbf{r}}(0)) \tag{B.7}$$

We proceed by evaluating equation(B.7) using equations (A.4) - (A.6) and without loss of generality we assume that $\mathbf{a}_0$ is located at the origin of our co-ordinate system. Therefore,

$$\dot{\mathbf{P}}(0) = \dot{\mathbf{r}}(0)W(0) \tag{B.8}$$

$$\ddot{\mathbf{P}}(0) = \ddot{\mathbf{r}}(0)W(0) + 2\dot{\mathbf{r}}(0)\dot{W}(0) \tag{B.9}$$

$$\dddot{\mathbf{P}}(0) = \dddot{\mathbf{r}}(0)W(0) + 3\ddot{\mathbf{r}}(0)\dot{W}(0) + 3\dot{\mathbf{r}}(0)\ddot{W}(0) \tag{B.10}$$

The triple scalar product of $\dot{\mathbf{P}}(0)$, $\ddot{\mathbf{P}}(0)$ and $\dddot{\mathbf{P}}(0)$ is,

$$\dot{\mathbf{P}}(0) \times \ddot{\mathbf{P}}(0) . \dddot{\mathbf{P}}(0) = \dot{\mathbf{r}}(0) \times \ddot{\mathbf{r}}(0) . \dddot{\mathbf{r}}(0)\ W^3(0)$$

Substituting u = 0 in equations (B.3) - (B.5) then,

$$12\ \mathbf{a}_1 \times \mathbf{a}_2 \cdot \mathbf{a}_3 = \dot{\mathbf{r}}(0) \times \ddot{\mathbf{r}}(0) \cdot \dddot{\mathbf{r}}(0)\ W^3(0)$$

If we assume that the weights, w_i, i=0,...,3 are all positive then the sign of torsion is determined by,

$$\mathrm{sgn}(\tau) = \mathrm{sgn}(\mathbf{a}_1 . \mathbf{a}_2 \times \mathbf{a}_3) \qquad \text{(B.11)}$$

Now from Appendix A, equations (A.2) and (A.10) we have,

$$P(0) = \mathbf{a}_0,\ P(1) = \mathbf{a}_0 + \mathbf{a}_1 + \mathbf{a}_2 + \mathbf{a}_3,\ \dot{P}(0) = \mathbf{a}_1,\ \dot{P}(1) = \mathbf{a}_1 + 2\mathbf{a}_2 + 3\mathbf{a}_3$$

Thus,

$$P(1) - P(0) = \mathbf{a}_1 + \mathbf{a}_2 + \mathbf{a}_3 \text{ and } \dot{P}(1) \times \dot{P}(0) = 2\ \mathbf{a}_2 \times \mathbf{a}_1 + 3\ \mathbf{a}_3 \times \mathbf{a}_1$$

Therefore,

$$\begin{aligned}(P(1) - P(0)).(\dot{P}(1) \times \dot{P}(0)) &= 3\ \mathbf{a}_2.\mathbf{a}_3 \times \mathbf{a}_1 + 2\ \mathbf{a}_3 . \mathbf{a}_2 \times \mathbf{a}_1 \\ &= 3\ \mathbf{a}_1.\mathbf{a}_2 \times \mathbf{a}_3 - 2\ \mathbf{a}_1.\mathbf{a}_2 \times \mathbf{a}_3 \\ &= \mathbf{a}_1.\mathbf{a}_2 \times \mathbf{a}_3\end{aligned}$$

Hence,

$$\mathrm{sgn}(\tau) = \mathrm{sgn}(\mathbf{a}_1.\mathbf{a}_2 \times \mathbf{a}_3) = \mathrm{sgn}(P(1) - P(0)).(\dot{P}(1) \times \dot{P}(0))$$

We now express this equation in terms of the end points and end tangents of the rational cubic segment $\mathbf{r}(u)$, $0 \le u \le 1$.

$$P(0) = \mathbf{r}(0)\ W(0),\ P(1) = \mathbf{r}(1)\ W(1),$$
$$\dot{P}(0) = \dot{\mathbf{r}}(0)\ W(0) + \mathbf{r}(0)\ \dot{W}(0),\ P(1) = \dot{\mathbf{r}}(1)\ W(1) + \mathbf{r}(1)\ \dot{W}(1)$$

But $P(0) = 0 = \mathbf{r}(0)$,

$$(P(1) - P(0)).(\dot{P}(1) \times \dot{P}(0)) = (P(1).(\dot{P}(1) \times \dot{P}(0)) =$$

$$\mathbf{r}(1)W(1).[\dot{\mathbf{r}}(1)W(1) + \mathbf{r}(1)\dot{W}(1)] \times \dot{\mathbf{r}}(0)W(0) = \mathbf{r}(1).\ \dot{\mathbf{r}}(1) \times \dot{\mathbf{r}}(0)W^2(1)\ W(0)$$

Therefore,

$\mathrm{sgn}(\tau) = \mathbf{r}(1)\ .\ \dot{\mathbf{r}}(1) \times \dot{\mathbf{r}}(0)\ W^2(1)\ W(0)$, and our theorem is proved.

APPENDIX C

Derivation of the Jacobian $\delta(u,v)/\delta(u^*,v^*)$.

Willmore [1972] states that for the relationship $u = u(u^*,v^*)$, $v = v(u^*,v^*)$ $u^*,v^* \in (0,1)$ to be single valued, the Jacobian $\delta(u,v)/\delta(u^*,v^*)$, defined by,

$$\frac{\delta(u,v)}{\delta(u^*,v^*)} = \begin{vmatrix} \frac{\delta u}{\delta u^*} & \frac{\delta u}{\delta v^*} \\ \frac{\delta v}{\delta u^*} & \frac{\delta v}{\delta v^*} \end{vmatrix} = \frac{\delta u}{\delta u^*}\frac{\delta v}{\delta v^*} - \frac{\delta u}{\delta v^*}\frac{\delta v}{\delta u^*} \qquad (C.1)$$

must be non-zero. To derive expressions for the partial derivatives in equation(C.1) we proceed in a way similar to Buck [1965].

We assume that a general point (u,v) on P and $u^*,v^* \in [0,1]$ on Q is defined in Chapter 4, section(4.1.1) by the equations :

$$\begin{aligned} a(u,v,u^*) &\equiv (\mathbf{p}(u,v) - \mathbf{c}(u^*)).\mathbf{N}^{ba} = 0 \\ b(u,v,v^*) &\equiv (\mathbf{p}(u,v) - \mathbf{d}).\hat{\mathbf{N}}_r(v^*) = 0 \end{aligned} \qquad (C.2)$$

Differentiating the left hand sides of equations(C.2) with respect to u^* we obtain :

$$\begin{aligned} \frac{\delta a}{\delta u}\frac{\delta u}{\delta u^*} + \frac{\delta a}{\delta v}\frac{\delta v}{\delta u^*} + \frac{\delta a}{\delta u^*} &= 0 \\ \frac{\delta b}{\delta u}\frac{\delta u}{\delta u^*} + \frac{\delta b}{\delta v}\frac{\delta v}{\delta u^*} &= 0 \end{aligned} \qquad (C.3)$$

We write equations(C.3) in matrix form :

$$A\,\underline{u}_{u^*} = -\,\underline{a}_{u^*} \tag{C.4}$$

where,

$$A = \begin{bmatrix} \dfrac{\delta a}{\delta u} & \dfrac{\delta a}{\delta v} \\ \dfrac{\delta b}{\delta u} & \dfrac{\delta b}{\delta v} \end{bmatrix}, \quad \underline{u}_{u^*} = \left[\frac{\delta u}{\delta u^*} , \frac{\delta v}{\delta u^*} \right]^T, \quad \underline{a}_{u^*} = \left[\frac{\delta a}{\delta u^*} , 0 \right]^T$$

For solutions to equations(C.4) we require that the determinant of A is non-zero :

$$\det(A) \neq 0 \tag{C.5}$$

If equation(C.5) holds then :

$$\underline{u}_{u^*} = -\,A^{-1}\,\underline{a}_{u^*} \tag{C.6}$$

where,

$$A^{-1} = \frac{1}{\det(A)} \begin{bmatrix} \dfrac{\delta b}{\delta v} & -\dfrac{\delta a}{\delta v} \\ -\dfrac{\delta b}{\delta u} & \dfrac{\delta a}{\delta u} \end{bmatrix}$$

Similarly we have,

$$\underline{u}_{v^*} = -\,A^{-1}\,\underline{a}_{v^*} \tag{C.7}$$

where,

$$\underline{u}_{v^*} = \left[\frac{\delta u}{\delta v^*} , \frac{\delta v}{\delta v^*} \right]^T, \quad \underline{a}_{v^*} = \left[0 , \frac{\delta b}{\delta v^*} \right]^T$$

Then, from equations(C.6) and (C.7) :

$$\frac{\delta u}{\delta u^*} = -\frac{1}{\det(A)}\frac{\delta b}{\delta v}\frac{\delta a}{\delta u^*}; \quad \frac{\delta v}{\delta u^*} = \frac{1}{\det(A)}\frac{\delta b}{\delta u}\frac{\delta a}{\delta u^*}$$

$$\frac{\delta u}{\delta v^*} = \frac{1}{\det(A)}\frac{\delta a}{\delta v}\frac{\delta b}{\delta v^*}; \quad \frac{\delta v}{\delta v^*} = -\frac{1}{\det(A)}\frac{\delta a}{\delta u}\frac{\delta b}{\delta v^*} \qquad (C.8)$$

Now,

$$\det(A) = \frac{\delta a}{\delta u}\frac{\delta b}{\delta v} - \frac{\delta a}{\delta v}\frac{\delta b}{\delta u}$$

Then from equations(C.2) :

$$\frac{\delta a}{\delta u} = \frac{\delta p}{\delta u} \cdot N^{ba}, \qquad \frac{\delta a}{\delta v} = \frac{\delta p}{\delta v} \cdot N^{ba}$$

$$\frac{\delta b}{\delta u} = \frac{\delta p}{\delta u} \cdot \hat{N}_r(v^*) \quad , \quad \frac{\delta b}{\delta v} = \frac{\delta p}{\delta v} \cdot \hat{N}_r(v^*)$$

$$\det(A) = \frac{\delta p}{\delta u} \cdot N^{ba} \frac{\delta p}{\delta v} \cdot \hat{N}_r(v^*) - \frac{\delta p}{\delta v} \cdot N^{ba} \frac{\delta p}{\delta u} \cdot \hat{N}_r(v^*)$$

$$= \left[\frac{\delta p}{\delta v} \cdot \hat{N}_r(v^*) \frac{\delta p}{\delta u} - \frac{\delta p}{\delta u} \cdot \hat{N}_r(v^*) \frac{\delta p}{\delta v} \right] \cdot N^{ba}$$

$$= \hat{N}_r(v^*) \times \left[\frac{\delta p}{\delta u} \times \frac{\delta p}{\delta v} \right] \cdot N^{ba} \qquad (C.9)$$

We recall,

$$\hat{N}(u,v) = \frac{H}{H} \; ; \; H = \frac{\delta p}{\delta u} \times \frac{\delta p}{\delta v} \text{ and } H \neq 0$$

Therefore,

$$\det(A) = H \; \hat{N}_r(v^*) \times \hat{N}(u,v) \cdot N^{ba} \qquad (C.10)$$

For the determinant of A to be non-zero then,

$$(\hat{N}_r(v^*) \times \hat{N}(u,v)) \cdot N^{ba} \neq 0$$

The Jacobian is defined by,

$$\frac{\delta(u,v)}{\delta(u^*,v^*)} = \frac{\delta u}{\delta u^*}\frac{\delta v}{\delta v^*} - \frac{\delta u}{\delta v^*}\frac{\delta v}{\delta u^*}$$

Substituting equations(C.8) then,

$$\frac{\delta(u,v)}{\delta(u^*,v^*)} = \frac{1}{\det(A)^2}\left[\frac{\delta b}{\delta v}\frac{\delta a}{\delta u^*}\frac{\delta a}{\delta u}\frac{\delta b}{\delta v^*} - \frac{\delta a}{\delta v}\frac{\delta b}{\delta v^*}\frac{\delta b}{\delta u}\frac{\delta a}{\delta v^*}\right]$$

$$= \frac{1}{\det(A)^2}\left[\frac{\delta b}{\delta v}\frac{\delta a}{\delta u} - \frac{\delta a}{\delta v}\frac{\delta b}{\delta u}\right]\frac{\delta a}{\delta u^*}\frac{\delta b}{\delta v^*}$$

$$= \frac{1}{\det(A)}\frac{\delta a}{\delta u^*}\frac{\delta b}{\delta v^*}$$

Now, from equations(C.2) we have,

$$\frac{\delta a}{\delta u^*} = -N^{ba}.N^{ba} \quad \text{and} \quad \frac{\delta b}{\delta v^*} = (p(u,v) - d).\frac{d\hat{N}_r(v^*)}{dv^*}$$

Using equation(C.10) then,

$$\frac{\delta(u,v)}{\delta(u^*,v^*)} = \frac{N^{ba}.N^{ba}\,(p(u,v) - d).\dfrac{d\hat{N}_r(v^*)}{dv^*}}{H\ \hat{N}(u,v) \times \hat{N}_r(v^*) \cdot N^{ba}} \qquad (C.11)$$

APPENDIX D

Application of torsion property.

We consider the application of the torsion property of the rational cubic segment, proved in Appendix B. In section(D.1) we discuss the application to composite rational cubic curves and the relevance to a new field of research : visual continuity [Boehm;1988], defined loosely by '*tangent and curvature continuity of composite curves and surfaces*'. In section (D.2) we discuss the application to the parametric curves of the rational bicubic patch.

D.1) Composite curves.

In this section we deduce that a composite twisted curve, with non-zero curvature, built-up of rational cubic segments cannot accommodate a planar segment and have curvature and torsion continuity.

A twisted curve adjoining a planar rational cubic segment would need to have zero torsion at the common boundary point. However this would determine the '*twisted segment*' to be planar, since from Theorem 5 we must have that the torsion is identically zero for the whole segment. Thus a higher order space curve would be required to ensure torsion continuity at the common boundary point : and Boehm [1987] has constructed torsion continuous composite curves for rational quartic β-splines.

D.2) Rational bicubic surface.

We deduce for a rational bicubic surface, $P(u,v)$, $0 \le u,v \le 1$, that if the signs of torsion for the boundary curves, $P_1(u) = P(u,0)$ and $P_2(u) = P(u,1)$, $0 \le u \le 1$, are different, then there exists a planar parametric segment for some $v = c$, $c \in (0,1)$, irrespective of how the surface $P(u,v)$, $0 \le u,v \le 1$, is constructed.

We consider the parametric curves defined by $\underline{\underline{P}}(u,v) = P(u,v) - P(0,v)$, $0 \le u \le 1$, $v \in [0,1]$. We define a continuous function,

$$\underline{\underline{s}}_\tau(v) = (\underline{\underline{P}}(1,v) - \underline{\underline{P}}(0,v)) \cdot \dot{\underline{\underline{P}}}(1,v) \times \dot{\underline{\underline{P}}}(0,v) = (\underline{\underline{P}}(1,v) \cdot \dot{\underline{\underline{P}}}(1,v) \times \dot{\underline{\underline{P}}}(0,v)$$

which by Theorem 6 determines the sign of torsion for each curve $\underline{\underline{P}}(u,v)$, $0 \le u \le 1$, $v \in [0,1]$.

By definition we must have $\underline{\underline{s}}_\tau(0)\underline{\underline{s}}_\tau(1) < 0$, then using the intermediate value theorem there must exist a $c \in (0,1)$ for which $\underline{\underline{s}}_\tau(c) = 0$.
By Theorem 5 the sign of torsion is constant, then torsion of the curve $\underline{\underline{P}}(u,c)$, $0 \le u \le 1$, $c \in (0,1)$ is identically zero and by Theorem 1, proved in section(3.2.3), must be planar.

Hence the parametric curve $P(u,c) = \underline{\underline{P}}(u,c) + P(0,c)$, $0 \le u \le 1$, $c \in (0,1)$ must also be planar.

BIBLIOGRAPHY

Ball, A.A. and Cripps, R.J. [1987] : 'A geometric analysis of springback in drawn panels'. Proc. ACME Conference, Cambridge Univ., SERC, Swindon.

Barnhill R.E., Farin G., Fayard L. and Hagen H. [1988] : 'Twists, curvature and surface interrogation', Computer Aided Geometric Design, Vol 20, no. 6, pp 341 - 347.

Baynham, J.M.W. and Zienkiewicz O.C. [1982] : 'Developments in Finite Element Analysis of thin sheet drawing and direct redrawing process, using the rigid - plastic approach', Num. Meth. in Ind. forming processes. Proc. of Conf., Univ. Swansea. pp 697 - 707.

Boehm, W. [1988] : 'Visual Continuity', Computer Aided Geometric Design, Vol 20, no. 6, pp 307 - 311.

Boehm, W. [1987] : 'Rational geometric splines', Computer Aided Geometric Design', Vol 4, pp 67 - 77.

Buck, R.C. [1965] : Advanced Calculus, McGraw-Hill Book Company.

Caddell, R.M. and Hosford, W.F. [1983] : 'Metal forming : mechanics and metallurgy', Ann Harbor, Michigan, Prentice Hall.

Chandra, A. [1986] : 'A generalized Finite Element Analysis of sheet metal forming with an elastic - viscoplastic material model', J. of Engn. for Ind., February, pp 9 - 15.

Chu, E., Samanta, S.K. and Tang, S.C. [1982] : 'Finite Element prediction of the formed shape of an automotive body panel during the pre-formed stage', Num. Meth. in Ind. forming processes. Proc. of Conf.), pp 629 - 641.

Chung, S.Y. and Swift, H.W. [1951] : 'Cup drawing from a flat blank', Proc. Inst. Mech. Eng., Vol. 165, pp 199-223.

Clarke, C. [1986] : Private communication.

Coltman, B. [1988] : Private communication.

Dahliquist, G. and Bjorck, A. [1974] : Numerical Methods, Prentice-Hall, Englewood Cliffs, N.J..

Dixon, P.R. [1988] : 'Preliminary compression Tests on 224 carbon steel at room temperature.', Internal Report, Department of Physics, Loughborough University of Technology.

Duncan, J.L., Sowerby, R. and Chu, E. [1985] : 'The development of sheet metal modelling', Computer modelling of sheet metal forming process : Theory, verification and application. (Proc. of Conf.) Ann Arbor, Michigan. pp 1 - 11.

Faux, I.D. and Pratt, M.J. [1983] : Computational geometry for design and manufacture, Ellis Horwood Ltd..

Farouki, R.T. [1987] : 'Graphical methods for surface differential geometry', The mathematics of surfaces II, IMA Conf., Cardiff, pp 363 - 385, Clarendon Press, Oxford.

Geisow, A.D. and Pratt, M.J. [1986] : 'Surface/surface intersection problems.', The mathematics of surfaces I, IMA Conf., Manchester, pp 117 - 142, Clarendon Press, Oxford.

Hall, I.H. [1968] : Deformation of solids, The University Press Ltd.

Honner, M.E., Mattiasson, K., Wood, R.D., Zienkiewicz, O.C. [1985] : 'Viscous flow and solid mechanical approaches to the analysis of thin sheet metal forming.', Computer modelling of sheet metal forming process : Theory, verification and application.(Proc. of Conf.),Ann Arbor, Michigan. pp 121 - 142.

Kobayayashi, S., Toh, C. H., and Shiau, Y.C. [1986] : 'Analysis of a Test Method of sheet metal formability using the Finite - Element Method', J. of Eng. in Ind., February, Vol 108, pp 3 - 8.

Kokken, V. [1985] : 'Modelling of forming process for Tool Design and Manufacturing at Volvo.' Computer modelling of sheet metal forming process : Theory, verification and application. (Proc. of Conf.) Ann Arbor, Michigan. pp 1 - 11.

Lee, D. [1982] : 'Computer - Aided control of sheet metal forming process', J. Metals, November, pp 20 - 29.

Lipschultz, M.M. [1969] : Differential Geometry, McGraw-Hill Book company.

Mitchel, A.R. and Wait, R. [1985] : Finite Element Analysis and Applications, John Wiley & Sons.

Munchmeyer, F. and Haw, R. [1982] : 'Applications of Differential Geometry to ship design', Computer applications in the automation of shipyard operation and ship design IV, pp 183 - 189.

Nutbourne, A.W. [1986] : 'A circle diagram for local differential geometry' The mathematics of surfaces I, IMA Conf., Manchester, pp 59 - 71. Clarendon Press, Oxford.

Richard, P.N. [1981a] : 'Forming and drawing of sheet steel' Part 1, Sheet Metal Industries, October pp 789 - 790.

Richard, P.N. [1981b] : 'Forming and drawing of sheet steel' Part 2, Sheet Metal Industries, November pp 913 - 917.

Sedgewich, R. [1983] : 'Algorithms', Addison-Wesley, pp 79 - 88.

Tennent, R.M. [1984] : 'Science data book', Oliver & Boyd, p60.

Wang, N. [1982] : 'A rigid - plastic rate - sensitive finite element method for modelling sheet metal forming process.' Num. Meth. in Ind. forming processes. Proc. of Conf., Univ. Swansea. pp 797 - 808.

Weatherburn, C.E. [1927] : Differential Geometry of three dimensions, Cambridge University Press.

Willmore, T.J. [1972] : An introduction to Differential Geometry, Oxford University Press.

Wood, R.D. [1981] : 'The finite element method and sheet metal forming', Sheet Metal Industries, August, pp. 561-567.

Zienkiewicz, O.C. [1985] : The Finite Element Method, 3rd edition, McGraw-Hill.